UNIVERSITY OF CALFORNIA SAN DIEGO

Role of PABP1 on Influenza A virus mRNA Translation Initiation

A dissertation submitted in partial satisfaction of the
requirements for the degree Doctor of Philosophy

in

Chemistry

by

Cyrus Marc de Rozières

Committee in charge:

Professor Simpson Joseph, Chair
Professor Thomas Hermann
Professor Amy Pasquinelli
Professor Navtej Toor
Professor Brian Zid

2021

The Dissertation of Cyrus Marc de Rozières is approved, and it is acceptable in quality and form for publication on microfilm and electronically.

University of California San Diego

2021

DEDICATION

I dedicate this body of work to my father, who I never got the chance to know, Jean Marie Guy de Rozières Gentilhomme de Laveline, Ph. D. and to my mother who raised and supported me all of my life, Sohela de Rozières Gentilhomme de Laveline, Ph. D. née Niroumand Rad.

EPIGRAPH

“Mother Nature is a serial killer. No one’s better. More creative. Like all serial killers, she can't help but the urge to get caught. What good are all those brilliant crimes if nobody takes the credit? So she leaves crumbs. Now, the hard part is, and why you spend decades in school, is seeing the crumbs for the clues they are. Sometimes the thing you thought to be the most brutal aspect of the virus, actually turns out to be the chink in its armor. She loves disguising her weaknesses as strengths.”

Character from World War Z, Andrew Fassbauch

TABLE OF CONTENTS

LIST OF ABBREVIATIONS

CDS	Coding sequence
CrPV	Cricket paralysis virus
cRNA	Copy ribonucleic acid
CTT	C-terminal tail
DNA	Deoxyribonucleic acid
dsRNA	Double-stranded ribonucleic acid
ED	Effector domain
ELISA	Enzyme-linked immunosorbent assay
EMCV	Encephalomyocarditis virus
EMSA	Electrophoretic mobility shift assay
FLuc	Firefly luciferase
GST	Glutathione S-transferase
HA	Hemagglutinin protein
IAV	Influenza A virus
IP	Immunoprecipitation
IRES	Internal ribosome entry site
IVTS	In vitro translation system
M1	Matrix protein 1
M2	Matrix protein 2
m^7G	7-Methylguanosine
mRNA	Messenger ribonucleic acid
NA	Neuraminidase protein

NGS	Next generation sequencing
NP	Nucleoprotein
NS1	Non-structural protein 1
NS2	Non-structural protein 2
PA	Polymerase acidic protein
PAGE	Polyacrylamide gel electrophoresis
PB1	Polymerase basic protein 1
PB2	Polymerase basic protein 2
PCR	Polymerase chain reaction
qPCR	Quantitative polymerase chain reaction
RBD	RNA binding domain
RLuc	Renilla luciferase
RNA	Ribonucleic acid
RRM	RNA recognition motif
RT	Reverse Transcription
ssRNA	Single-stranded ribonucleic acid
SUMO	Small ubiquitin-like modifier
tRNA	Transfer ribonucleic acid
UTR	Untranslated region
vRNA	Viral ribonucleic acid

LIST OF FIGURES

LIST OF TABLES

ACKNOWLEDGMENTS

I would like to thank Professor Simpson Joseph for his support and guidance these past years. He always gave me the freedom to pursue the research that interested me at the pace that I wanted. He also supported the times when I needed a break and to experience important events in my life and for that I am eternally grateful.

I also thank my committee members for their continued support over the years. I always received great feedback and genuine enthusiasm from each member and am grateful for the time that they shared with me.

I would also like to thank the colleagues and friends I made across the department. The sharing of ideas, equipment, resources and time within and outside of the Joseph lab all culminated in my ability to progress in my goals and serves as proof of the virtues of collaboration and fostering positive relationships.

Lastly, I would like to thank my brother, family and friends who have always been supportive and a positive distraction to keep me focused on the present. I would especially like to thank Audrey Rose Zak for her support throughout this experience having helped me through all the ups and downs of this process. Finally, I would like to thank my mother for having done so much to get me to this point. As my role model and greatest supporter, all of the good things that I do in this life I do thanks to her and for her.

Chapter 2, in full, has been submitted for publication of the material. Cyrus M de Rozières, Alberto Pequeno, Shandy Shahabi, Taryn M Lucas, Kamil Godula,

Gourisankar Ghosh and Simpson Joseph. The dissertation author was the primary investigator and author of this material.

Chapter 3, in full, is a reprint of the material as it appears in Influenza A Virus NS1 Protein Binds as a Dimer to RNA-Free PABP1 but Not to the PABP1·Poly(A) RNA Complex, Biochemistry, 2020. de Rozieres, Cyrus M.; Joseph, Simpson, 2020. The dissertation author was the primary investigator and author of this paper.

VITA

2013	Bachelor of Science, University of California San Diego
2013-2014	Research Assistant, Sanford Burnham Medical Research Institute
2015	Laboratory Assistant, Sanford Burnham Medical Research Institute
2015-2016	Research Associate, Illumina
2018	Master of Chemistry, University of California San Diego
2021	Doctor of Philosophy, University of California San Diego

PUBLICATIONS

Arias-Mireles BH, de Rozieres CM, Ly K, Joseph S. (2018). RNA Modulates the Interaction Between Influenza A Virus NS1 and Human PABP1. *Biochemistry*, 57 (26) 3590-3598.

de Rozières CM, Joseph S. (2020). Influenza A virus NS1 protein binds as a dimer to the RNA-free PABP1 but not to the PABP1-Poly(A) RNA Complex. *Biochemistry*, 59 4439-4448.

de Rozières CM, Pequeno A, Shahabi S, Lucas TM, Godula K, Ghosh G, Joseph S. (2021). PABP1 drives the Selective Translation of Influenza A Virus mRNA. *IN SUBMISSION*

ABSTRACT OF THE DISSERTATION

Role of PABP1 on Influenza A virus mRNA Translation Initiation

by

Cyrus Marc de Rozières

Doctor of Philosophy in Chemistry

University of California San Diego, 2021

Professor Simpson Joseph, Chair

The Influenza A virus (IAV) is a pathogen with a long-standing history of seasonal spread across human communities. Infection by IAV can cause upper respiratory distress in humans that can be fatal especially for those with weakened immune systems. The reservoirs of IAV in animals as well as the rapid mutation rate makes IAV challenging to prevent and eradicate, therefore more understanding of its mechanisms of hijacking host cellular machinery is required to find new solutions for treating this disease.

Results from the field suggests that Influenza RNA are acted upon by translation factors in the same manner as host mRNA. Capped and poly (A) tailed viral mRNA are recognized by eIF4E at the 5' end and PABP1 at the 3' end to recruit the subsequent initiation factors until the ribosome is assembled and can commence translation. This mechanism of translation initiation however, fails to explain why viral proteins are synthesized to such a high degree.

We set out to study the role PABP1 plays on IAV RNA due to it being targeted by the IAV protein NS1. Using qualitative and quantitative binding assays we have further characterized the PABP1-NS1 interaction by discovering that it occurs in the absence of Poly(A). This suggests that NS1 acts upon PABP1 independent of PABP1 binding to a poly(A) tail.

Furthermore, we discovered a novel interaction that PABP1 has to the 5' UTR regions of viral mRNAs. The differences in binding affinity correlate with the protein production measured for those segments. We thus tested the validity of these observations by studying the benefits of IAV 5' UTRs in a cell free *in vitro* translation system where cap dependent translation was inhibited. We found that RNAs driven with

the viral 5’ UTRs are more resistant to suppression of cap-dependent translation than RNAs driven by a eukaryotic 5’ UTR. To follow up on our *in vitro* results, we pulled down PABP1 from IAV infected cells and found via RT-qPCR that the 5’ UTRs of IAV RNAs are enriched post pulldown. This suggests that IAV mRNA translation can be initiated by PABP1 acting on the 5’ end.

Chapter 1: Introduction

1.1 Viruses

Viruses are small parasites incapable of reproducing themselves without a host. Viruses, therefore, require host cells whose molecular machinery and resources can be directed towards the synthesis and assembly of new viral particles known as virions. In general, virions are made up of a protein coat containing the virus's genetic material in the form of DNA or RNA [1]. The viral genome generally contains all of the necessary information in order to successfully replicate and proliferate new progenitor virions that infect other cells.

The genomes of different viruses vary in length and number of encoded proteins. The number of encoded proteins range from as few as four to as many as hundreds of unique proteins [1]. Most proteins encoded by viruses can be categorized as either structural proteins, enzymes necessary for viral replication, or proteins that inhibit host-cell functions such as DNA, RNA, and protein synthesis. Each of these types of proteins are needed in varying amounts with structural proteins typically synthesized in abundance relative to the other two types [1].

While many different viruses exist, most are limited in the range of hosts and cell types that can be successfully infected for subsequent replication. Bacteriophages, plant viruses, and animal viruses will typically infect within a phylum but may transfer across species given sufficient evolutionary pressure and sufficient cellular machinery to proliferate. Often the ability to jump across species will promote viral fitness in order to maximize its ability to rapidly infect cells, known as virulence.

Viruses have had a long-standing influence on humans, their evolution, the societies they form, and their history [2]. It has been estimated that roughly 10% of the human genome is made up of genes incorporated by early interactions between viruses and early vertebrates [3]. For example, syncytin is a protein expressed in humans important for cell-cell fusion pivotal for the development of the placenta, which aids in embryo attachment to the uterus and nutrient exchange [4]. The gene encoding syncytin stems from the envelope gene of the retrovirus HERV-W whose genome was incorporated when early mammals diverged from birds 25 to 40 million years ago [5,6]. It is believed that viruses have driven roughly 30% of adaptive amino acid changes in the human genome, making them one of the most dominant drivers of evolutionary change in mammalian genomes [2].

While viruses have provided evolutionary advantages to human fitness over large timescales, they can also be destructive to human populations [2,7]. Viruses have shaped our societies, policies, behaviors, and lifespan, and have caused major paradigm shifts in modern history [8]. The transmission of viruses across populations can range from local communities (epidemics) to the world (pandemics). Smallpox ravaged Europe between the 15th and 17th centuries, killing millions before Edward Jenner's vaccine was developed [9]. The AIDS pandemic stemming from the HIV retrovirus that began in the 1980s destroyed communities and continues to be a source of intense focus to this day [10]. The SARS pandemic in 2003 and the ongoing COVID-19 pandemic come from coronaviruses that spread rapidly through human populations and have shaped modern protocols towards global health responses and strategies for mitigating the spread of these viruses [11,12]. The Ebola virus pandemic in 2014 exhibited the sensitivity of

communities that are least equipped to defend against the most lethal of viruses [13]. And finally, the influenza viruses have caused the most frequent pandemics in the last century, the rapid mutations of these viruses and their immune evasion strategies make them a looming threat year after year to society [14].

1.2 Effects of the Influenza A Virus on the World

Influenza viruses are a zoonotic pathogen known to infect a variety of species including humans, domesticated animals, and birds [15]. These viruses are predominantly found in the gastrointestinal tracts of aquatic birds, however they have had a long history of transmitting to humans via adaptive re-assortment of its genome in domesticated animals, namely swine [16]. These viruses can be classified into four genera distinguished as type A, B, C, and D viruses [17]. Influenza A virus (IAV) is the type most prevalent in modern society. IAV is the only type to cause a human pandemic and has had a long history of doing so [18].

Influenza has been around for millennia having first been described by Hippocrates in 412 B.C.E. The first well-documented IAV pandemic occurred in 1889, starting in Russia before spreading globally, with its characteristic mortality pattern of the most deaths in the elderly and young children [19]. This pandemic was followed by the 1918 Spanish flu pandemic, known to be one of the most fatal IAV pandemics with a global death estimate of at least 50 million people [20]. The IAV outbreak of 1957 reported in Hong Kong led to 1.5 million deaths on the Asian continent with another IAV outbreak in 1968 leading to another million deaths in Hong Kong alone [21]. Over the following

decades many more smaller IAV outbreaks occurred until 2009 when the most recent Swine flu pandemic caught the world by surprise **(Figure 1.1)** [22].

In humans, IAV is a contagious respiratory disease, with symptoms like coughing, sneezing, and fever that can lead to viral pneumonia and death [23]. While more studies are recommended to legitimize this, the Centers for Disease Control and Prevention (CDC) warns that people over 65 years of age, under 5 years of age, and pregnant women are at greatest risk of developing life-threatening complications from the influenza infection [19,24]. Furthermore, studies show a correlation between influenza-related hospitalization and lower socioeconomic status believed to be due to lower vaccination rates, poverty-related crowding, and increased comorbidities that make people more at risk of developing health-related complications [25]. While many of these studies were performed in the United States due to its surveillance programs, these risk-related factors can be extrapolated to also affect the rest of the world.

One reason for the continued prevalence of influenza can be attributed to a growing and more interconnected global population. Since the 1800's the global population has seen a roughly 1.1% growth year-over-year from 1 billion to 7.8 billion by the late 2010's according to the United Nations (UN) [26]. It is projected that at the current rate the global population can reach 11 billion by 2100 [26]. Furthermore, 95% of the global population lives on only 10% of the world's available land with an expected rise from 33 megacities (metropolitan areas with a population of 10 million people or more) in 2018 to 43 megacities by 2030 [27].

The World Health Organization (WHO) estimates on average that about 1 billion cases of seasonal influenza infection occur, leading to 300,000 – 650,000 deaths each

year [28]. It is estimated that within the United States alone, the economic burden due to seasonal influenza costs $10.4 billion for direct medical costs and $87.1 billion for the total economic impact per year [29].

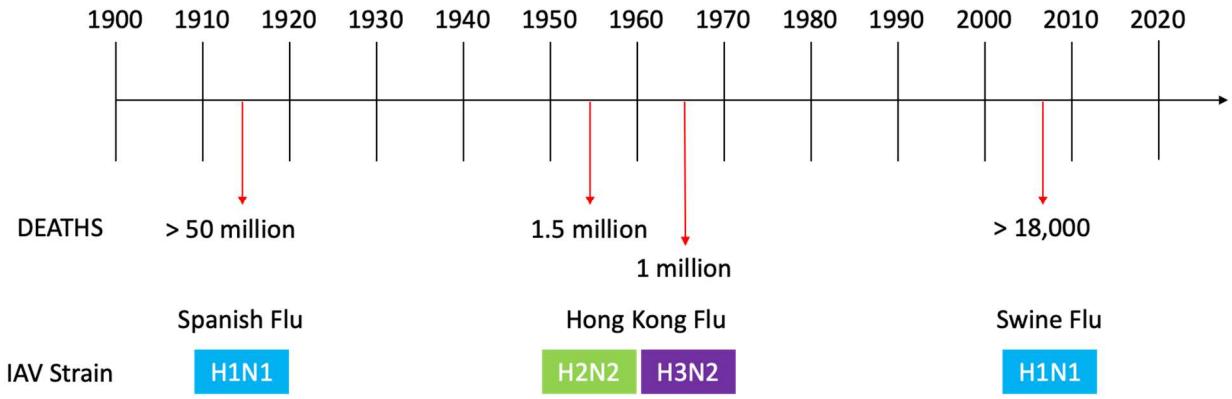

Figure 1.1: IAV pandemic events and strains in the past century. A timeline describing official IAV pandemics since 1900 with an estimate of the number of deaths caused by the virus and the predominant strain.

1.3 Influenza A Virus Structure & Components

Influenza viruses are members of the Orthomyxoviridae family which are characterized by having an enveloped segmented genome [30]. IAV is classified as a V.b.

virus due to its genomic makeup of 8 negative-sense single-stranded RNAs [1]. The segments code for the roughly dozen viral proteins necessary to successfully infect and replicate within a host cell for subsequent infections **(Figure 1.2)**. The segments range in size from ~1 to 3 kilobases (kb) in length and each is named according to the name of the major protein product that it codes for.

Segments 1 and 2 are primarily known for coding the RNA polymerases PB2 and PB1, respectively, responsible for synthesis of viral RNA. Segment 3 codes for the polymerase protein, PA, that acts as an endonuclease important for the synthesis of the RNA. Segment 4 codes for the hemagglutinin (HA) proteins responsible for viral entry into a host cell. Segment 5 codes for the nucleoprotein (NP), which serves to protect the integrity of the IAV genome from nucleases by acting as a scaffold for the viral RNA to wrap around. Segment 6 codes for the neuraminidase (NA) proteins allowing for newly formed virions to exit the cell. Segment 7 codes for the matrix (M) proteins which form the viral capsid. Finally segment 8 codes for the non-structural (NS) proteins, responsible for the host cellular mechanisms hijacking and directing of energy and resources for successful viral proliferation [17].

Influenza viruses are made up of a lipid membrane enveloping the 8 segments that is acquired when packaged virions bud from a host cell [31]. The surfaces of these lipid membranes display the glycoproteins HA and NA **(Figure 1.3a)**. HA is the viral protein that recognizes the sialic acid receptors on target cells allowing for viral entry. Because infection and subsequent proliferation is dependent on viral entry, it is unsurprising that HA proteins consist of ~80% of the surface proteins on any given virion. NA on the other hand is responsible for viral exit of the infected host cell and

makes up less than 20% of the viral proteins found on the virus surface. The remaining surface proteins of IAV is the M2 protein that serves as a proton pump, spanning the lipid bilayer and maintaining the pH of the interior of the virus.

Housed underneath the lipid membrane is the viral capsid made up of an oligomeric assembly of pairs of M1 proteins [32]. Finally, the interior of the virus contains one copy of each of the 8 viral RNA segments whose 3' end is bound by the heterotrimeric polymerase complex of PB2, PB1, and PA [31]. The rest of the RNA is coiled around the nucleoprotein (NP), which allows the RNA to be packaged efficiently within the virus.

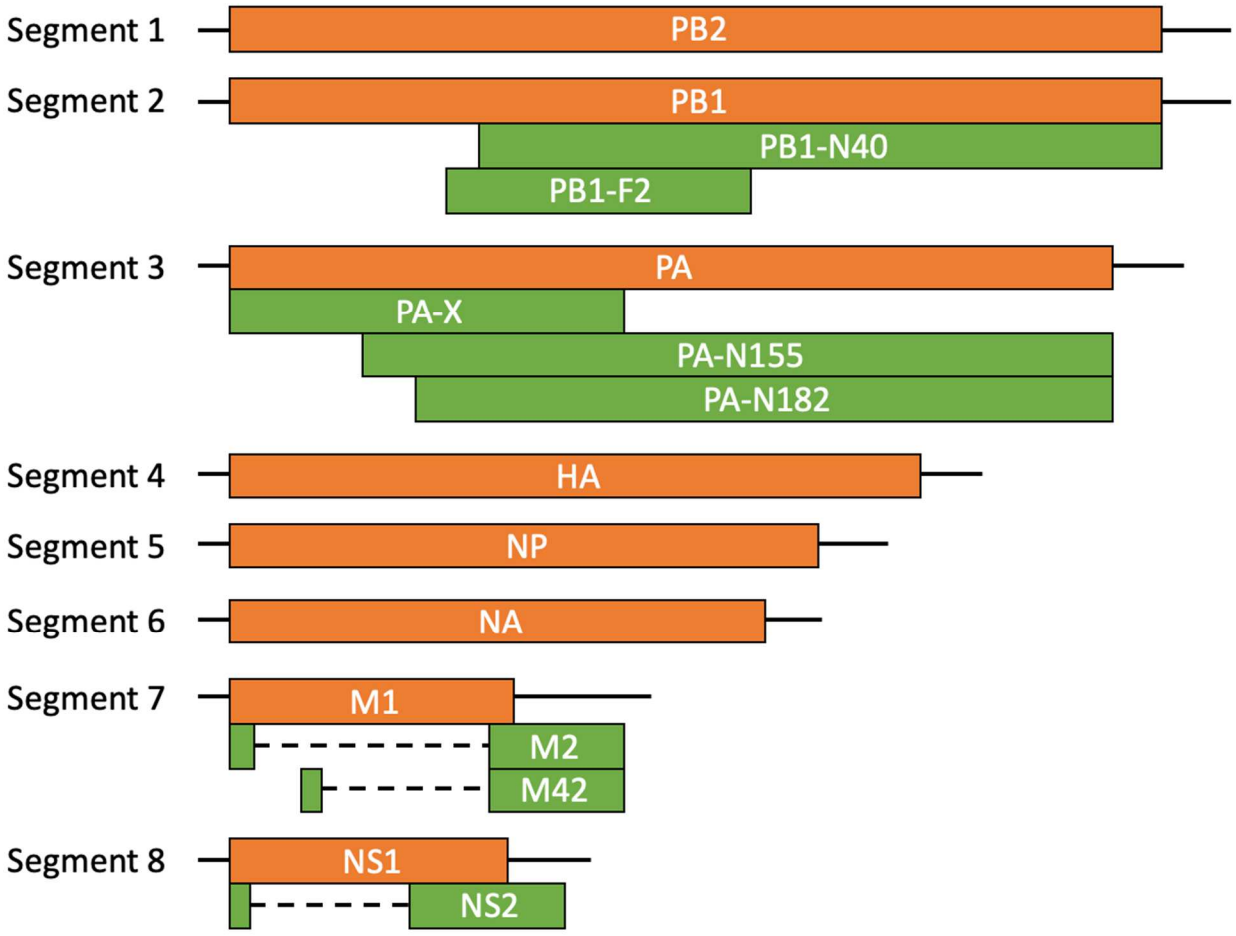

Figure 1.2: 8 IAV segments and the proteins encoded. The 8 segments, their relative lengths and the major proteins encoded are depicted in orange rectangles with the black lines flanking either side representing the UTRs. The green rectangles represent alternative protein products due to alternative reading frames (PA and PB1 segments) or splicing (dashed lines).

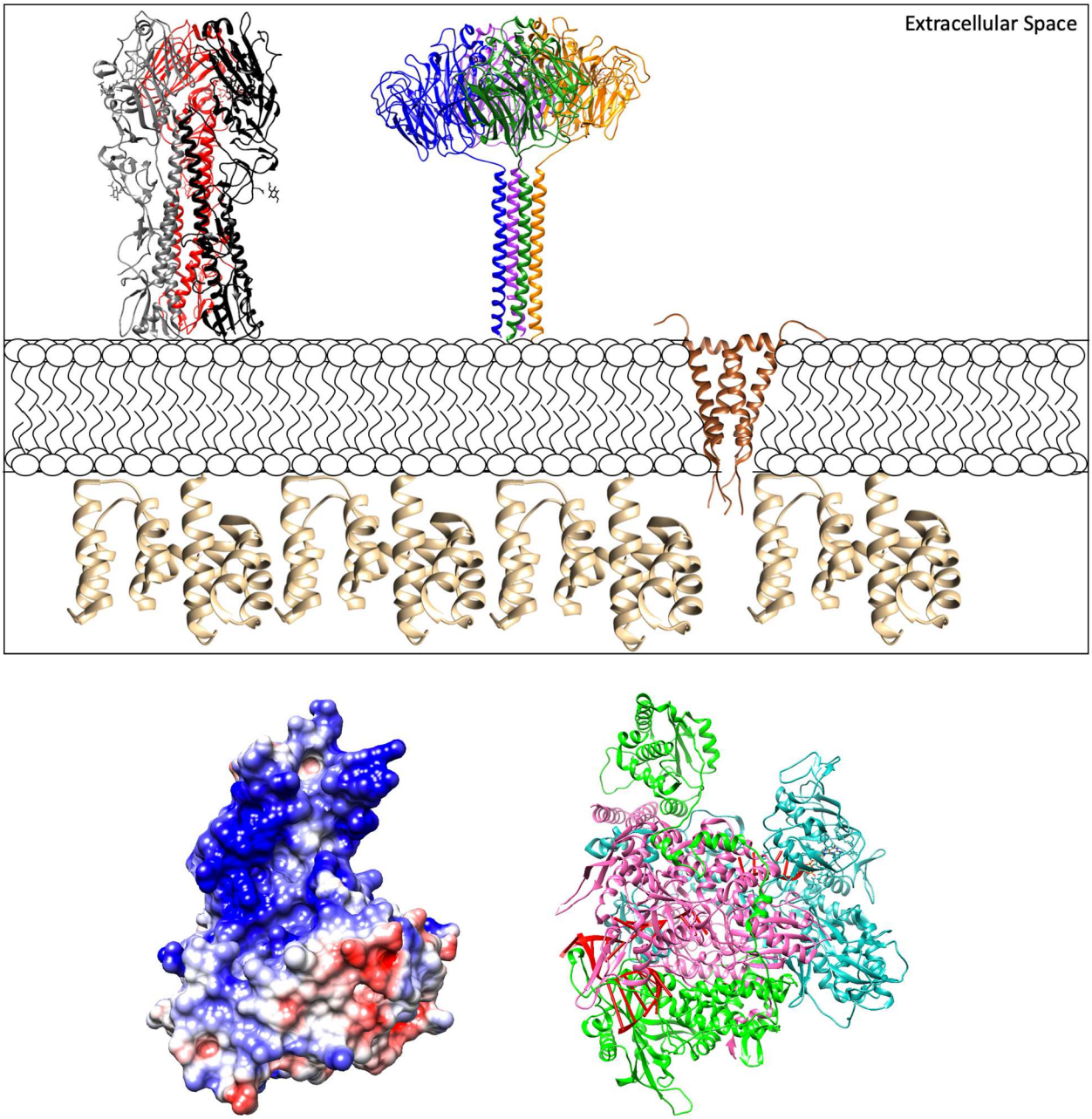

Figure 1.3: Structural depictions of the viral proteins that make up IAV. (A) Cross-sectional depiction of the viral enveloped membrane with the solved structures of HA (black, red and gray) and NA (blue, purple, green, and orange) on a lipid bilayer with an M2 (brown) proton pump embedded. On the other side of the membrane is a rough oligomer of the M1 (tan) viral capsid that forms the structure of the virion. (B) A heatmap of the nucleocapsid structure where areas of increased positively and negatively charged residues are depicted in blue and red, respectively. (C) The structure of the heterotrimeric polymerase complex with PB1 (pink), PA (teal), PB2 (green) bound to cRNA (RNA in red).

1.4 Influenza A Virus Life Cycle

The life cycle of IAV upon entering into the airway passages of a human host begins with the recognition by HA, on the surface of the virion, of the sialic acid receptors of a lung epithelial cell. Recognition by this receptor triggers endocytosis into the cell whereupon entry the virus is transported as cargo towards the nucleus whereby upon reaching its destination will release its genome into the cell's nucleus [33].

Upon entry into the nucleus the heterotrimeric polymerase complex bound to the 3' end of each segment begins the process of transcription. During transcription, the PA subunit of the polymerase complex uses its endonucleolytic abilities to capture the 5' ends of mRNA, specifically targeting mRNAs with an m^7G cap and the first 12-13 nucleotides of the mRNA sequence, in a process called cap-snatching. Studies have suggested that certain sequences and mRNAs are preferred depending on the IAV strain and the IAV segment being transcribed [34,35]. Multiple studies have identified the endogenous U2 snRNA, whose sequence contains an m^7G cap, but is not typically translated, as most targeted by IAV during this cap-snatching process [35–37]. These sequences are then positioned and used as a primer for subsequent transcription by the PB2 polymerase subunit to synthesize the positive-sense RNA.

At the end of this transcription process the polymerase will reach a stretch of uracils at the 5'end of the vRNA [38]. This end is positioned such that the RNA is not capable of further translocation after the polymerase incorporates the next nucleotide [39]. This causes a stuttering event whereby the polymerase remains stuck on this uracil stretch and thus will begin to incorporate a series of adenines to the 3'end of the

transcribed mRNA. Studies have shown that approximately 150 adenines are added to the 3' end of the transcribed mRNA [40]. At some point the newly synthesized mRNA is released into the cytoplasm to undergo translation. It is worth noting that the transcription process does not contain any error recognition process to ensure correct synthesis of the mRNA. This actually serves as an advantage for the virus since it allows for an increase in mutation rate that keeps IAV evolutionarily fit. It is estimated that the IAV genome's mutation rate ranges between 1×10^{-3} and 8×10^{-3} mutations per base every year [41,42].

Due to the capped and tailed nature of the mRNA synthesized during viral transcription, the viral mRNAs have all of the necessary components to be recognized and translated by the host's canonical cap-dependent translational machinery (described in more detail in Chapter 1.5). Upon translation the newly synthesized viral proteins can then begin the process of hijacking the cellular machinery in order to further direct resources towards the synthesis of more viral proteins, vRNA, and eventually virions.

While the majority of the viral proteins synthesized are predominantly structural in nature, a select few serve as agents for the overall success of virus production. Notable players are NS1, NS2 (also known as NEP) from the NS segment, and PA-X from the PA segment. NS1 whose functions will be described in more detail in Chapter 1.7 is primarily responsible for the immune suppression of the host cell by recognizing and sequestering the RIG-I complex. PA-X contains the endonucleolytic activity of the PA protein and is believed to serve as a method to degrade host mRNAs in the cytoplasm to increase the relative concentrations and competitiveness of the viral mRNAs.

The process of viral transcription and translation continues throughout the infection causing exponential amounts of viral molecules to be produced at its peak. During this time, a new version of the positive-sense viral RNA (cRNA) is synthesized without a cap and tail to serve as the template for the production of new vRNAs. vRNAs will then be synthesized and assembled upon by newly synthesized NP, PB2, PB1, and PA proteins. These newly assembled vRNAs will then be transported to the host cell membrane with all of the necessary structural proteins, namely M1, M2, HA, and NA, to form new virions each containing a single copy of the 8 viral segments [31]. The assembled virions then bud off from the host cell membrane taking with them a portion of the cell membrane whereby the NA proteins perform the final cleavage necessary to be released into the extracellular space for subsequent infection and proliferation.

1.5 Canonical Eukaryotic Translation & Translation Initiation

Due to the nature of viral mRNA transcription by which a 5' cap and 3' poly (A) tail are incorporated onto the coding sequence of the (+)-sense RNA, it is clear that IAV utilizes the canonical methods by which host mRNAs are translated. The process of translation is heavily regulated in order to ensure that correct RNAs are translated while non-coding RNAs serving alternative functions are left alone. The process begins when a capped and tailed mRNA enters the cytoplasm of the cell. The 5' m^7G cap of the RNA is recognized and bound by the eukaryotic initiation factor 4E (eIF4E). This protein is part of an even larger protein complex bound to eukaryotic initiation factor 4G and 4A (eIF4G and eIF4A respectively) to make the eIF4F complex. At the 3'end the poly (A)

tail, the mRNA is bound by multiple poly A binding proteins (PABP1). The recognition and binding of both ends of the mRNA molecule to either protein is very specific, indicated by the very high affinities each have for their respective sites. PABP1, which has an estimated 4 μM concentration in the cell, binds to the poly (A) tail with an equilibrium dissociation constant (K_D) of 2 - 7 nM affinity [43–45]. It has been reported that eIF4E binds to the m7G cap with a K_D of ~ 1 nM, however its cellular abundance is much lower than that of PABP1 and its binding is considered the rate limiting step in translation initiation [46].

Once both ends of the mRNA have been bound to their respective proteins, the mRNA undergoes a circularization event due to the affinity that PABP1 and eIF4G have for each other [47]. After circularization, more initiation factors can begin to assemble onto the mRNA until the recruitment of the 40S ribosomal subunit to form the 43S pre-initiation complex. The 40S ribosome then begins to scan the RNA sequence until it reaches the first AUG start codon which is then locked in place by the interaction of the initiator tRNA. Once in place, the 60S ribosome can then bind the RNA opposite the 40S to form the 80S ribosomal complex. At this point the initiation phase of translation is complete and the elongation phase can commence.

During elongation the mRNA will be translocated by three nucleotides in the ribosome and tRNA with the correct anticodon sequence will recognize the next codon made available by translocation of the ribosome along the mRNA. Each tRNA brings with it an amino acid that can be ligated with the growing polypeptide chain that is being formed. This process of tRNA recognition, amino acid ligation to the polypeptide, and

subsequent translocation continues until the ribosome comes upon a stop codon (UAA, UAG or UGA) whereby translation elongation stops and termination begins.

Translation termination involves recognition of the stop codons by the release factor eRF1, which will bind to the ribosome-mRNA complex and prompt the release of the newly synthesized polypeptide chain. This is followed by a process whereby the ribosome can be disassembled from the mRNA and recycled for translation of other mRNAs.

1.6 Poly(A) Binding Protein

Poly (A) binding proteins are a class of RNA-binding proteins found in eukaryotic organisms. They are ubiquitous in the cell with concentrations measured to be approximately 4 μM, and have a variety of functions revolving around polyadenylated RNA [43]. In vertebrates there are five different PABP1 proteins in the cell with their own function [48]. Nuclear PABP (PABPN1), X-linked PABP (PABPC5) and the cytoplasmic PABPs (iPABP, PABPC3 and PABPC1) have been identified thus far [49]. While PABPN1 is involved with maturing mRNA and export in the nucleus, the cytoplasmic PABPs protect mRNA from degradation, initiate translation, and have been reported to bind to the 5'UTR of certain mRNA to regulate expression [50–53]. The bulk of studies on these proteins focus predominantly on PABPC1 which is the protein we are referring to whenever we mention PABP1.

PABP1 is a 72 kDa globular protein made up of four RNA recognition motifs (RRM), a homodimerization domain, and a C-terminal motif termed PABC **(Figure**

1.4A). The RRMs are responsible for binding to RNA, with RRM 1 and RRM 2 mediating PABP1 binding to the poly(A) sequence. RRM 3 and RRM 4 have their own specificity to different RNA sequences with a preference for AU repeats (K_D = 2.9 nM) [54]. The homodimerization domain is a roughly 200 amino acid sequence without a predominant structural motif and is predicted to be intrinsically disordered in solution **(Figure 1.4B)** [55,56]. This portion of the protein is involved in the multimerization that occurs between PABP1 molecules that allows for the coordinated assembly of these proteins on poly(A) tails [49,57].The C-terminal PABC domain interacts with other proteins believed to be important for modulating PABP1's ability to bind to RNAs at different times.

On a poly(A) tail, PABP1 will oligomerize in a unidirectional fashion with recent NMR studies suggesting that the coordination and orientation is dictated by the homodimerization domain of one PABP1 molecule interacting with RRM 2 of its neighbor [57]. While poly(A) tails are believed to reach lengths of 150 to 200 nucleotides in the nucleus, these tails are believed to be shortened down to lengths that fit only a single PABP1 on transcripts that are highly translated [58]. PABP1 requires a minimum of 18 adenosines for RRM 1 and 2 to bind properly, however the protein itself has a roughly 30 nucleotide foot-print. While PABP1's greatest affinity is for poly(A) sequences (K_D = 2 – 7 nM), it has been shown to also have affinities for poly(G) and poly(U) sequences but not poly(C) [44,45,59,60].

Crystal structures of PABP1 on poly(A) have revealed the possible mechanism by which PABP1 – Poly(A) can interact with eIF4G to cause circularization of an mRNA

(Figure 1.4A) [61]. These studies also reveal an allosterically based mechanism to promote this complex formation.

While PABP1 is canonically associated with the 3' end of mRNA, there are more and more studies surfacing that implicate PABP1 with having possible roles at the 5' end as well [62]. For example, PABP1 has been shown in humans and mice to bind to an A-rich sequence of its own RNA at the 5' end [50,52]. It is thought that this suppresses the translation of its own mRNA by preventing canonical cap-dependent translation initiation from occurring. Other groups have shown, in yeast cells under stress, that certain genes important in stress response have poly-A tracks in their 5'UTR [63]. They observed in their studies that these sequences in the 5'UTR allowed for continued translation of the mRNA when cap-dependent translation was inhibited and that this continuing translation was due to PABP1 localization at the 5' end of the mRNA [63]. While more needs to be understood regarding this protein, it is clear that its importance cannot be understated.

The role PABP1 plays in cells has not gone unnoticed by viruses, of which some have developed mechanisms to either harness or neutralize the protein during infection. For example, the herpes simplex virus 1 genome codes for a protein called ICP27. It is an essential mRNA-binding protein serving as a key regulator during infection [64]. This viral protein will selectively initiate translation of specific RNAs by binding to the RNA and recruiting PABP1 to subsequently recruit eIF4G and the following initiation factors independent of eIF4E [64]. Other viruses like those of the picornavirius family encode proteases that cleave PABP1 to direct translation in a manner that is beneficial to proliferation of those viruses [65]. It therefore comes as no surprise that influenza has also been found to have ties to PABP1.

To date, multiple groups have demonstrated biochemically that PABP1 interacts with the NS1 protein [66]. Furthermore the K_D of this interaction has been measured via FRET studies to be roughly 20 nM [60]. Additionally, in immunoprecipitation pull-down studies, influenza viral mRNA also pulled down PABP1 suggesting that PABP1 is involved during IAV replication [67]. It does remain to be seen, however, how exactly PABP1 functions in the context of IAV and thus more studies are needed to examine its role.

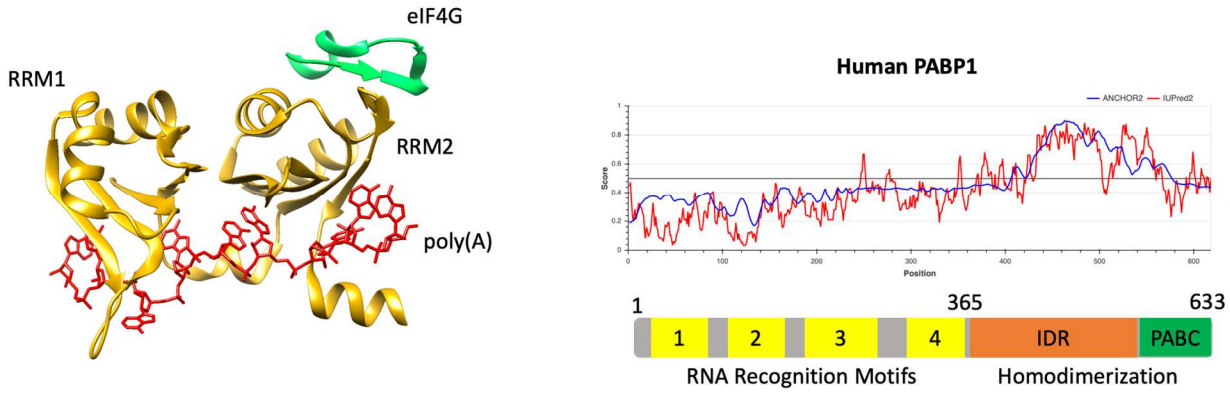

Figure 1.4: PABP1 binding to eIF4G and poly(A) RNA. (A) Structure of RRM 1 and 2 of PABP (gold) bound by a portion of eIF4G (green) and bound to poly(A) RNA (red). (B) Structure prediction of PABP1 protein by IUPRED where a score below 0.5 is predicted to be ordered and above 0.5 is disordered. Below it is a schematic of the major domains and their positions in the PABP1 primary sequence.

1.7 NS1 Structure, Roles, and Importance

The major protein translated from the NS segment of IAV is called Non-structural protein 1 because it is one of the few proteins synthesized that is not included in the newly formed virion during infection. NS1 however is a necessary protein whose multifunctional roles lend it great importance for the proliferation of the virus. Reverse genetic studies of IAV with truncations or deletions in their NS segment have been shown to produce attenuated viruses [68]. This is due to NS1's primary function of downregulating the host innate immune response [69]. In addition to this role NS1 has been implicated in dozens of other aspects and changes to the cellular state during IAV infection. Among other roles, NS1 interferes with the processing of pre-mRNA in the cell by binding to CPSF30 [70]; inhibits double stranded RNA-activated protein kinase (PKR) to maintain normal cellular translation [71]; and delaying apoptosis by inhibiting PI3K among other roles [72]. Extensive interaction mapping has identified over 24 different roles for NS1 with upwards of 30 different interactions [73,74]. Needless to say, this remarkable protein is imperative for successful IAV proliferation.

NS1 is 26 kDa in size and made up of four different domains, the RNA-binding domain (RBD), linker region, effector domain (ED) and the C terminal tail (CTT). The RBD at the N-terminal end is made up of a three alpha helix bundle capable of dimerizing with the RBD of another NS1 protein via the Arg35 and Arg46 residues [75]. Following the RBD is a disordered linker region whose flexibility allows NS1 to adopt different structural conformations [76,77]. The ED of NS1 is made up of a seven strand antiparallel beta sheet with a single alpha helix [78]. Similar to the RBD, the ED can also

dimerize with the ED of another NS1 molecule allowing for the multimerization of long oligomeric NS1 structures that have been found to wrap around RNA [79,80]. Finally, the CTT is a disordered region at the C-terminal end of NS1 believed to enhance NS1's functions while not being completely necessary for viral proliferation [81].

One of the least characterized roles of NS1 is its involvement in translation. Evidence has been mounting implicating NS1's role in translation. Binding studies have demonstrated that NS1 is capable of binding to translation initiation factors such as PABP1, eIF4G and RNA **(Figure 1.5)** [60,66,75,82]. These binding studies have been corroborated by immunoprecipitation and interaction mapping experiments [67,83]. Furthermore, a multitude of evidence has linked NS1 to enhanced translation *in vitro* and *in vivo*. Multiple *in vitro* translation based studies have shown the presence of NS1 to enhance the translation of reporter RNAs [84–86]. *In vivo* work has also shown that the translation of viral mRNAs is improved when NS1 is present [87,88]. Based on this evidence it stands to reason that a link might exist between the interactions NS1 has with translation initiation factors and the enhanced rate of protein synthesis when NS1 is present. This connection has not yet been found and thus more work is recommended to uncover how this protein influences translation.

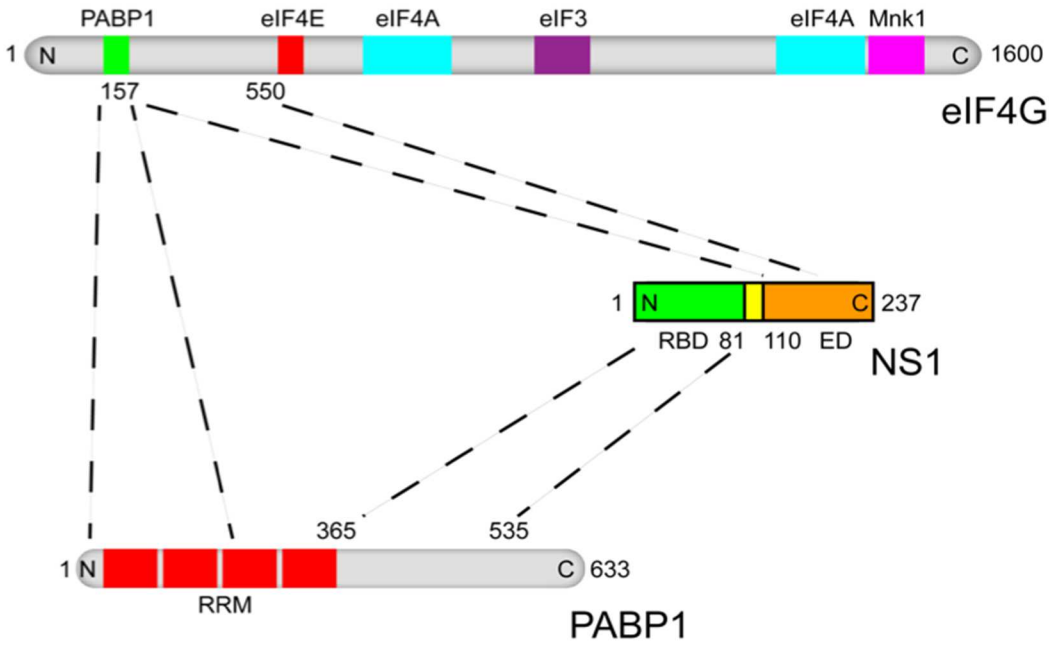

Figure 1.5: Binding map between NS1, PABP1, and eIF4G. The primary sequences of NS1, eIF4G and PABP1 are depicted with each domain labelled based on function or binding partner. The dashed lines represent what is known about the relative binding locations between each protein. The N-terminal domain of eIF4G interacts with RRM 1 and 2 of PABP1. The RBD of NS1 is known to be responsible for binding the homodimerization domain of PABP1 (residues 365-535), while the ED of NS1 binds to eIF4G somewhere between residues 157-550.

1.8 Elucidating the Relationship between NS1 and PABP1 during IAV Infection & the Mechanism behind Translation Initiation of vRNAs

Studies that examined translation during the course of influenza infection have yielded great insights into the temporal changes that occur during the course of infection. What has been clear for a long time is the speed at which viral proteins are synthesized during the course of infection. Qualitative experiments using radiolabeled methionine incorporated in infected cells followed by gel electrophoresis at different time points indicated back in the 1980s how more and more viral proteins are synthesized at the expense of host cell protein synthesis [89]. Later on, more quantitative proteomics studies looking at protein synthesis during human cell infection with two different IAV strains determined that over the course of infection, host cell protein production dropped by an order of magnitude while viral protein production increased two to three orders of magnitude over host cell protein production[90]. These studies are indicative of both an effective host shutoff mechanism and an efficient viral protein production process.

Another aspect of IAV protein synthesis that has been well-characterized is the differences in the abundance of each viral protein. Contemporary quantitative proteomics studies have measured the relative abundance of each viral protein synthesized during the course of each infection, and their findings corroborate the qualitative observations from earlier influenza studies [89,91]. The results from these studies show that proteins like the three polymerase proteins and neuraminidase proteins are not synthesized to the same extent as the M1, HA, NP, and NS1 proteins.

The conclusion is that not all viral proteins are required in equal amounts and thus suggests there is some level of control over the translation of the 8 viral segments.

This difference in abundance of the major proteins from each viral segment cannot be readily explained due to a difference in segment-specific mRNA abundance. It has been shown quantitatively that throughout the course of infection the amount of each type of segment-specific RNA (vRNA, mRNA, and cRNA) remain relatively the same [92]. Furthermore, ribosome profiling methods looking at the occupancy of ribosomes along both host and IAV mRNAs do not show any significant difference [93]. This suggests viral mRNAs are not translated better or worse than host mRNAs while further extrapolation might suggest that the same is likely to be true of the 8 viral segments relative to each other. Some contribution to the differences in protein abundance may stem from the length of the transcripts being translated. To elaborate, the transcripts of M1 and NS1 code for ~250 amino acids each, the transcripts for the three polymerase subunits code for ~800 amino acids, and the transcripts of HA, NA, and NP code for ~500 amino acids. While it would clearly take a ribosome less time to translate the M1 and NS1 mRNAs as opposed to the polymerase mRNAs, the difference in translation time does not seem sufficient to explain the exponential differences in protein production measured experimentally [89–91]. If true, then this suggests IAV employs a mechanism to selectively translate mRNAs based on the amount of each protein necessary for successful viral proliferation.

One final hint that the translation of viral mRNAs is specially regulated during IAV infection stems from several experiments looking at the effects of IAV infection on translation initiation factors. Burgui and co-workers first examined how cap-dependent

the translation initiation on viral mRNAs truly was by studying the rates of translation when cells were deficient in the cap-binding protein, eIF4E [94]. In this study two alternative methods were used to inhibit eIF4E's effect in cells: (1) they used rapamycin to stimulate the mTOR pathway, which dephosphorylates the eIF4E binding protein (4E-BP) and enables 4E-BP to prevent eIF4E from binding to eIF4G, or (2) by silencing expression of the eIF4E gene in a cell line using a plasmid that expresses the short hairpin corresponding to position 447 to 465 of eIF4E mRNA. With both methods, when looking at the expression of viral mRNAs during infection, they found that viral protein synthesis was unaffected by the absence of eIF4E while endogenous cellular protein levels were diminished [94]. Other studies have shown that the translation initiation factors eIF4G and PABP1 are actually recognized and bound by the viral NS1 protein [66,82]. Finally, *in vitro* translation studies looking at the effects of protein synthesis in the presence of the NS1 protein have demonstrated a global enhancement in mRNA translation based on translation of reporter mRNAs [84–86]. Altogether, these disparate results all point to some level of regulation by IAV on translation initiation and may be the key to explaining the selective viral translation hinted at by the various proteomics studies mentioned earlier.

My studies into the roles of NS1 and PABP1 in translation initiation will shed light on the role PABP1 plays in initiating translation of influenza mRNAs and further characterize the PABP1 – NS1 interaction to better understand how IAV hijacks host cells and regulates the translation of viral mRNAs.

References

(1) *Molecular Cell Biology*, 4th ed.; Lodish, H. F., Ed.; W.H. Freeman: New York, 2000.

(2) Enard, D.; Cai, L.; Gwennap, C.; Petrov, D. A. Viruses Are a Dominant Driver of Protein Adaptation in Mammals. 25.

(3) Griffiths, D. J. Endogenous Retroviruses in the Human Genome Sequence. 5.

(4) Soygur, B.; Sati, L. The Role of Syncytins in Human Reproduction and Reproductive Organ Cancers. *Reproduction* **2016**, *152* (5), R167–R178. https://doi.org/10.1530/REP-16-0031.

(5) Mi, S.; Lee, X.; Li, X.; Veldman, G. M.; Finnerty, H.; Racie, L.; LaVallie, E.; Tang, X.-Y.; Edouard, P.; Howes, S.; Keith, J. C.; McCoy, J. M. Syncytin Is a Captive Retroviral Envelope Protein Involved in Human Placental Morphogenesis. *Nature* **2000**, *403* (6771), 785–789. https://doi.org/10.1038/35001608.

(6) Dupressoir, A.; Lavialle, C.; Heidmann, T. From Ancestral Infectious Retroviruses to Bona Fide Cellular Genes: Role of the Captured Syncytins in Placentation. *Placenta* **2012**, *33* (9), 663–671. https://doi.org/10.1016/j.placenta.2012.05.005.

(7) Huremović, D. Brief History of Pandemics (Pandemics Throughout History). In *Psychiatry of Pandemics*; Huremović, D., Ed.; Springer International Publishing: Cham, 2019; pp 7–35. https://doi.org/10.1007/978-3-030-15346-5_2.

(8) Sankaran, N.; Weiss, R. A. Viruses: Impact on Science and Society. In *Encyclopedia of Virology*; Elsevier, 2021; pp 671–680. https://doi.org/10.1016/B978-0-12-814515-9.00075-8.

(9) Riedel, S. Edward Jenner and the History of Smallpox and Vaccination. *Bayl. Univ. Med. Cent. Proc.* **2005**, *18* (1), 21–25. https://doi.org/10.1080/08998280.2005.11928028.

(10) Sharp, P. M.; Hahn, B. H. Origins of HIV and the AIDS Pandemic. *Cold Spring Harb. Perspect. Med.* **2011**, *1* (1), a006841–a006841. https://doi.org/10.1101/cshperspect.a006841.

(11) Smith, R. D. Responding to Global Infectious Disease Outbreaks: Lessons from SARS on the Role of Risk Perception, Communication and Management. *Soc. Sci. Med.* **2006**, *63* (12), 3113–3123. https://doi.org/10.1016/j.socscimed.2006.08.004.

(12) Sood, S.; Aggarwal, V.; Aggarwal, D.; Upadhyay, S. K.; Sak, K.; Tuli, H. S.; Kumar, M.; Kumar, J.; Talwar, S. COVID-19 Pandemic: From Molecular Biology, Pathogenesis, Detection, and Treatment to Global Societal Impact. *Curr. Pharmacol. Rep.* **2020**, *6* (5), 212–227. https://doi.org/10.1007/s40495-020-00229-2.

(13) Redding, D. W.; Atkinson, P. M.; Cunningham, A. A.; Lo Iacono, G.; Moses, L. M.; Wood, J. L. N.; Jones, K. E. Impacts of Environmental and Socio-Economic Factors on Emergence and Epidemic Potential of Ebola in Africa. *Nat. Commun.* **2019**, *10* (1), 4531. https://doi.org/10.1038/s41467-019-12499-6.

(14) Potter, C. W. A History of Influenza. *J. Appl. Microbiol.* **2001**, *91* (4), 572–579. https://doi.org/10.1046/j.1365-2672.2001.01492.x.

(15) Forrest, H. L.; Webster, R. G. Perspectives on Influenza Evolution and the Role of Research. *Anim. Health Res. Rev.* **2010**, *11* (1), 3–18. https://doi.org/10.1017/S1466252310000071.

(16) Fuller, T. L.; Gilbert, M.; Martin, V.; Cappelle, J.; Hosseini, P.; Njabo, K. Y.; Abdel Aziz, S.; Xiao, X.; Daszak, P.; Smith, T. B. Predicting Hotspots for Influenza Virus Reassortment. *Emerg. Infect. Dis.* **2013**, *19* (4), 581–588. https://doi.org/10.3201/eid1904.120903.

(17) Krammer, F.; Smith, G. J. D.; Fouchier, R. A. M.; Peiris, M.; Kedzierska, K.; Doherty, P. C.; Palese, P.; Shaw, M. L.; Treanor, J.; Webster, R. G.; García-Sastre, A. Influenza. *Nat. Rev. Dis. Primer* **2018**, *4* (1), 3. https://doi.org/10.1038/s41572-018-0002-y.

(18) Hay, A. J.; Gregory, V.; Douglas, A. R.; Lin, Y. P. The Evolution of Human Influenza Viruses. *Philos. Trans. R. Soc. Lond. B. Biol. Sci.* **2001**, *356* (1416), 1861–1870. https://doi.org/10.1098/rstb.2001.0999.

(19) Uyeki, T. M. High-Risk Groups for Influenza Complications. *JAMA* **2020**, *324* (22), 2334. https://doi.org/10.1001/jama.2020.21869.

(20) Morens, D. M.; Fauci, A. S. The 1918 Influenza Pandemic: Insights for the 21st Century. *J. Infect. Dis.* **2007**, *195* (7), 1018–1028. https://doi.org/10.1086/511989.

(21) Honigsbaum, M. Revisiting the 1957 and 1968 Influenza Pandemics. *The Lancet* **2020**, *395* (10240), 1824–1826. https://doi.org/10.1016/S0140-6736(20)31201-0.

(22) Mena, I.; Nelson, M. I.; Quezada-Monroy, F.; Dutta, J.; Cortes-Fernández, R.; Lara-Puente, J. H.; Castro-Peralta, F.; Cunha, L. F.; Trovão, N. S.; Lozano-Dubernard, B.; Rambaut, A.; van Bakel, H.; García-Sastre, A. Origins of the 2009 H1N1 Influenza Pandemic in Swine in Mexico. *eLife* **2016**, *5*, e16777. https://doi.org/10.7554/eLife.16777.

(23) Ghebrehewet, S.; MacPherson, P.; Ho, A. Influenza. *BMJ* **2016**, i6258. https://doi.org/10.1136/bmj.i6258.

(24) Mertz, D.; Kim, T. H.; Johnstone, J.; Lam, P.-P.; Science, M.; Kuster, S. P.; Fadel, S. A.; Tran, D.; Fernandez, E.; Bhatnagar, N.; Loeb, M. Populations at Risk for Severe or Complicated Influenza Illness: Systematic Review and Meta-Analysis. *BMJ* **2013**, *347* (aug23 1), f5061–f5061. https://doi.org/10.1136/bmj.f5061.

(25) Hadler, J. L.; Yousey-Hindes, K.; Pérez, A.; Anderson, E. J.; Bargsten, M.; Bohm, S. R.; Hill, M.; Hogan, B.; Laidler, M.; Lindegren, M. L.; Lung, K. L.; Mermel, E.; Miller, L.; Morin, C.; Parker, E.; Zansky, S. M.; Chaves, S. S. Influenza-Related Hospitalizations and Poverty Levels — United States, 2010–2012. *MMWR Morb. Mortal. Wkly. Rep.* **2016**, *65* (05), 101–105. https://doi.org/10.15585/mmwr.mm6505a1.

(26) United Nations; Department of Economic and Social Affairs; Population Division. *World Population Prospects Highlights, 2019 Revision Highlights, 2019 Revision*; 2019.

(27) United Nations; Department of Economic and Social Affairs; Population Division. *World Urbanization Prospects: The 2018 Revision*; 2019.

(28) Iuliano, A. D.; Roguski, K. M.; Chang, H. H.; Muscatello, D. J.; Palekar, R.; Tempia, S.; Cohen, C.; Gran, J. M.; Schanzer, D.; Cowling, B. J.; Wu, P.; Kyncl, J.; Ang, L. W.; Park, M.; Redlberger-Fritz, M.; Yu, H.; Espenhain, L.; Krishnan, A.; Emukule, G.; van Asten, L.; Pereira da Silva, S.; Aungkulanon, S.; Buchholz, U.; Widdowson, M.-A.; Bresee, J. S.; Azziz-Baumgartner, E.; Cheng, P.-Y.; Dawood, F.; Foppa, I.; Olsen, S.; Haber, M.; Jeffers, C.; MacIntyre, C. R.; Newall, A. T.; Wood, J. G.; Kundi, M.; Popow-Kraupp, T.; Ahmed, M.; Rahman, M.; Marinho, F.; Sotomayor Proschle, C. V.; Vergara Mallegas, N.; Luzhao, F.; Sa, L.; Barbosa-Ramírez, J.; Sanchez, D. M.; Gomez, L. A.; Vargas, X. B.; Acosta Herrera, aBetsy; Llanés, M. J.; Fischer, T. K.; Krause, T. G.; Mølbak, K.; Nielsen, J.; Trebbien, R.; Bruno, A.; Ojeda, J.; Ramos, H.; an der Heiden, M.; del Carmen Castillo Signor, L.; Serrano, C. E.; Bhardwaj, R.; Chadha, M.; Narayan, V.; Kosen, S.; Bromberg, M.; Glatman-Freedman, A.; Kaufman, Z.; Arima, Y.; Oishi, K.; Chaves, S.; Nyawanda, B.; Al-Jarallah, R. A.; Kuri-Morales, P. A.; Matus, C. R.; Corona, M. E. J.; Burmaa, A.; Darmaa, O.; Obtel, M.; Cherkaoui, I.; van den Wijngaard, C. C.; van der Hoek, W.; Baker, M.; Bandaranayake, D.; Bissielo, A.; Huang, S.; Lopez, L.; Newbern, C.; Flem, E.; Grøneng, G. M.; Hauge, S.; de Cosío, F. G.; de Moltó, Y.; Castillo, L. M.; Cabello, M. A.; von Horoch, M.; Medina Osis, J.; Machado, A.; Nunes, B.; Rodrigues, A. P.; Rodrigues, E.; Calomfirescu, C.; Lupulescu, E.; Popescu, R.; Popovici, O.; Bogdanovic, D.; Kostic, M.; Lazarevic, K.; Milosevic, Z.; Tiodorovic, B.; Chen, M.; Cutter, J.; Lee, V.; Lin, R.; Ma, S.; Cohen, A. L.; Treurnicht, F.; Kim, W. J.; Delgado-Sanz, C.; de mateo Ontañón, S.; Larrauri, A.; León, I. L.; Vallejo, F.; Born, R.; Junker, C.; Koch, D.;

Chuang, J.-H.; Huang, W.-T.; Kuo, H.-W.; Tsai, Y.-C.; Bundhamcharoen, K.; Chittaganpitch, M.; Green, H. K.; Pebody, R.; Goñi, N.; Chiparelli, H.; Brammer, L.; Mustaquim, D. Estimates of Global Seasonal Influenza-Associated Respiratory Mortality: A Modelling Study. *The Lancet* **2018**, *391* (10127), 1285–1300. https://doi.org/10.1016/S0140-6736(17)33293-2.

(29) Molinari, N.-A. M.; Ortega-Sanchez, I. R.; Messonnier, M. L.; Thompson, W. W.; Wortley, P. M.; Weintraub, E.; Bridges, C. B. The Annual Impact of Seasonal Influenza in the US: Measuring Disease Burden and Costs. *Vaccine* **2007**, *25* (27), 5086–5096. https://doi.org/10.1016/j.vaccine.2007.03.046.

(30) Influenza Virus. *Transfus. Med. Hemotherapy* **2009**, *36* (1), 32–39. https://doi.org/10.1159/000197314.

(31) Chou, Y. -y.; Vafabakhsh, R.; Doganay, S.; Gao, Q.; Ha, T.; Palese, P. One Influenza Virus Particle Packages Eight Unique Viral RNAs as Shown by FISH Analysis. *Proc. Natl. Acad. Sci.* **2012**, *109* (23), 9101–9106. https://doi.org/10.1073/pnas.1206069109.

(32) Sha, B.; Luo, M. Structure of a Bifunctional Membrane-RNA Binding Protein, Influenza Virus Matrix Protein M1. *Nat. Struct. Biol.* **1997**, *4* (3), 239–244. https://doi.org/10.1038/nsb0397-239.

(33) *Textbook of Influenza*, 2nd edition.; Webster, R. G., Braciale, T. J., Monto, A. S., Lamb, R. A., Eds.; Wiley-Blackwell: Chichester, West Sussex, UK ; Hoboken, NJ, 2013.

(34) Sikora, D.; Rocheleau, L.; Brown, E. G.; Pelchat, M. Deep Sequencing Reveals the Eight Facets of the Influenza A/HongKong/1/1968 (H3N2) Virus Cap-Snatching Process. *Sci. Rep.* **2015**, *4* (1), 6181. https://doi.org/10.1038/srep06181.

(35) Sikora, D.; Rocheleau, L.; Brown, E. G.; Pelchat, M. Influenza A Virus Cap-Snatches Host RNAs Based on Their Abundance Early after Infection. *Virology* **2017**, *509*, 167–177. https://doi.org/10.1016/j.virol.2017.06.020.

(36) Gu, W.; Gallagher, G. R.; Dai, W.; Liu, P.; Li, R.; Trombly, M. I.; Gammon, D. B.; Mello, C. C.; Wang, J. P.; Finberg, R. W. Influenza A Virus Preferentially Snatches Noncoding RNA Caps. *RNA* **2015**, *21* (12), 2067–2075. https://doi.org/10.1261/rna.054221.115.

(37) Koppstein, D.; Ashour, J.; Bartel, D. P. Sequencing the Cap-Snatching Repertoire of H1N1 Influenza Provides Insight into the Mechanism of Viral Transcription Initiation. *Nucleic Acids Res.* **2015**, *43* (10), 5052–5064. https://doi.org/10.1093/nar/gkv333.

(38) Poon, L. L. M.; Pritlove, D. C.; Fodor, E.; Brownlee, G. G. Direct Evidence That the Poly(A) Tail of Influenza A Virus MRNA Is Synthesized by Reiterative Copying of a U Track in the Virion RNA Template. *J. Virol.* **1999**, *73* (4), 3473–3476. https://doi.org/10.1128/JVI.73.4.3473-3476.1999.

(39) te Velthuis, A. J. W.; Fodor, E. Influenza Virus RNA Polymerase: Insights into the Mechanisms of Viral RNA Synthesis. *Nat. Rev. Microbiol.* **2016**, *14* (8), 479–493. https://doi.org/10.1038/nrmicro.2016.87.

(40) Plotch, S. J.; Krug, R. M. Influenza Virion Transcriptase: Synthesis in Vitro of Large, Polyadenylic Acid-Containing Complementary RNA. *J. Virol.* **1977**, *21* (1), 24–34. https://doi.org/10.1128/JVI.21.1.24-34.1977.

(41) Rambaut, A.; Pybus, O. G.; Nelson, M. I.; Viboud, C.; Taubenberger, J. K.; Holmes, E. C. The Genomic and Epidemiological Dynamics of Human Influenza A Virus. *Nature* **2008**, *453* (7195), 615–619. https://doi.org/10.1038/nature06945.

(42) Chen, R.; Holmes, E. C. Avian Influenza Virus Exhibits Rapid Evolutionary Dynamics. *Mol. Biol. Evol.* **2006**, *23* (12), 2336–2341. https://doi.org/10.1093/molbev/msl102.

(43) Görlach, M.; Burd, C. G.; Dreyfuss, G. The MRNA Poly(A)-Binding Protein: Localization, Abundance, and RNA-Binding Specificity. *Exp. Cell Res.* **1994**, *211* (2), 400–407. https://doi.org/10.1006/excr.1994.1104.

(44) Sachs, A. B.; Davis, R. W.; Kornberg, R. D. A Single Domain of Yeast Poly(A)-Binding Protein Is Necessary and Sufficient for RNA Binding and Cell Viability. *Mol. Cell. Biol.* **1987**, *7* (9), 3268–3276. https://doi.org/10.1128/mcb.7.9.3268.

(45) Kühn, U.; Pieler, T. Xenopus Poly(A) Binding Protein: Functional Domains in RNA Binding and Protein-Protein Interaction. *J. Mol. Biol.* **1996**, *256* (1), 20–30. https://doi.org/10.1006/jmbi.1996.0065.

(46) Niedzwiecka, A.; Marcotrigiano, J.; Stepinski, J.; Jankowska-Anyszka, M.; Wyslouch-Cieszynska, A.; Dadlez, M.; Gingras, A.-C.; Mak, P.; Darzynkiewicz, E.; Sonenberg, N.; Burley, S. K.; Stolarski, R. Biophysical Studies of EIF4E Cap-Binding Protein: Recognition of MRNA 5′ Cap Structure and Synthetic Fragments of EIF4G and 4E-BP1 Proteins. *J. Mol. Biol.* **2002**, *319* (3), 615–635. https://doi.org/10.1016/S0022-2836(02)00328-5.

(47) Vicens, Q.; Kieft, J. S.; Rissland, O. S. Revisiting the Closed-Loop Model and the Nature of MRNA 5′–3′ Communication. *Mol. Cell* **2018**, *72* (5), 805–812. https://doi.org/10.1016/j.molcel.2018.10.047.

(48) Goss, D. J.; Kleiman, F. E. Poly(A) Binding Proteins—Are They All Created Equal? **2014**, 17.

(49) Eliseeva, I. A.; Lyabin, D. N.; Ovchinnikov, L. P. Poly(A)-Binding Proteins: Structure, Domain Organization, and Activity Regulation. *Biochem. Mosc.* **2013**, *78* (13), 1377–1391. https://doi.org/10.1134/S0006297913130014.

(50) de Melo Neto, O. P.; Standart, N.; de Sa, C. M. Autoregulation of Poly(A)-Binding Protein Synthesis *in Vitro*. *Nucleic Acids Res.* **1995**, *23* (12), 2198–2205. https://doi.org/10.1093/nar/23.12.2198.

(51) Wu, J.; Bag, J. Negative Control of the Poly(A)-Binding Protein MRNA Translation Is Mediated by the Adenine-Rich Region of Its 5′-Untranslated Region. *J. Biol. Chem.* **1998**, *273* (51), 34535–34542. https://doi.org/10.1074/jbc.273.51.34535.

(52) Bag, J.; Wu, J. Translational Control of Poly(A)-Binding Protein Expression. *Eur. J. Biochem.* **1996**, *237* (1), 143–152. https://doi.org/10.1111/j.1432-1033.1996.0143n.x.

(53) Kahvejian, A.; Svitkin, Y. V.; Sukarieh, R.; M'Boutchou, M.-N.; Sonenberg, N. Mammalian Poly(A)-Binding Protein Is a Eukaryotic Translation Initiation Factor, Which Acts via Multiple Mechanisms. *Genes Dev.* **2005**, *19* (1), 104–113. https://doi.org/10.1101/gad.1262905.

(54) Sladic, R. T.; Lagnado, C. A.; Bagley, C. J.; Goodall, G. J. Human PABP Binds AU-Rich RNA via RNA-Binding Domains 3 and 4. *Eur. J. Biochem.* **2004**, *271* (2), 450–457. https://doi.org/10.1046/j.1432-1033.2003.03945.x.

(55) Erdős, G.; Dosztányi, Z. Analyzing Protein Disorder with IUPred2A. *Curr. Protoc. Bioinforma.* **2020**, *70* (1). https://doi.org/10.1002/cpbi.99.

(56) Mészáros, B.; Erdős, G.; Dosztányi, Z. IUPred2A: Context-Dependent Prediction of Protein Disorder as a Function of Redox State and Protein Binding. *Nucleic Acids Res.* **2018**, *46* (W1), W329–W337. https://doi.org/10.1093/nar/gky384.

(57) Sawazaki, R.; Imai, S.; Yokogawa, M.; Hosoda, N.; Hoshino, S.; Mio, M.; Mio, K.; Shimada, I.; Osawa, M. Characterization of the Multimeric Structure of Poly(A)-Binding Protein on a Poly(A) Tail. *Sci. Rep.* **2018**, *8* (1), 1455. https://doi.org/10.1038/s41598-018-19659-6.

(58) Lima, S. A.; Chipman, L. B.; Nicholson, A. L.; Chen, Y.-H.; Yee, B. A.; Yeo, G. W.; Coller, J.; Pasquinelli, A. E. Short Poly(A) Tails Are a Conserved Feature of Highly Expressed Genes. *Nat. Struct. Mol. Biol.* **2017**, *24* (12), 1057–1063. https://doi.org/10.1038/nsmb.3499.

(59) Burd, C. G.; Matunis, E. L.; Dreyfuss, G. The Multiple RNA-Binding Domains of the MRNA Poly(A)-Binding Protein Have Different RNA-Binding Activities. *Mol. Cell. Biol.* **1991**, *11* (7), 3419–3424. https://doi.org/10.1128/MCB.11.7.3419.

(60) Arias-Mireles, B. H.; de Rozieres, C. M.; Ly, K.; Joseph, S. RNA Modulates the Interaction between Influenza A Virus NS1 and Human PABP1. *Biochemistry* **2018**, *57* (26), 3590–3598. https://doi.org/10.1021/acs.biochem.8b00218.

(61) Safaee, N.; Kozlov, G.; Noronha, A. M.; Xie, J.; Wilds, C. J.; Gehring, K. Interdomain Allostery Promotes Assembly of the Poly(A) MRNA Complex with PABP and EIF4G. *Mol. Cell* **2012**, *48* (3), 375–386. https://doi.org/10.1016/j.molcel.2012.09.001.

(62) Kini, H. K.; Silverman, I. M.; Ji, X.; Gregory, B. D.; Liebhaber, S. A. Cytoplasmic Poly(A) Binding Protein-1 Binds to Genomically Encoded Sequences within Mammalian MRNAs. *RNA* **2016**, *22* (1), 61–74. https://doi.org/10.1261/rna.053447.115.

(63) Gilbert, W. V.; Zhou, K.; Butler, T. K.; Doudna, J. A. Cap-Independent Translation Is Required for Starvation-Induced Differentiation in Yeast. *Science* **2007**, *317* (5842), 1224–1227. https://doi.org/10.1126/science.1144467.

(64) Smith, R. W. P.; Anderson, R. C.; Larralde, O.; Smith, J. W. S.; Gorgoni, B.; Richardson, W. A.; Malik, P.; Graham, S. V.; Gray, N. K. Viral and Cellular MRNA-Specific Activators Harness PABP and EIF4G to Promote Translation Initiation Downstream of Cap Binding. *Proc. Natl. Acad. Sci.* **2017**, *114* (24), 6310–6315. https://doi.org/10.1073/pnas.1610417114.

(65) Smith, R. W. P.; Gray, N. K. Poly(A)-Binding Protein (PABP): A Common Viral Target. *Biochem. J.* **2010**, *426* (1), 1–12. https://doi.org/10.1042/BJ20091571.

(66) Burgui, I.; Aragón, T.; Ortín, J.; Nieto, A. PABP1 and EIF4GI Associate with Influenza Virus NS1 Protein in Viral MRNA Translation Initiation Complexes. *J. Gen. Virol.* **2003**, *84* (12), 3263–3274. https://doi.org/10.1099/vir.0.19487-0.

(67) Bier, K.; York, A.; Fodor, E. Cellular Cap-Binding Proteins Associate with Influenza Virus MRNAs. *J. Gen. Virol.* **2011**, *92* (7), 1627–1634. https://doi.org/10.1099/vir.0.029231-0.

(68) Richt, J. A.; García-Sastre, A. Attenuated Influenza Virus Vaccines with Modified NS1 Proteins. In *Vaccines for Pandemic Influenza*; Compans, R. W., Orenstein, W. A., Eds.; Current Topics in Microbiology and Immunology; Springer Berlin Heidelberg: Berlin, Heidelberg, 2009; Vol. 333, pp 177–195. https://doi.org/10.1007/978-3-540-92165-3_9.

(69) Marcus, P. I.; Sekellick, M. J. Interferon Induction by Viruses XIII. Detection and Assay of Interferon Induction-Suppressing Particles. *Virology* **1985**, *142* (2), 411–415. https://doi.org/10.1016/0042-6822(85)90349-6.

(70) Ayllon, J.; García-Sastre, A. The NS1 Protein: A Multitasking Virulence Factor. In *Influenza Pathogenesis and Control - Volume II*; Oldstone, M. B. A., Compans, R. W., Eds.; Current Topics in Microbiology and Immunology; Springer International Publishing: Cham, 2014; Vol. 386, pp 73–107. https://doi.org/10.1007/82_2014_400.

(71) Schierhorn, K. L.; Jolmes, F.; Bespalowa, J.; Saenger, S.; Peteranderl, C.; Dzieciolowski, J.; Mielke, M.; Budt, M.; Pleschka, S.; Herrmann, A.; Herold, S.; Wolff, T. Influenza A Virus Virulence Depends on Two Amino Acids in the N-Terminal Domain of Its NS1 Protein To Facilitate Inhibition of the RNA-Dependent Protein Kinase PKR. *J. Virol.* **2017**, *91* (10), e00198-17, e00198-17. https://doi.org/10.1128/JVI.00198-17.

(72) Hale, B. G.; Kerry, P. S.; Jackson, D.; Precious, B. L.; Gray, A.; Killip, M. J.; Randall, R. E.; Russell, R. J. Structural Insights into Phosphoinositide 3-Kinase Activation by the Influenza A Virus NS1 Protein. *Proc. Natl. Acad. Sci.* **2010**, *107* (5), 1954–1959. https://doi.org/10.1073/pnas.0910715107.

(73) Shapira, S. D.; Gat-Viks, I.; Shum, B. O. V.; Dricot, A.; de Grace, M. M.; Wu, L.; Gupta, P. B.; Hao, T.; Silver, S. J.; Root, D. E.; Hill, D. E.; Regev, A.; Hacohen, N. A Physical and Regulatory Map of Host-Influenza Interactions Reveals Pathways in H1N1 Infection. *Cell* **2009**, *139* (7), 1255–1267. https://doi.org/10.1016/j.cell.2009.12.018.

(74) de Chassey, B.; Aublin-Gex, A.; Ruggieri, A.; Meyniel-Schicklin, L.; Pradezynski, F.; Davoust, N.; Chantier, T.; Tafforeau, L.; Mangeot, P.-E.; Ciancia, C.; Perrin-Cocon, L.; Bartenschlager, R.; André, P.; Lotteau, V. The Interactomes of Influenza Virus NS1 and NS2 Proteins Identify New Host Factors and Provide Insights for ADAR1 Playing a Supportive Role in Virus Replication. *PLoS Pathog.* **2013**, *9* (7), e1003440. https://doi.org/10.1371/journal.ppat.1003440.

(75) Wang, W.; Riedel, K.; Lynch, P.; Chien, C.-Y.; Montelione, G. T.; Krug, R. M. RNA Binding by the Novel Helical Domain of the Influenza Virus NS1 Protein Requires Its Dimer Structure and a Small Number of Specific Basic Amino Acids. *RNA* **1999**, *5* (2), 195–205. https://doi.org/10.1017/S1355838299981621.

(76) Carrillo, B.; Choi, J.-M.; Bornholdt, Z. A.; Sankaran, B.; Rice, A. P.; Prasad, B. V. V. The Influenza A Virus Protein NS1 Displays Structural Polymorphism. *J. Virol.* **2014**, *88* (8), 4113–4122. https://doi.org/10.1128/JVI.03692-13.

(77) Hale, B. G. Conformational Plasticity of the Influenza A Virus NS1 Protein. *J. Gen. Virol.* **2014**, *95* (10), 2099–2105. https://doi.org/10.1099/vir.0.066282-0.

(78) Xia, S.; Robertus, J. D. X-Ray Structures of NS1 Effector Domain Mutants. *Arch. Biochem. Biophys.* **2010**, *494* (2), 198–204. https://doi.org/10.1016/j.abb.2009.12.008.

(79) Bornholdt, Z. A.; Prasad, B. V. V. X-Ray Structure of Influenza Virus NS1 Effector Domain. *Nat. Struct. Mol. Biol.* **2006**, *13* (6), 559–560. https://doi.org/10.1038/nsmb1099.

(80) Nemeroff, M. E.; Qian, X. Y.; Krug, R. M. The Influenza Virus NS1 Protein Forms Multimers in Vitro and in Vivo. *Virology* **1995**, *212* (2), 422–428. https://doi.org/10.1006/viro.1995.1499.

(81) Abdelwhab, E.-S. M.; Veits, J.; Breithaupt, A.; Gohrbandt, S.; Ziller, M.; Teifke, J. P.; Stech, J.; Mettenleiter, T. C. Prevalence of the C-Terminal Truncations of NS1 in Avian Influenza A Viruses and Effect on Virulence and Replication of a Highly Pathogenic H7N1 Virus in Chickens. *Virulence* **2016**, *7* (5), 546–557. https://doi.org/10.1080/21505594.2016.1159367.

(82) Aragón, T.; de la Luna, S.; Novoa, I.; Carrasco, L.; Ortín, J.; Nieto, A. Eukaryotic Translation Initiation Factor 4GI Is a Cellular Target for NS1 Protein, a Translational Activator of Influenza Virus. *Mol. Cell. Biol.* **2000**, *20* (17), 6259–6268. https://doi.org/10.1128/MCB.20.17.6259-6268.2000.

(83) Thulasi Raman, S. N.; Zhou, Y. Networks of Host Factors That Interact with NS1 Protein of Influenza A Virus. *Front. Microbiol.* **2016**, *7*. https://doi.org/10.3389/fmicb.2016.00654.

(84) Panthu, B.; Terrier, O.; Carron, C.; Traversier, A.; Corbin, A.; Balvay, L.; Lina, B.; Rosa-Calatrava, M.; Ohlmann, T. The NS1 Protein from Influenza Virus Stimulates Translation Initiation by Enhancing Ribosome Recruitment to MRNAs. *J. Mol. Biol.* **2017**, *429* (21), 3334–3352. https://doi.org/10.1016/j.jmb.2017.04.007.

(85) Anastasina, M.; Terenin, I.; Butcher, S. J.; Kainov, D. E. A Technique to Increase Protein Yield in a Rabbit Reticulocyte Lysate Translation System. *BioTechniques* **2014**, *56* (1). https://doi.org/10.2144/000114125.

(86) Kainov, D. E.; Müller, K. H.; Theisen, L. L.; Anastasina, M.; Kaloinen, M.; Muller, C. P. Differential Effects of NS1 Proteins of Human Pandemic H1N1/2009, Avian Highly Pathogenic H5N1, and Low Pathogenic H5N2 Influenza A Viruses on Cellular Pre-MRNA Polyadenylation and MRNA Translation. *J. Biol. Chem.* **2011**, *286* (9), 7239–7247. https://doi.org/10.1074/jbc.M110.203489.

(87) de la Luna, S.; Fortes, P.; Beloso, A.; Ortín, J. Influenza Virus NS1 Protein Enhances the Rate of Translation Initiation of Viral MRNAs. *J. Virol.* **1995**, *69* (4), 2427–2433. https://doi.org/10.1128/JVI.69.4.2427-2433.1995.

(88) Enami, K.; Sato, T. A.; Nakada, S.; Enami, M. Influenza Virus NS1 Protein Stimulates Translation of the Ml Protein. **1994**, *68*, 6.

(89) Shapiro, G. I.; Gurney, T.; Krug, R. M. Influenza Virus Gene Expression: Control Mechanisms at Early and Late Times of Infection and Nuclear-Cytoplasmic Transport of Virus-Specific RNAs. *J. Virol.* **1987**, *61* (3), 764–773. https://doi.org/10.1128/JVI.61.3.764-773.1987.

(90) Bogdanow, B.; Eichelbaum, K.; Sadewasser, A.; Wang, X.; Husic, I.; Paki, K.; Hergeselle, M.; Vetter, B.; Hou, J.; Chen, W.; Wiebusch, L.; Meyer, I. M.; Wolff, T.; Selbach, M. *The Dynamic Proteome of Influenza A Virus Infection Identifies M Segment Splicing as a Host Range Determinant*; preprint; Systems Biology, 2018. https://doi.org/10.1101/438176.

(91) Kummer, S.; Flöttmann, M.; Schwanhäusser, B.; Sieben, C.; Veit, M.; Selbach, M.; Klipp, E.; Herrmann, A. Alteration of Protein Levels during Influenza Virus H1N1 Infection in Host Cells: A Proteomic Survey of Host and Virus Reveals Differential Dynamics. *PLoS ONE* **2014**, *9* (4), e94257. https://doi.org/10.1371/journal.pone.0094257.

(92) Hatada, E.; Hasegawa, M.; Mukaigawa, J.; Shimizu, K.; Fukuda, R. Control of Influenza Virus Gene Expression: Quantitative Analysis of Each Viral RNA Species in Infected Cells. *J. Biochem. (Tokyo)* **1989**, *105* (4), 537–546. https://doi.org/10.1093/oxfordjournals.jbchem.a122702.

(93) Bercovich-Kinori, A.; Tai, J.; Gelbart, I. A.; Shitrit, A.; Ben-Moshe, S.; Drori, Y.; Itzkovitz, S.; Mandelboim, M.; Stern-Ginossar, N. A Systematic View on Influenza Induced Host Shutoff. *eLife* **2016**, *5*, e18311. https://doi.org/10.7554/eLife.18311.

(94) Burgui, I.; Yángüez, E.; Sonenberg, N.; Nieto, A. Influenza Virus MRNA Translation Revisited: Is the EIF4E Cap-Binding Factor Required for Viral MRNA Translation? *J. Virol.* **2007**, *81* (22), 12427–12438. https://doi.org/10.1128/JVI.01105-07.

Chapter 2: PABP1 Drives the Selective Translation of Influenza A Virus mRNA

Abstract

Influenza A virus (IAV) is a human infecting pathogen with a history of causing seasonal epidemics and on several occasion worldwide pandemics. Infection by IAV causes a dramatic decrease in host mRNA translation, whereas viral mRNAs are efficiently translated. The IAV mRNAs have a highly conserved 5'-untranslated region (5'UTR) that is rich in adenosine residues. We show that the human polyadenylate binding protein 1 (PABP1) binds to the 5'UTR of the viral mRNAs. The interaction of PABP1 with the viral 5'UTR makes the translation of viral mRNAs more resistant to canonical cap-dependent translation inhibition. Additionally, PABP1 bound to the viral 5'UTR can recruit eIF4G in an eIF4E-independent manner. These results indicate that PABP1 bound to the viral 5'UTR may function as an IRES to promote eIF4E-independent translation initiation.

Introduction

Influenza A virus (IAV) is a zoonotic pathogen capable of infecting the epithelial cells of the upper respiratory tract in humans. Infection by IAV can lead to acute respiratory distress such as coughing, sneezing and even pneumonia and be fatal to those that are most vulnerable in our society [1]. Seasonal influenza is the cause for an estimated 350,000 deaths worldwide each year while IAV pandemics have been known to cause millions of deaths on several occasions in the past century [2,3]. An estimated economic burden of $10.4 billion for direct medical costs and $87.1 billion for the total economic impact per year has been attributed to IAV in the United States alone [4]. These reasons among others make IAV an important subject for research into the mechanisms of infection and viral proliferation to better defend the global community from this disease.

A hallmark of efficient viral infection and proliferation is the ability to direct host resources and cellular machinery towards the production of new virions. Much of our understanding of how cells operate stem from how viruses modulate specific signaling pathways and host proteins. One of the most important mechanisms that a virus must influence is that of mRNA translation, since it is only through viral protein production that more viruses can be made. Host mRNAs have a 7-methyl guanosine cap structure (m^7G cap) at the 5'-end and a 3' poly adenosine tail sequence. The m^7G cap is recognized by the eukaryotic initiation factor 4E (eIF4E) while the poly A tail is bound by multiple polyadenylate binding proteins (PABP1) [5,6]. With both ends of the mRNA bound, subsequent initiation factors can assemble on the mRNA including the

eukaryotic initiation factor 4G (eIF4G) that leads to the eventual recruitment of the 40S and 60S ribosomal subunits necessary for translating the mRNA sequence into a protein [5,6].

IAV has evolved its own mechanism to best take advantage of the translation mechanism in host cells. During the course of infection, IAV will release its eight segmented (-)-sense RNAs into the host cell which enter the nucleus. In the nucleus, the viral polymerase subunits bound to each RNA will begin to cleave off the first dozen or so nucleotides of host mRNAs, which include the 5'-m^{7}G cap [7–11]. This cap snatched sequence then serves as a primer to synthesize the (+)-sense mRNA and a final stuttering event on a poly(U) stretch allows for the synthesis of a 3' poly(A) tail [12]. The viral mRNAs are then exported to the cytoplasm where they are believed to be translated in the canonical cap-dependent manner like host mRNAs.

While cap-dependent translation of viral mRNA seems to be the primary method for IAV protein synthesis, there exists some gaps in our understanding regarding the temporal translation of viral mRNA that cannot be explained solely by this mechanism. Firstly, measurements of host versus viral mRNA levels during the course of viral infection have shown that during peak infection the mRNA pool in the cell will contain roughly a little more than 50% viral mRNA relative to host mRNA [13]. Contrary to this however, are the findings that during peak infection the cell will produce 100 to 1000 fold more viral proteins compared to only a roughly 10 fold decrease in host protein production [14]. Additionally, the major proteins coded by each viral segment are also known to be synthesized at different levels while viral mRNA levels are fairly equal throughout infection [15,16]. The disparity in protein synthesis cannot be explained simply

by differences in translation efficiency, since ribosome profiling show no difference in translation rates of the mRNAs [13]. Furthermore, it has been suggested that IAV infection will stimulate the mTOR pathway and activate the 4E binding proteins (4EBP) which can sequester eIF4E, in a similar fashion, as found in the case of poliovirus and encephalomyocarditis virus (EMCV) infection [17]. Sequestration of eIF4E by 4EBP prevents the association between eIF4E and eIF4G, thus halting canonical cap-dependent translation initiation. This suggests the possibility of a selective mechanism, whereby viral mRNAs are translated more than host mRNAs in a manner that can be independent of 5' cap recognition by eIF4E.

In this study, we examine the IAV mRNA sequences found across different strains and show that PABP1 binds to the 5'UTR of all eight viral segments. The affinity of PABP1 for the 5'UTR correlates with the level of translation of each individual segment as measured by proteomics studies done by other groups [14,15,18]. We demonstrate using a cell-free protein synthesis system that the translation of reporter mRNAs containing the viral 5'UTR is more resistant to cap-dependent translation inhibition than host mRNAs. We further used immunoprecipitation of PABP1 in IAV infected cells to demonstrate that PABP1 enriches the 5'UTRs of viral mRNAs. We propose that the recognition of the 5'UTR by PABP1 serves, in an IRES-like manner, to recruit eIF4G and the subsequent initiation factors to selectively translate viral mRNAs over those of the host in the infected cell.

Results and Discussion

2.1 5'UTR sequence is conserved across most IAV strains.

To better understand the mechanism by which IAV mRNA are so highly translated, we began by analyzing the sequence identity and conservation of the 5'UTRs of each of the eight segments across several strains. To do so, we analyzed all unique IAV sequences that are present in the Influenza Research Database (www.fludb.org) whose sequences begin with the universally conserved sequence: 5'-AGCRAAAGC-3'. The database provided roughly 1000 – 4000 unique sequences for each viral segment. These sequences were separated by the 5'UTR length up to the AUG start codon and conservation was analyzed by LOGO **(Figure 2.1A)** [19,20]. The results exhibited a significant degree of conservation across the vast majority of IAV strains for each individual segment [21]. In the few cases where a nucleotide was not fully conserved, the alternative possible nucleotides were usually consistent as either a purine or a pyrimidine. Furthermore, the 5'UTRs are notably purine rich, primarily made up of adenines with several segments containing stretches of adenines **(Figure 2.1B)**. Minor populations of specific segments (HA, NP, NA and M1) with varying lengths were also highly conserved and purine rich **(Figure 2.2)**. Mutation rates of IAV are known to be quite high, believed to promote its evolutionary fitness, and yet the high conservation found in the 5'UTRs of each segment suggests an importance to this particular stretch of nucleotides [22–25].

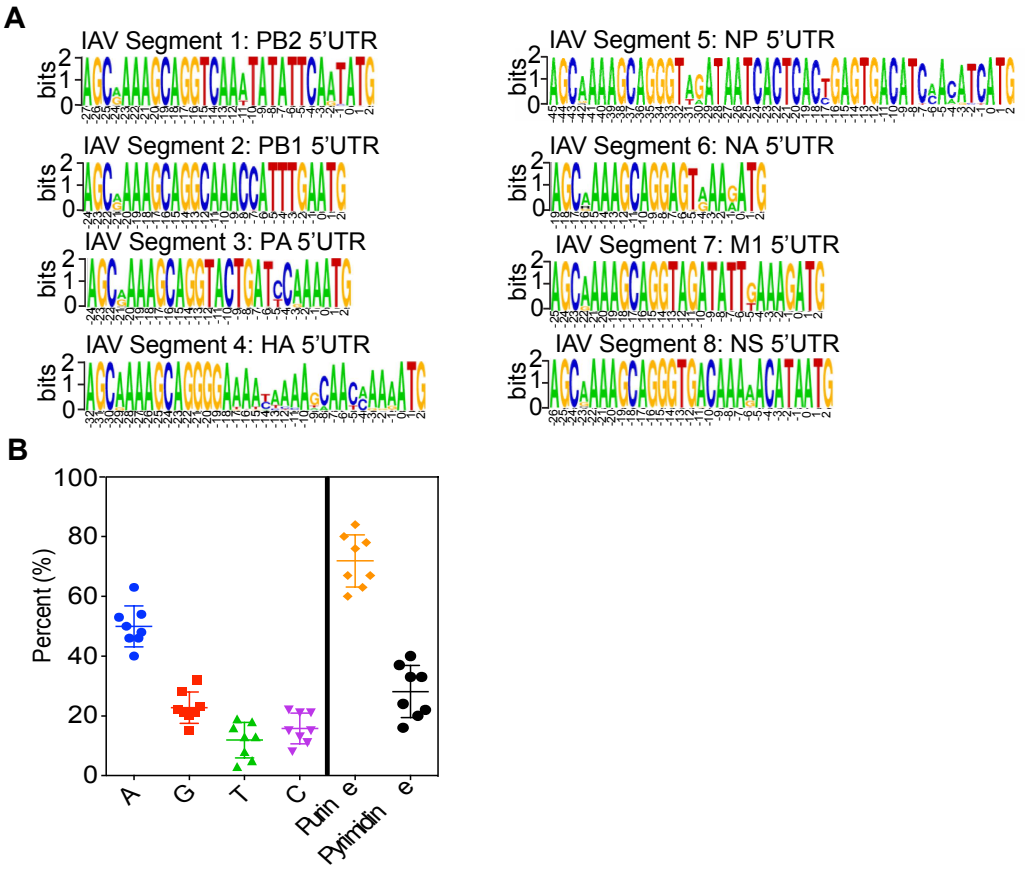

Figure 2.1 IAV 5'UTR Sequence Conservation. (A) LOGO analysis of the eight IAV 5'UTR sections found across strains. Analysis is based on DNA sequencing files and thus the RNA would have an uracil instead of a thymine. For each segment, the last three nucleotides (ATG) correspond to the mRNA start codon. (B) Estimated nucleotide percent representation per IAV 5'UTR. The sum of each individual nucleotide was calculated relative to the total number of nucleotides making up the 5'UTR. In cases where a position had low conservation, the most conserved nucleotide was chosen for that position and used as part of the calculation. The plot is separated based on individual nucleotide or purine versus pyrimidine prevalence.

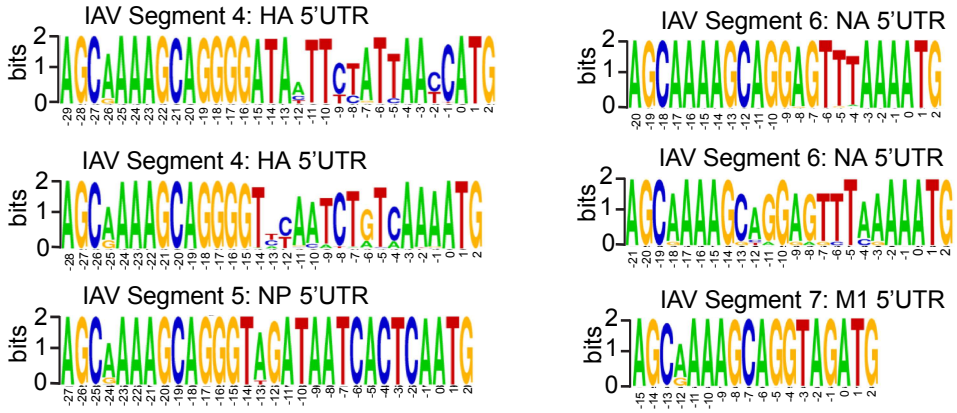

Figure 2.2: IAV 5'UTR Sequence Conservation of minor population. (A) LOGO analysis of several alternative IAV 5'UTR sections found across segments. For the HA segment 35% and 19% of total UTR sequences analyzed were 28 nt and 27 nt respectively. The alternative NP and M1 segments LOGO made up 19% of total sequences. The NA segment had 6% of sequences with 20 nt and 1% with 21 nt. Analysis is based on DNA sequencing files and thus the RNA would have an uracil instead of a thymine.

2.2 PABP1 has a significant affinity for the M1 portion of the 5'UTR.

Given the richness in adenines of these UTR's, we wondered whether PABP1, which is known to bind poly(A) and to a lesser extent poly(G) sequences will bind to the 5'UTR [26–28]. Previous studies have shown that during the cap snatching process the 5'UTR of the M1 segment contains the first 12 nucleotides of the U2 snRNA [8–11]. We were curious therefore, to see how PABP1 would interact with an RNA segment of the M1 5'UTR with or without the cap-snatched sequence. Therefore, we purified recombinant human PABP1 and synthesized the RNA of the M1 5'UTR segment for A/WSN/1933 (H1N1) strain, with and without the U2 snRNA cap-snatched sequence **(Figure 2.3A)**. An EMSA was performed to qualitatively analyze the binding of PABP1 to the M1 5'UTR and control RNAs. We observed a shift of the $Poly(A)_{18}$ RNA and M1 5'UTR with and without the cap-snatch sequence in the presence of PABP1 **(Figure 2.3B)**. PABP1 binds as a monomer and dimer to $Poly(A)_{18}$ RNA, which was resolved by the EMSA [27,29]. A shift was also observed with the U2 snRNA cap-snatch sequence and PABP1, but to a lesser extent. No shift was observed with a single-stranded control RNA (ssCR1) in the presence of PABP1. These results indicate that PABP1 binds to the M1 5'UTR and to a lesser extent to the cap-snatched sequence. We next performed fluorescence anisotropy studies to quantitatively determine the binding affinity of PABP1 for M1 5'UTR. Fluorescence anisotropy studies showed that PABP1 binds to the M1 5'UTR with an equilibrium dissociation constant (K_D) of 86 ± 7 nM, regardless of the presence of the cap snatch sequences **(Figure 2.3C and Table 2.1)**. Despite the affinity being an order of magnitude weaker than PABP1's affinity to poly(A) sequences, the

binding affinity suggest biological relevance given the high concentration (~ 4 μM) of PABP1 found in the cell [30]. Absence of PABP1 binding to other control RNAs demonstrates the specificity it has for the M1 5'UTR sequence **(Figures 2.3C and 2.4 and Table 2.2)**.

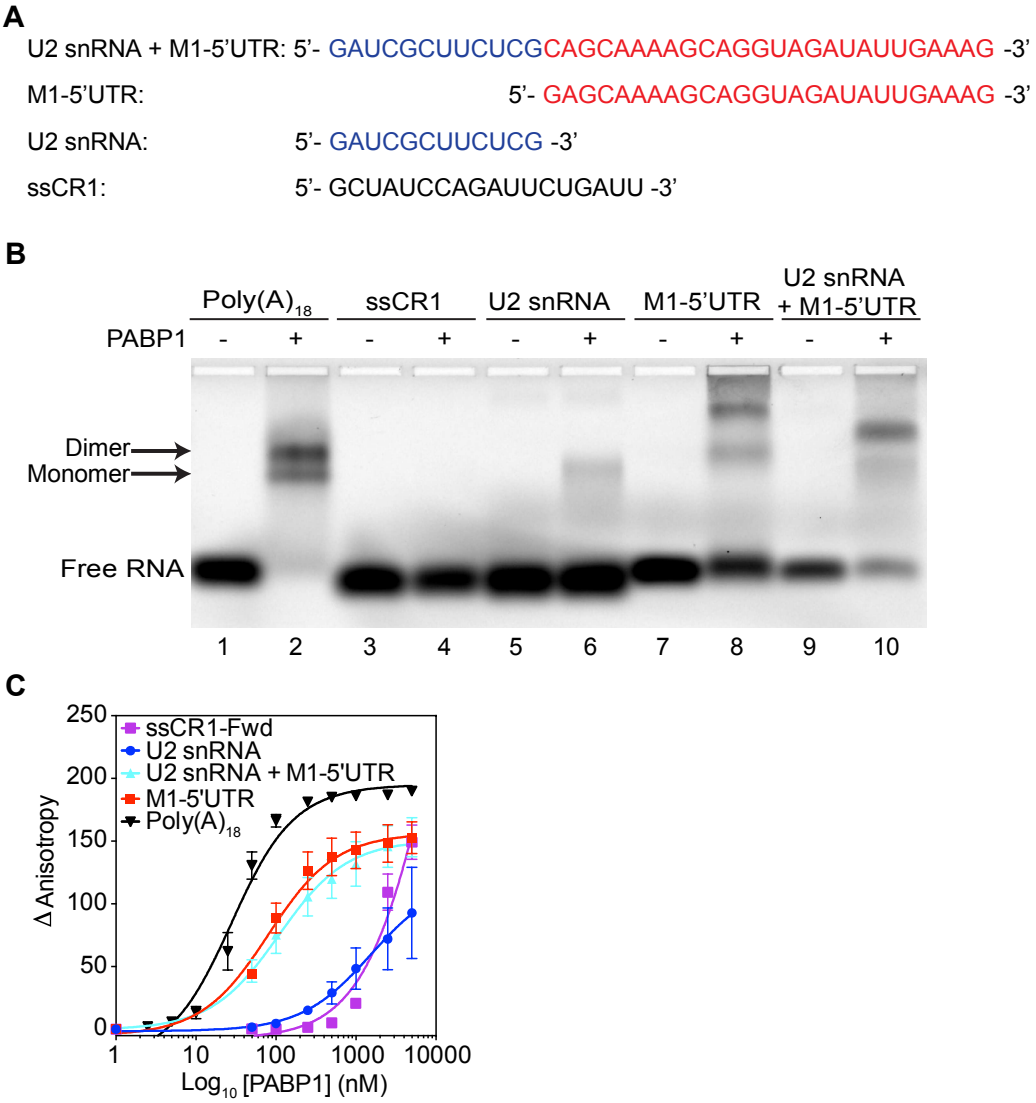

Figure 2.3: PABP1 binds to the 5'UTR of M1 mRNA. (A) The sequences used in the binding studies. The U2 snRNA (blue) and M1-5'UTR (red) sequences are color coded for visual clarity. (B) EMSA assay comparing the binding of PABP1 to the sections that make up the M1 5'UTR RNA and control RNAs. Minus sign indicates no PABP1 was added to the reaction. Arrow points to the shifted PABP1 monomer•Poly(A)$_{18}$ complex and PABP1 dimer•Poly(A)$_{18}$ complex. (C) Anisotropy assay of PABP1 binding to the sections that make up the M1 5'UTR RNA and control RNAs. The final concentration of the RNAs was 10 nM, and the final concentration of PABP1 was increased from 0 to 5 μM. The change in anisotropy is shown on the y-axis. The error bars represent the standard deviation from three independent experiments.

Table 2.1. Equilibrium Dissociation Constants (K_D) for PABP1 binding to the model IAV 5'UTR RNA

Sequence Name	Length (nt)	Sequence	K_D
U2 snRNA + M1-5'UTR	38	5'-GAUCGCUUCUCGCAGCAAAAGCAGGUAGAUAUUGAAAG-3'	106 nM ± 21 nM
U2 snRNA	12	5'-GAUCGCUUCUCG-3'	1519 nM ± 720 nM
M1-5'UTR	26	5'-GAGCAAAAGCAGGUAGAUAUUGAAAG-3'	86 nM ± 7 nM

A

ssIAV:	5'- AGCAAAGCCGG -3'
dsIAV:	5'- AGCAAAGCCGG -3' 3'- UCGUUUCGGCC -5'
ssCR1:	5'- GCUAUCCAGAUUCUGAUU -3'
dsCR1:	5'- GCUAUCCAGAUUCUGAUU -3' 3'- CGAUAGGUCUAAGACUAAG -5'
ssRK1:	5'- CCAUCCUCUACAGGGCG -3'
dsRK1:	5'- CCAUCCUCUACAGGGCG -3' 3'- GGUAGGAGAUGUCCCGC -5'

B

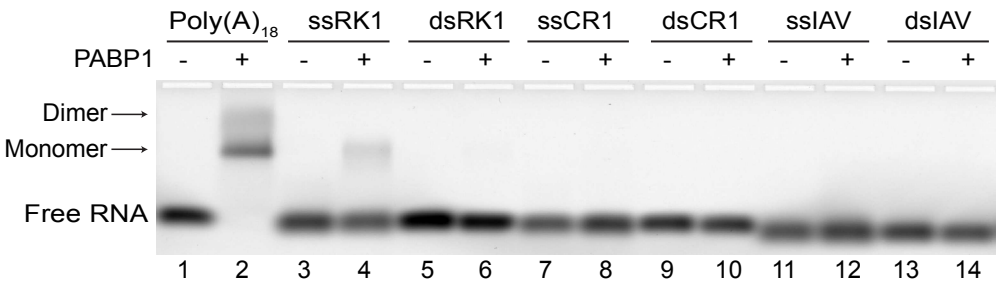

C

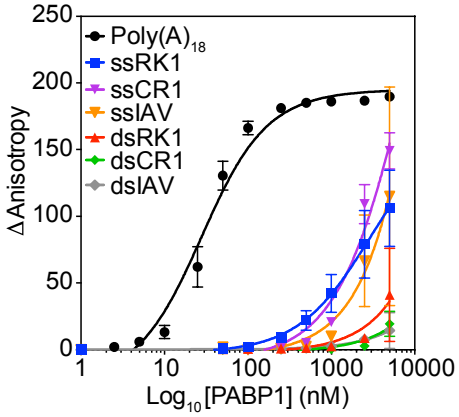

Figure 2.4: PABP1 does not bind to all RNA. (A) The sequences of the RNA used in the binding studies. (B) EMSA assay comparing binding of PABP1 to different control RNA. Minus sign indicates no PABP1 was added to the reaction. Arrow points to the shifted PABP1 monomer•Poly(A)$_{18}$ complex and PABP1 dimer•Poly(A)$_{18}$ complex. (C) Anisotropy assay to analyze the binding of PABP1 to the different control RNAs. The final concentration of the RNAs was 10 nM, and the final concentration of PABP1 was increased from 0 to 5 μM. The change in anisotropy is shown on the y-axis. The error bars represent the standard deviation from three independent experiments.

Table 2.2. Equilibrium Dissociation Constants (K_D) for PABP1 binding to short control RNAs

Sequence Name	Length (nt)	Sequence	K_D
ssIAV	12	5'- AGCAAAAGCCGG -3'	No Binding
dsIAV	12	5'- AGCAAAAGCCGG -3' 3'- UCGUUUUCGUCC -5'	No Binding
ssCR1	18	5'- GCUAUCCAGAUUCUGAUU -3'	9.7 μM ± 4.6 μM
dsCR1	19	5'- GCUAUCCAGAUUCUGAUU -3' 3'- CGAUAGGUCUAAGACUAAG -5'	No Binding
ssRK1	16	5'- CCAUCCUCUACAGGCG -3'	3.0 μM ± 1.5 μM
dsRK1	16	5'- CCAUCCUCUACAGGCG -3' 3'- GGUAGGAGAUGUCCGC -5'	No Binding

2.3 PABP1 has varying affinities for the eight IAV 5'UTRs.

We were curious then to see how PABP1 interacted with the 5'UTRs of the remaining IAV segments of A/WSN/1933 (H1N1). The seven 5'UTR RNAs were synthesized without the cap-snatch sequence and binding to PABP1 was analyzed using EMSA and fluorescence anisotropy. Our studies showed that PABP1 has varying affinities to each IAV 5'UTR ranging from 20 nM up to 1 μM **(Figure 2.5 and Table 2.3)**. Interestingly, the affinities seem to correlate with the expression levels that have been reported of the major proteins measured for these segments. Segments such as HA, NP and M1, whose proteins are required in abundance, have the highest affinities for PABP1 and other segments like PB1 and PA which are translated at lower levels have weaker affinities for PABP1 [14,15,18].

Furthermore, we measured the binding affinity PABP1 has to the eight 5'UTRs of two other human infecting strains used most prevalently in the literature, namely A/Puerto Rico/8/34 (H1N1) and A/Udorn/307/1972 (H3N2) **(Figures 2.6 and 2.7, Tables 2.4 and 2.5)**. We found that while affinities varied for different strain segments, the overall trend remained true that highly expressed segments have a 5'UTR that bind with a high affinity to PABP1.

To test whether PABP1 is recognizing the sequence or the structure of the RNA, we took the U2 snRNA + M1-5'UTR sequence and mutated different sections looking primarily at how modifying the 5'-AGCAAAAGCA-3' stem loop or the unique conserved sequence of the M1 segment affects the K_D **(Figure 2.8 and Table 2.6)** [31]. We found overall that changes to the conserved sequence unique to the M1 segment had the

greatest effect on the affinity to PABP1 with some influence provided by the stem loop and no change when modifying the cap snatch sequence. This, in addition to the findings that UTRs of the eight different segments have different affinities for PABP1, suggests that the unique UTR sequence is dictating PABP1's binding affinity.

A

A/WSN/1933 (H1N1)

PB2: 5'- GAGCGAAAGCAGGUCAAUUAUAUUCAAU -3'
PB1: 5'- GAGCGAAAGCAGGCAAACCAUUUGA -3'
PA: 5'- GAGCGAAAGCAGGUACUGAUUCAAA -3'
HA: 5'- GAGCAAAAGCAGGGGAAAAUAAAAACAACCAAA -3'
NP: 5'- GAGCAAAAGCAGGGUAGAUAAUCACUCACAGAGUGACAUCGAAAUC -3'
NA: 5'- GAGCGAAAGCAGGAGUUUAA -3'
M1: 5'- GAGCAAAAGCAGGUAGAUAUUGAAAG -3'
NS: 5'- GAGCAAAAGCAGGGUGACAAAGACAUA -3'

B

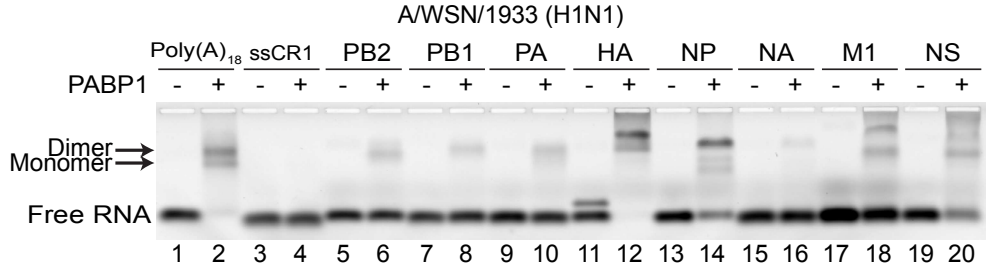

C

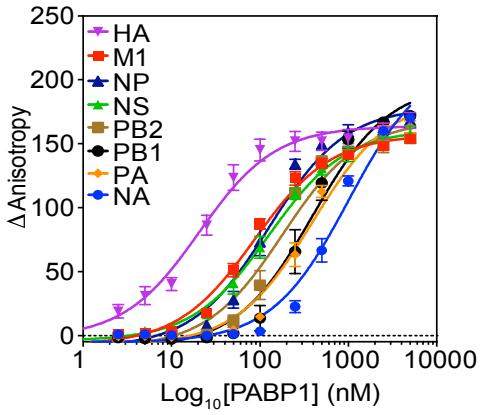

Figure 2.5: PABP1 binds to the 5'UTR of all eight segments of A/WSN/1933 (H1N1) IAV. (A) The sequences of the 5'UTRs of A/WSN/1933 (H1N1) used in the binding studies. (B) EMSA assay comparing the binding of PABP1 to the different 5'UTR RNA of each IAV segment. Minus sign indicates no PABP1 was added to the reaction. Arrow points to the shifted PABP1•Poly(A)$_{18}$ complexes. (C) Anisotropy assay to determine the binding affinity of PABP1 for the different 5'UTR RNA of each IAV segment. The final concentration of the RNAs was 1 nM, and the final concentration of PABP1 was increased from 0 to 5 μM. The change in anisotropy is shown on the y-axis. The error bars represent the standard deviation from three independent experiments.

Table 2.3. Equilibrium Dissociation Constants (K_D) for PABP1 binding to the eight 5'UTR RNA of A/WSN/1933 (H1N1) IAV.

Sequence Name	Length (nt)	A/WSN/1933 (H1N1) 5'UTR Sequence	K_D
PB2 5'UTR	28	5'- GAGCGAAAGCAGGUCAAUUAUAUUCAAU -3'	181 nM ± 26 nM
PB1 5'UTR	25	5'- GAGCGAAAGCAGGCAAACCAUUUGA -3'	394 nM ± 52 nM
PA 5'UTR	25	5'- GAGCGAAAGCAGGUACUGAUUCAAA -3'	395 nM ± 44 nM
HA 5'UTR	33	5'- GAGCAAAAGCAGGGGAAAAUAAAAACAACCAAA -3'	20 nM ± 2 nM
NP 5'UTR	46	5'- GAGCAAAAGCAGGGUAGAUAAUCACUCACAGAGUGACAUCGAAAUC -3'	126 nM ± 14 nM
NA 5'UTR	21	5'- GAGCGAAAGCAGGAGUUUAA -3'	1004 nM ± 122 nM
M1 5'UTR	26	5'- GAGCAAAAGCAGGUAGAUAUUGAAAG -3'	86 nM ± 7 nM
NS 5'UTR	27	5'- GAGCAAAAGCAGGGUGACAAAGACAUA -3'	126 nM ± 9 nM

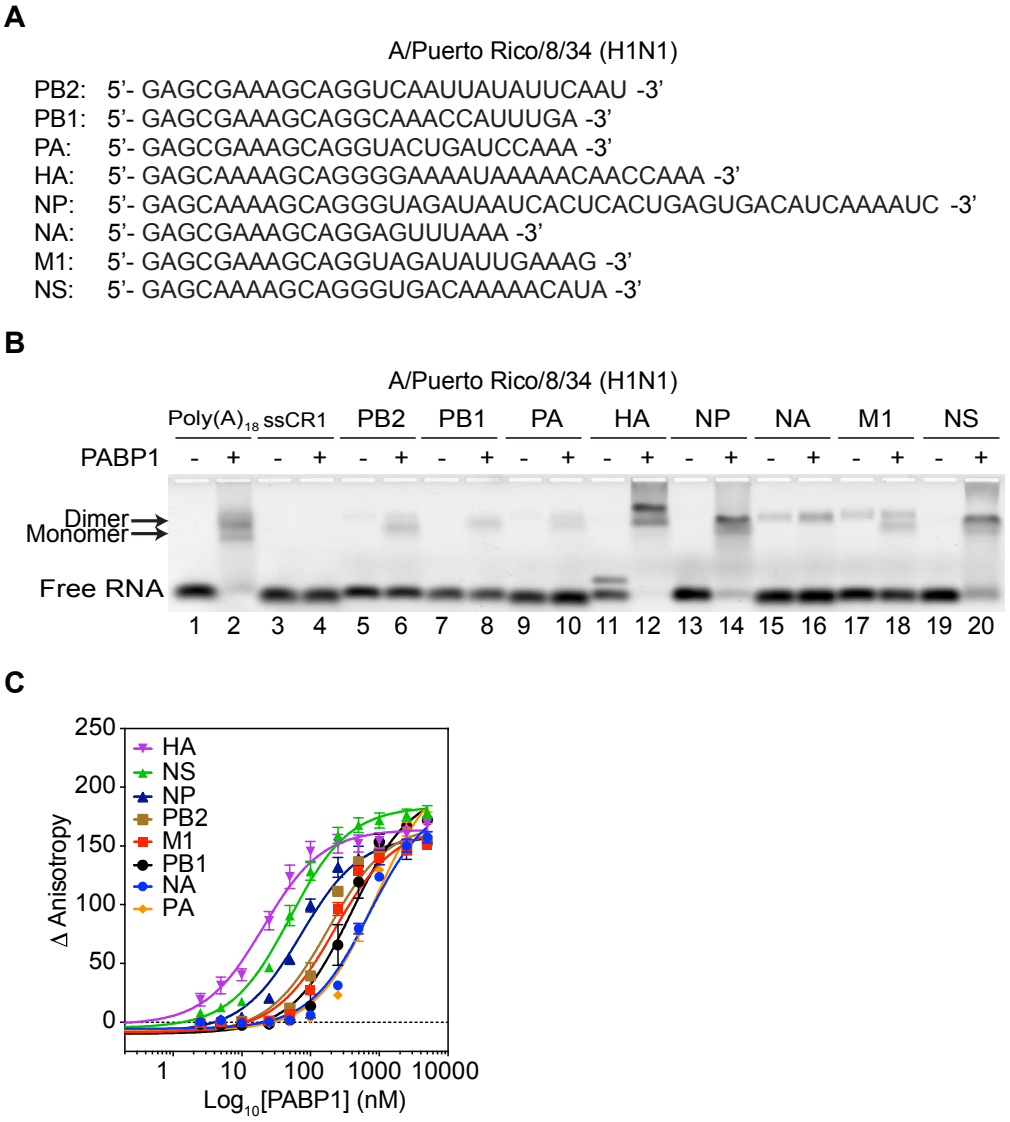

Figure 2.6: PABP1 binds to the 5'UTR of all eight segments of A/Puerto Rico/8/34 (H1N1) IAV. (A) The sequences of the 5'UTRs of A/Puerto Rico/8/34 (H1N1) used in the binding studies. (B) EMSA assay comparing binding of PABP1 to the different 5'UTR RNA of each IAV segment. Minus sign indicates no PABP1 was added to the reaction. Arrow points to the shifted PABP1 monomer•Poly(A)$_{18}$ complex and PABP1 dimer•Poly(A)$_{18}$ complex. (C) Anisotropy assay to determine the binding affinity of PABP1 for the different 5'UTR RNA of each IAV segment. The final concentration of the RNAs was 1 nM, and the final concentration of PABP1 was increased from 0 to 5 μM. The change in anisotropy is shown on the y-axis. The error bars represent the standard deviation from three independent experiments.

Table 2.4. Equilibrium Dissociation Constants (K_D) for PABP1 binding to the eight 5'UTR RNA of A/Puerto Rico/8/34 (H1N1) IAV.

Sequence Name	Length (nt)	A/Puerto Rico/8/34 (H1N1) 5'UTR Sequence	K_D
PB2 5'UTR	28	5'- GAGCGAAAGCAGGUCAAUUAUAUUCAAU -3'	181 nM ± 26 nM
PB1 5'UTR	25	5'- GAGCGAAAGCAGGCAAACCAUUUGA -3'	394 nM ± 53 nM
PA 5'UTR	25	5'- GAGCGAAAGCAGGUACUGAUCCAAA -3'	883 nM ± 114 nM
HA 5'UTR	33	5'- GAGCAAAAGCAGGGGAAAAUAAAAACAACCAAA -3'	20 nM ± 2 nM
NP 5'UTR	46	5'- GAGCAAAAGCAGGGUAGAUAAUCACUCACUGAGUGACAUCAAAAUC -3'	73 nM ± 8 nM
NA 5'UTR	21	5'- GAGCGAAAGCAGGAGUUUAAA -3'	711 nM ± 83 nM
M1 5'UTR	26	5'- GAGCGAAAGCAGGUAGAUAUUGAAAG -3'	224 nM ± 31 nM
NS 5'UTR	27	5'- GAGCAAAAGCAGGGUGACAAAAACAUA -3'	50 nM ± 4 nM

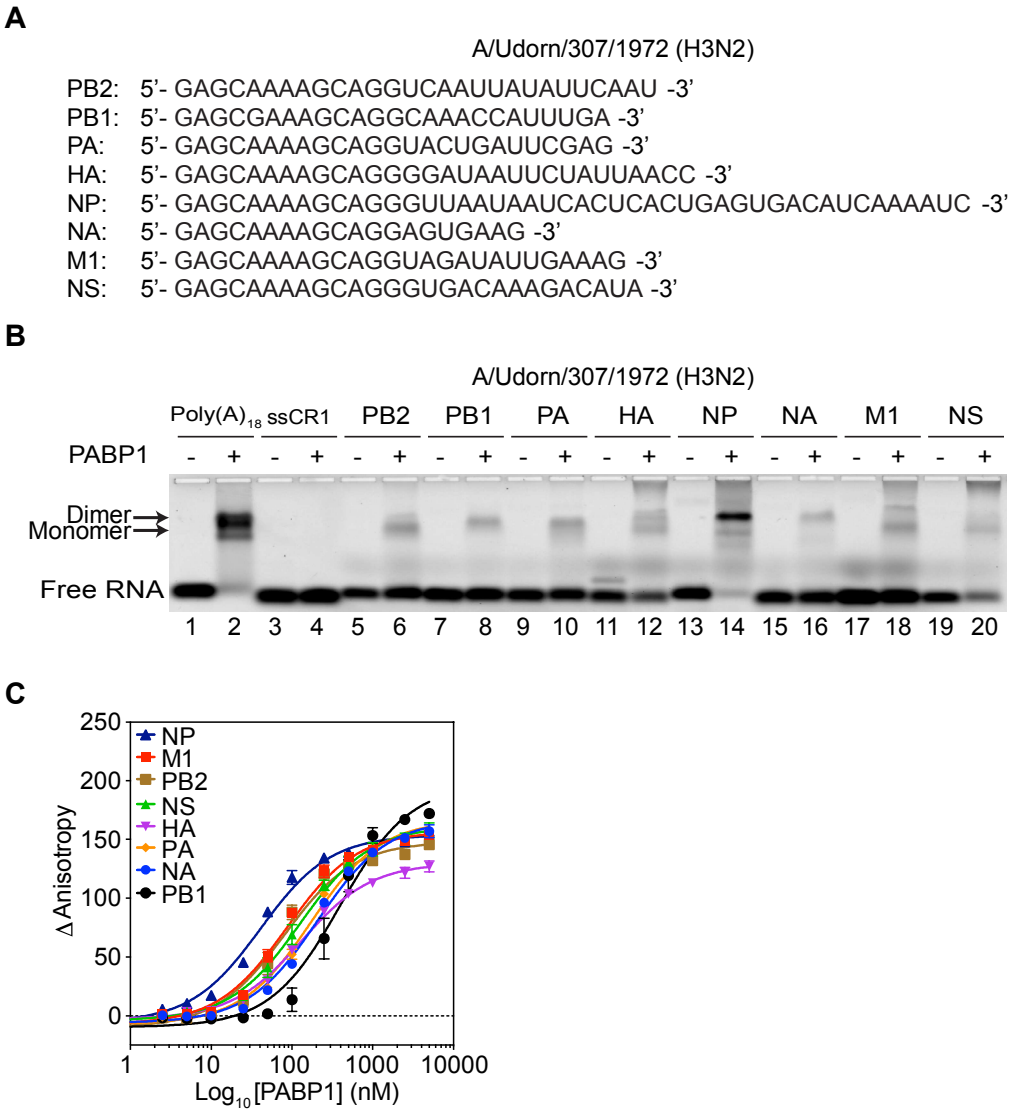

Figure 2.7: PABP1 binds to the 5'UTR of all eight segments of A/Udorn/307/1972 (H3N2) IAV. (A) The sequences of the 5'UTRs of A/Udorn/307/1972 (H3N2) used in the binding studies. (B) EMSA assay comparing binding of PABP1 to the different 5'UTR RNA of each IAV segment. Minus sign indicates no PABP1 was added to the reaction. Arrow points to the shifted PABP1 monomer•Poly(A)$_{18}$ complex and PABP1 dimer•Poly(A)$_{18}$ complex. (C) Anisotropy assay to determine the binding affinity of PABP1 for the different 5'UTR RNA of each IAV segment. The final concentration of the RNAs was 1 nM, and the final concentration of PABP1 was increased from 0 to 5 μM. The change in anisotropy is shown on the y-axis. The error bars represent the standard deviation from three independent experiments.

Table 2.5. Equilibrium Dissociation Constants (K_D) for PABP1 binding to the eight 5'UTR RNA of A/Udorn/307/1972 (H3N2) IAV.

Sequence Name	Length (nt)	A/Udorn/307/1972 (H3N2) 5'UTR Sequence	K_D
PB2 5'UTR	28	5'- GAGCAAAAGCAGGUCAAUUAUAUUCAAU -3'	81 nM ± 9 nM
PB1 5'UTR	25	5'- GAGCGAAAGCAGGCAAACCAUUUGA -3'	394 nM ± 53 nM
PA 5'UTR	25	5'- GAGCAAAAGCAGGUACUGAUUCGAG -3'	171 nM ± 13 nM
HA 5'UTR	30	5'- GAGCAAAAGCAGGGGAUAAUUCUAUUAACC -3'	131 nM ± 7 nM
NP 5'UTR	46	5'- GAGCAAAAGCAGGGUUAAUAAUCACUCACUGAGUGACAUCAAAAUC -3'	40 nM ± 3 nM
NA 5'UTR	20	5'- GAGCAAAAGCAGGAGUGAAG -3'	205 nM ± 14 nM
M1 5'UTR	26	5'- GAGCAAAAGCAGGUAGAUAUUGAAAG -3'	86 nM ± 7 nM
NS 5'UTR	27	5'- GAGCAAAAGCAGGGUGACAAAGACAUA -3'	126 nM ± 9 nM

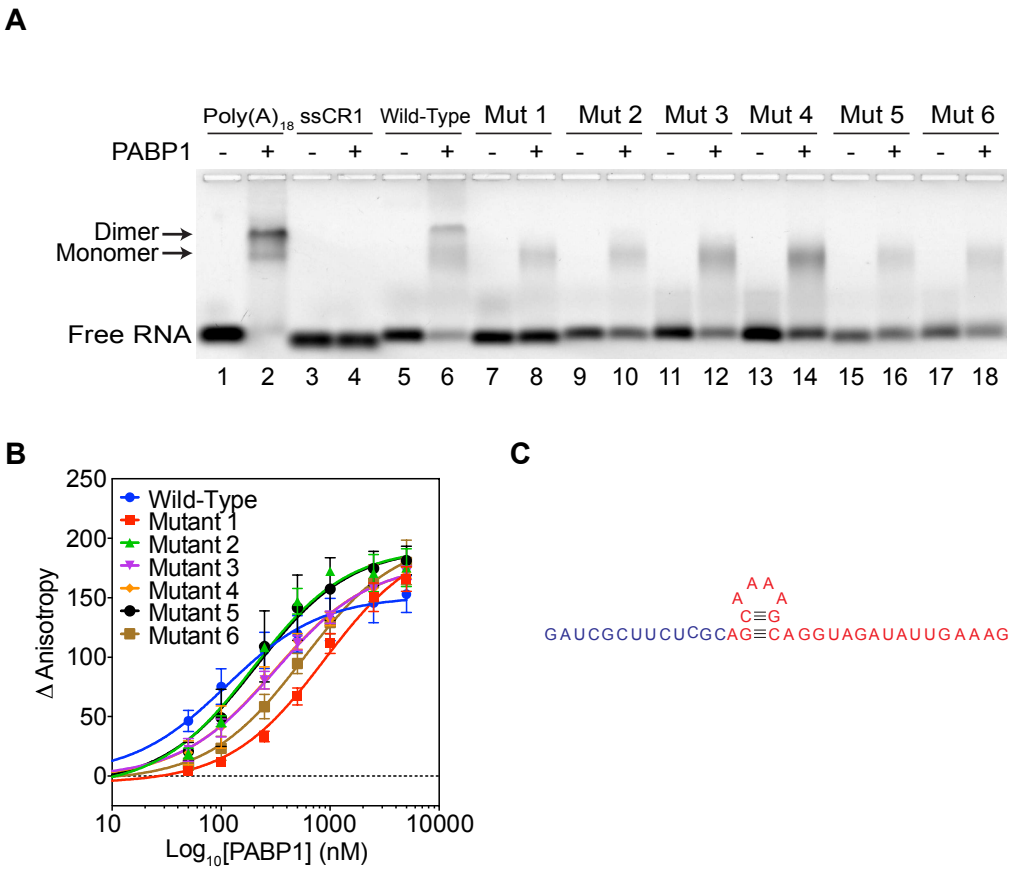

Figure 2.8: Binding of PABP1 to U2 snRNA + M1-5'UTR RNA mutant sequences. (A) EMSA assay comparing binding of PABP1 to different mutants of the U2 snRNA + M1-5'UTR RNA. Minus sign indicates no PABP1 was added to the lane. Arrow points to the shifted PABP1 monomer•Poly(A)$_{18}$ complex and PABP1 dimer•Poly(A)$_{18}$ complex. (B) Anisotropy assay to determine the binding affinity of PABP1 for the different mutants of the U2 snRNA + M1-5'UTR RNA sequence. The final concentration of the RNAs was 1 nM, and the final concentration of PABP1 was increased from 0 to 5 μM. The change in anisotropy is shown on the y-axis. The error bars represent the standard deviation from three independent experiments. (C) Secondary structure prediction of the U2 snRNA + M1-5'UTR sequence with the cap-snatch U2 snRNA in blue and M1-5'UTR in red.

Table 2.6. Equilibrium Dissociation Constants (K_D) for PABP1 binding to the variant U2 snRNA + M1-5'UTR RNA

Sequence Name	Length (nt)	Sequence	K_D
Wild-Type	38	5'- G*AUCGCUUCUCGC*AGCAAAAGCAGGUAGAUAUUGAAAG -3'	106 nM ± 21 nM
Mutant 1	38	5'- G*AUCGCUUCUCGC*AGCAAAAGCA**UCCUCCUCCUCCUCC** -3'	870 nM ± 104 nM
Mutant 2	38	5'- G**UCCUCCUCCU***GC*AGCAAAAGCAGGUAGAUAUUGAAAG -3'	189 nM ± 30 nM
Mutant 3	38	5'- G**UCCUCCUCCU***GC*AGCAAAAGCA**UCCUCCUCCUCCUCC** -3'	309 nM ± 25 nM
Mutant 4	38	5'- G**UCCUCCUCCUCCUCC**AAAA**UCCUCCUCCUCCUCCUCC**- 3'	299 nM ± 34 nM
Mutant 5	38	5'- G*AUCGCUUCUCGC*AGC**CCCC**GCAGGUAGAUAUUGAAAG- 3'	202 nM ± 47 nM
Mutant 6	38	5'- G**UCCUCCUCCUCCUCCCCCCUCCUCCUCCUCCUCCUCC** -3'	554 nM ± 75 nM

[a] The U2 snRNA cap snatched sequence is italicized, the changes in sequence are shown as bold.

2.4 Translation initiation with IAV 5'UTR are resistant to cap-dependent downregulation.

Given the evidence that PABP1 binds to the 5'UTRs with significant affinity, we set out to examine the biological relevance of this binding. We hypothesized that due to PABP1's canonical role of initiating translation by binding to the 3' end, perhaps it could do the same for viral mRNAs from the 5' end. To test this, we took the viral 5'UTR sequences of M1 with and without the cap snatch sequence (shown in Figure 2.2A) and incorporated them upstream of a *Renilla* luciferase coding sequence with a poly(A)$_{25}$ sequence at the 3' end. The viral 5'UTR containing *Renilla* luciferase mRNAs were synthesized by in vitro transcription. Additionally, we made a control *Renilla* luciferase mRNA with the Kozak sequence (5'-GCCACCAUG-3'), which is known to be found in the 5'UTR of highly expressed mRNAs [32]. All mRNAs were capped at the 5' end with a m^{7}G cap using the vaccinia virus capping enzyme. We tested the baseline *Renilla* expression of these mRNAs in a HeLa cell-derived *in vitro* translation system (IVTS) and found that the IAV 5'UTR sequences does not confer any significant advantage compared to the Kozak driven mRNA **(Figure 2.9A)** [33]. This suggests that under normal cellular conditions viral mRNAs would not have any advantage over host mRNA with regard to translation. This runs counter to what has been measured in the past where at peak infection viral mRNA levels are similar to host mRNA levels but viral protein expression is significantly higher than host protein expression [13,14,18].

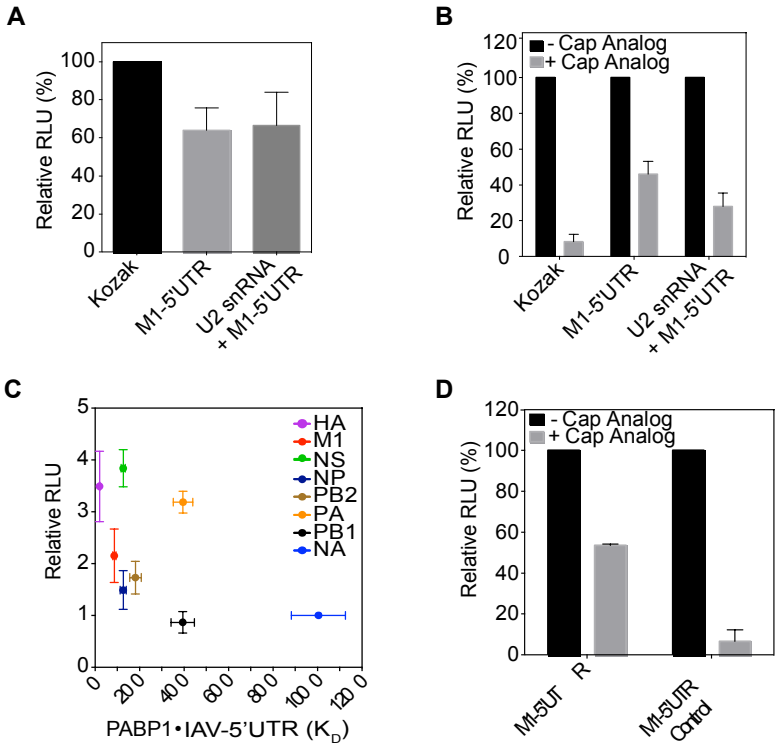

Figure 2.9: The IAV 5'UTR confer resistance to cap-dependent translation inhibition. (A) Translation of Kozak sequence driven *Renilla* luciferase mRNA, M1-5' UTR driven *Renilla* luciferase mRNA, and U2 snRNA + M1-5' UTR driven *Renilla* luciferase mRNA in HeLa lysate monitored by relative luminescence units (RLU). RNAs are capped at the 5' end with m^7G and have a 25-nucleotide long adenine tail at the 3' end. The RLU was normalized relative to the control Kozak driven *Renilla* mRNA translation. (B) Translation of Kozak sequence driven *Renilla* luciferase mRNA, M1-5' UTR driven *Renilla* luciferase mRNA, and U2 snRNA + M1-5' UTR driven *Renilla* luciferase mRNA in HeLa lysate in the presence or absence of 1 mM m^7G cap analog. RNAs are capped at the 5' end with m^7G and have a 25-nucleotide long adenine tail at the 3' end. In each case, the RLU with the cap analog was normalized to the absence of cap analog arbitrarily set as 100%. (C) Correlation between the translation of the eight *Renilla* luciferase mRNAs driven by the 5' UTR sequence of the eight segments of A/WSN/1933 (H1N1) IAV in HeLa lysate in the presence of 1 mM m^7G cap analog relative to the K_D measured for each 5' UTR binding to PABP1. RNAs are capped at the 5' end with m^7G and have a 25-nucleotide long adenine tail at the 3' end. Each point is as follows, HA (purple), M1 (red), NS (green), NP (dark blue), PB2 (brown), PA (orange), PB1 (black), NA (blue). The RLU was normalized relative to the NA 5' UTR driven *Renilla* mRNA. (D) Translation of M1-5' UTR driven *Renilla* luciferase mRNA, and M1-5' UTR Control driven *Renilla* luciferase mRNA in HeLa lysate in the presence or absence of 1 mM m^7G cap analog. RNAs are capped at the 5' end with m^7G and have a 25-nucleotide long adenine tail at the 3' end. The RLU in the presence of the cap analog was normalized relative to the signal in the absence of the cap analog arbitrarily set as 100%. The standard deviations from three experiments are shown.

Interestingly, previous studies have shown that the translation of influenza viral mRNA is independent of eIF4E activity [17,34–36]. We therefore determined how expression of the M1 5'UTR mRNAs handled shut-off of eIF4E driven translation initiation by including an m^7G cap analog in the IVTS **(Figures 2.9B and 2.10)**) [37]. Results show that 90% of the Kozak driven mRNA translation is dependent on eIF4E availability, whereas only ~ 50% of the translation of the mRNA driven by the M1 5'UTR is dependent on eIF4E. The same trend was found to be true when comparing the relative translation rates of the same mRNAs that were capped and poly(A) tailed to versions that contained no cap and a long randomized 3'UTR sequence **(Figure 2.10B)**. This suggests, that while knockdown of cap-dependent translation creates an environment that decreases translation for all mRNAs, it does give mRNAs with the viral 5'UTR sequence a distinct advantage over the host mRNAs. In order to ensure that this advantage was due primarily to the 5'UTR sequence and not an artifact of the *in vitro* system, RNA sequence or secondary structure, we used a bicistronic RNA where the varying 5'UTR's and the cricket-paralysis virus (CrPV) IRES drove the production of firefly and *Renilla* luciferase, respectively **(Figure 2.10D)**. By measuring the production of firefly luciferase and normalizing it to the production of the CrPV IRES driven *Renilla* luciferase, we found that the downregulation of eIF4E had the most inhibitory effect on the Kozak driven mRNA than on the M1-5'UTR driven mRNA. In fact, the translation of the varying 5'UTR of the bicistronic mRNAs resemble those of the monocistronic mRNAs, indicating the importance of the 5'UTR sequence on its resistance to cap-dependent translation inhibition.

Figure 2.10: Cap-dependent translation inhibition. (A) Translation of Kozak sequence driven *Renilla* luciferase mRNA in HeLa lysate in the presence of increasing amount of m^7G cap analog. mRNA is capped at the 5' end with m^7G and have a 25-nucleotide long adenine tail at the 3' end. Translation was monitored by luminescence and shown as relative luminescence units (RLU). The RLU in the presence of the cap analog was normalized to the control reaction without the cap analog. (B) Translation of Kozak sequence driven *Renilla* luciferase mRNA, M1-5' UTR driven *Renilla* luciferase mRNA, and U2 snRNA + M1-5' UTR driven *Renilla* luciferase mRNA in HeLa lysate. mRNAs are either capped at the 5' end with m^7G and have a 25-nucleotide long adenine tail at the 3' end (+ Cap/ + Tail) or do not contain an m^7G cap and have a 100 nt long random UTR at the 3' end (- Cap/ - Tail). The RLU of the mRNAs without the cap and tail were normalized to their respective mRNAs with the cap and tail. (C) Translation of eight *Renilla* luciferase mRNAs driven by the different 5' UTR sequence of the 8 segments of A/WSN/1933 (H1N1) IAV in HeLa lysate in the presence or absence of 1 mM m^7G cap analog. (D) Translation of Kozak sequence driven *Firefly* luciferase and CrPV driven *Renilla* luciferase bicistronic mRNA in HeLa lysate in the presence of increasing amount of m^7G cap analog. RNA is capped at the 5' end with m^7G and has a 25-nucleotide long adenine tail at the 3' end. The signal for the firefly luciferase in reactions with the cap analog were normalized to the control Kozak driven mRNA translation in the absence of the cap analog. Additionally, the signals for the firefly luciferase were normalized to the *Renilla* luciferase signals for each reaction conditions to normalize for variability. (E) Translation of Kozak, M1-5' UTR, or U2 snRNA + M1-5' UTR sequence driven *Firefly* luciferase and CrPV driven *Renilla* luciferase bicistronic mRNA in HeLa lysate in the presence or absence of 1 mM m^7G cap analog. RNAs are capped at the 5' end with m^7G and have a 25-nucleotide long adenine tail at the 3' end. The RLU in the presence of the cap analog was normalized to the control reaction without the cap analog. The standard deviations from three experiments are shown.

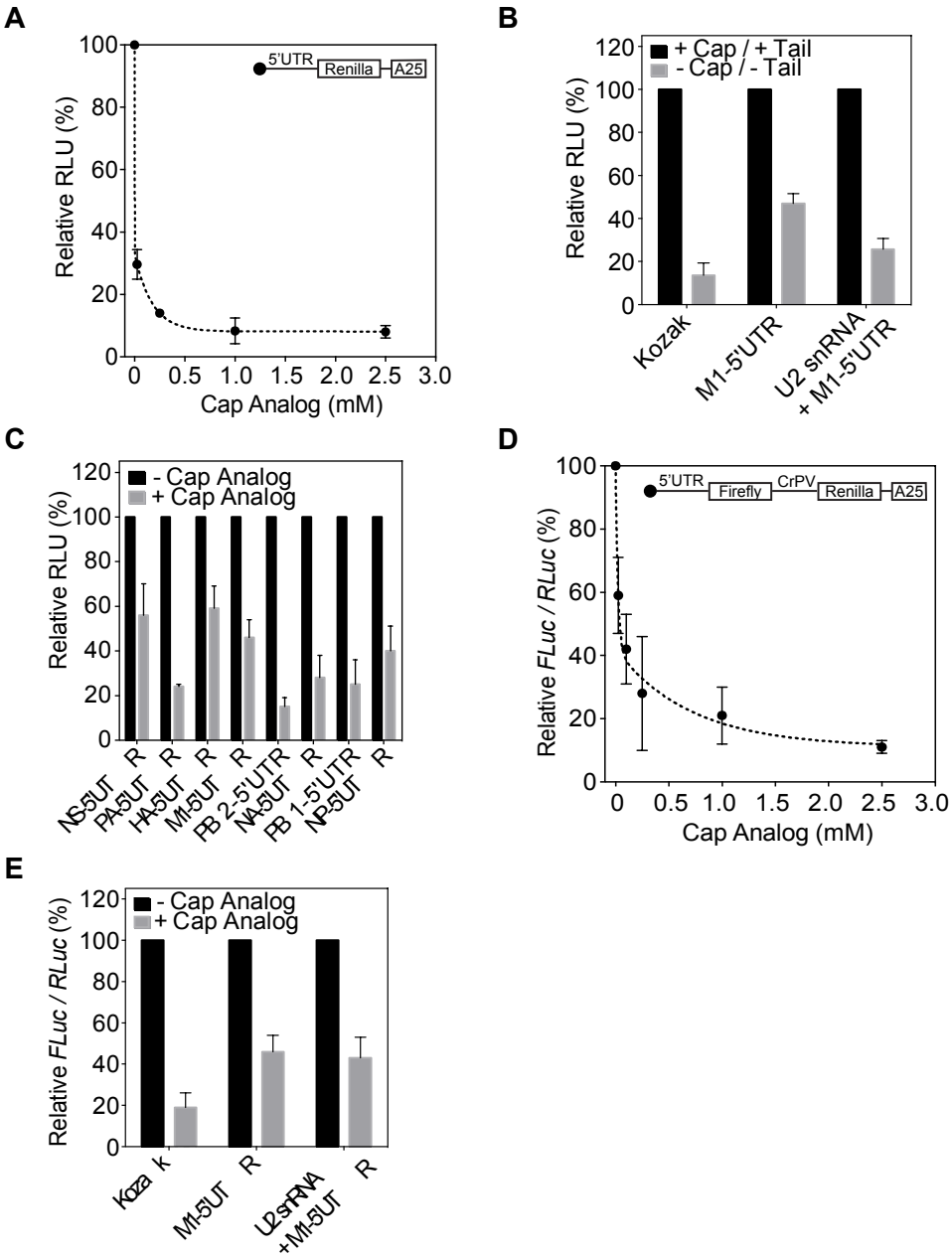
A
Relative RLU (%)
5'UTR
Renilla
A25
Cap Analog (mM)
B
+ Cap / + Tail
- Cap / - Tail
Relative RLU (%)
Kozak
M1-5'UTR
U2 snRNA + M1-5'UTR
C
- Cap Analog
+ Cap Analog
Relative RLU (%)
NS-5UT
PA-5UT
HA-5UT
M1-5UT
PB 2-5'UTR
NA-5UT
PB 1-5'UTR
NP-5UT
D
5'UTR
Firefly
CrPV
Renilla
A25
Relative FLuc / RLuc (%)
Cap Analog (mM)
E
- Cap Analog
+ Cap Analog
Relative FLuc / RLuc (%)
Kozak
M1-5UT
U2 snRNA +M1-5UT

We wanted to see whether this translational advantage during eIF4E inhibition correlated with the affinity PABP1 has to different 5'UTRs. We thus incorporated the different 5'UTRs of each IAV viral segment upstream of the monocistronic *Renilla* mRNA reporter. The translation of these mRNAs was tested in the HeLa IVTS in the presence of cap analog and the relative translation was compared to the affinities measured by our binding studies **(Figure 2.9C)**. The results were in agreement with our prediction that sequences whose 5'UTR had a high affinity for PABP1 also translated more than those whose affinity to PABP1 were weaker. Additionally, all reporters containing a 5'UTR of each IAV segment were found to be more resistant to the presence of the cap analog compared to the Kozak sequence **(Figure 2.10C)**.These results suggest that if eIF4E is sequestered or inhibited during the course of IAV infection, the viral mRNAs are capable of overcoming cap-dependent translation inhibition.

To further validate that the translational levels observed in the *in vitro* translation system is due to PABP1 binding to the 5'UTR, we compared the translational efficiency of an M1 5'UTR driven *Renilla* construct with a *Renilla* sequence whose 5'UTR is the complementary sequence of the M1 5'UTR (Control). Binding studies reveal that PABP1 does not bind with significant affinity to the M1 5'UTR Control **(Figure 2.11)**. The translation assay showed that the M1-5'UTR Control driven mRNA is more susceptible to knocking down cap-dependent translation initiation than the M1-5'UTR driven mRNA sequence **(Figure 2.9D)**.

A

M1 5'UTR: 5'- G A G C A A A A G C A G G U A G A U A U U G A A A G-3'
M1 5'UTR Control: 5'- G U C G U U U U C G U C C A U C U A U A A C U U U C-3'

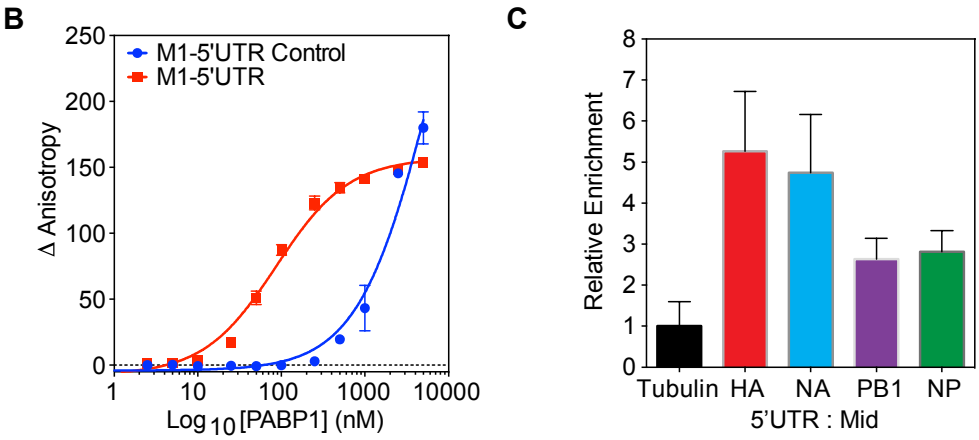

Figure 2.11: PABP1 binding to the M1-5'UTR and M1-5'UTR Control RNAs and additional RT-qPCR analysis. (A) Sequence of the M1-5'UTR RNA and the M1-5'UTR control RNA. The M1-5'UTR control RNA is the complement counterpart to the M1-5'UTR sequence. Both sequences contain a guanine at the 5' end to improve transcription of RNAs. (B) Anisotropy assay to determine the binding affinity of PABP1 for the M1-5'UTR and the M1-5'UTR control RNAs. The final concentration of the RNAs was 1 nM, and the final concentration of PABP1 was increased from 0 to 5 μM. The change in anisotropy is shown on the y-axis. The error bars represent the standard deviation from three independent experiments. (C) Results of qPCR comparing the enrichment of RNA fragments from the 5' end relative to fragments from the middle of IAV mRNAs. The data was normalized relative to the tubulin mRNA fragments from the 5' end over middle set to 1 and the error was propagated for all conditions. The cells were infected with A/Puerto Rico/8/34 (H1N1). The standard deviations from three biological replicates.

2.5 eIF4G binds to PABP1•IAV 5'UTR complex.

During canonical cap-dependent translation initiation, PABP1 utilizes RRM1 and RRM2 to bind to the poly(A) tail and interacts with eIF4G bound to the 5'-end of the mRNA. Studies have shown that eIF4G will bind to RRM2 and that this interaction is allosterically driven by PABP1 binding to its target RNA sequence [38]. For IAV to utilize PABP1 for translation initiation from the 5' end of the mRNA, it may recruit eIF4G to the 5' end in an eIF4E independent manner. To test this hypothesis, we purified a fragment of eIF4G (88-653) which contains the PABP1 binding site and confirmed its ability to recognize PABP1 on a poly(A) sequence by EMSA **(Figure 2.12A, indicated by blue circle)**. We then tested the binding of eIF4G to PABP1 bound to the M1 5'UTR by EMSA. At low concentration of PABP1, we observed the monomer of PABP1 bound to the M1 5'UTR **(Figure 2.12B, indicated by the red circle in lane 3)**. While at higher concentration of PABP1, we observed the dimer of PABP1 bound to the M1 5'UTR **(Figure 2.12B, indicated by the purple circle in lane 5)**. This is consistent with previous data showing that at high concentrations PABP1 binds as a dimer to RNA [27,29,39]. In both cases, the presence of eIF4G causes the PABP1 RNA complex to shift up even further **(Figure 2.12B, indicated by the blue and green circles in lanes 4 and 6, respectively)**. In the absence of PABP1, eIF4G has little to no affinity for the M1 5'UTR **(Figure 2.12B, lane 2)**. These results show that PABP1 is capable of binding to the 5' end of the viral mRNA and recruit eIF4G, which should be sufficient for the recruitment of the subsequent initiation factors and the ribosome to commence translation.

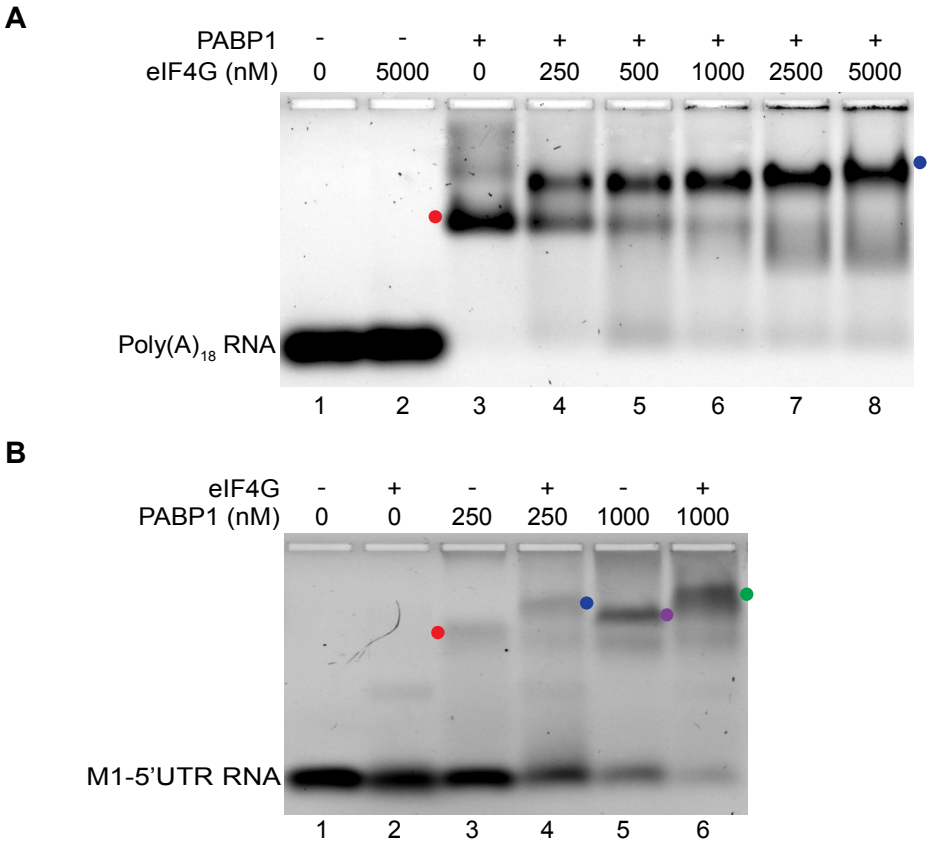

Figure 2.12: eIF4G is recruited by PABP1 to the 5' UTR of M1 mRNA. (A) EMSA assay monitoring the binding of PABP1 to poly $(A)_{18}$ RNA in the presence of varying amounts of eIF4G. Minus sign indicates no PABP1 was added to the reaction. The red circle points to the shifted PABP1•poly $(A)_{18}$ complex (lane 3) and the blue circle points to the PABP1•poly $(A)_{18}$•eIF4G complex (lanes 4 to 8). (B) EMSA assay monitoring the binding of PABP1 to M1-5'UTR RNA in the presence or absence of eIF4G. Minus sign indicates no eIF4G was added to the reaction. The red circle points to the PABP1 monomer•M1-5'UTR complex (lane 3), the blue circle points to the PABP1 monomer•M1-5'UTR•eIF4G complex (lane 4), the purple circle points PABP1 dimer•M1-5'UTR complex (lane 5), and the green circle points to the PABP1 dimer•M1-5'UTR •eIF4G complex (lane 6).

2.6 PABP1 is enriched on IAV 5'UTR sequences in infected cells.

To further support the possibility that the 5'UTR of IAV sequences can serve as an IRES, we determined whether PABP1 would preferentially enrich RNA pools with the IAV 5'UTR. To this end, we took A549 cells that were infected for 24 hours with the A/Puerto Rico/8 (H1N1) virus (MOI = 1) and used formaldehyde to crosslink proteins bound to RNA sequences. We then used sonication to lyse the cells and fragment the RNA to shortened sequences of 100 nt to 500 nt in length. Using an antibody against PABP1, we performed an immunoprecipitation (IP) reaction to pull down PABP1 and any RNAs it was bound to during infection. After isolating the RNAs by reversing the crosslinks, we used qPCR to amplify different portions of the IAV segment to examine the relative preference PABP1 has for different portions of an mRNA **(Figures 2.13A and B)**. Using the actin gene as a housekeeping control, we find that the PABP1 IP enriches the RNA pool with the 3' end of the mRNA by about 4-fold higher than the middle region. This trend is expected given that the 3' end of the actin mRNA abuts the poly (A) tail and should be enriched during the IP. We also find that these results are consistent regardless of whether the cells were MOCK infected or IAV infected. Furthermore, we examined the abundance of the 5' end of the actin mRNA in the IP to test whether the closed loop model of translation initiation would cause the IP to enrich the 5' ends of mRNAs **(Figure 2.13C)**. We find that the relative enrichment of the 5' mRNA ends are 5-fold less than the 3' ends indicating that the background we may encounter due to the closed loop model is very low [40].

Next, we decided to analyze four of the longer IAV mRNAs coding for HA, NP, NA and PB1 because they are similar in length to the actin mRNA, which serves as an internal control for the RNA shearing process during the IP. Examination of the relative enrichment of the four IAV mRNA 5' ends shows a 2 to 4-fold increase over that of actin mRNA when normalized against the middle sections of the same mRNA **(Figures 2.12D)**. We also compared the 5' end enrichment of tubulin mRNA, a different housekeeping gene, and found the relative differences to be similar **(Figure 2.11C)**. These results indicate that the IP of PABP1 is enriching the RNA pool with the 5' ends of each viral mRNA in line with what might be expected if PABP1 is bound to the 5'UTR.

Figure 2.13: PABP1 pulldown from IAV infected cells enriches for viral 5'UTR RNAs. (A) The workflow of the immunoprecipitation experiment from live IAV infected cells. Briefly, lysate containing PABP1 crosslinked to RNA are sheared into fragments by the sonication step, followed by recognition of PABP1 by specific antibody and pulldown of the PABP1•RNA complex. Proteins are digested and total RNA fragments are purified. Primers for reverse transcription and qPCR were designed to amplify the 5', 3' and middle section of the mRNAs of interest. RT-qPCR was performed to determine the enrichment for the 5', 3' and middle section of selected mRNAs. (B) Results of qPCR comparing the enrichment of actin mRNA fragments from the 3' end (Actin 3'UTR) relative to the middle fragments (Actin Mid). MOCK refers to cells that were mock infected while IAV refers to cells infected with A/Puerto Rico/8/34 (H1N1) IAV strain. (C) Results of qPCR comparing the enrichment of actin mRNA fragments from the 3' end (Actin 3'UTR) relative to fragments from the 5' end (Actin 5'UTR). MOCK refers to cells that were mock infected while IAV refers to cells infected with A/Puerto Rico/8/34 (H1N1) IAV strain. (D) Results of qPCR comparing the enrichment of RNA fragments from the 5' end relative to fragments from the middle of IAV mRNAs. The data was normalized relative to the actin mRNA fragments from the 5' end over middle set to 1 and the error was propagated for all conditions. The cells were infected with A/Puerto Rico/8/34 (H1N1). The standard deviations from three biological replicates are shown. $P < 0.05$ is denoted with one asterisks, $P < 0.01$ is denoted with two asterisks, and $P < 0.0001$ is denoted with four asterisks.

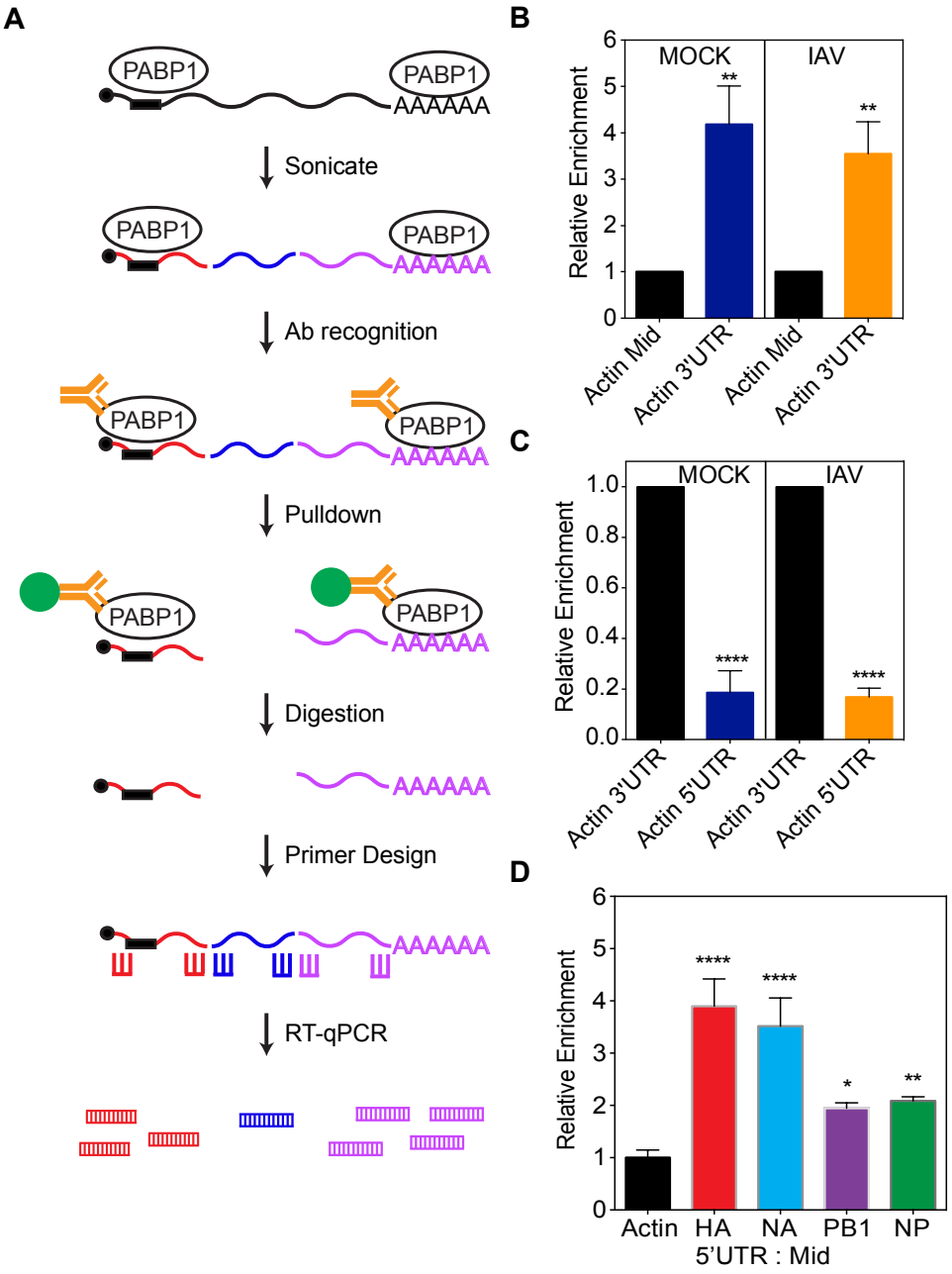
A
PABP1
PABP1
AAAAAA
Sonicate
Ab recognition
Pulldown
Digestion
Primer Design
RT-qPCR
B
MOCK
IAV
Relative Enrichment
Actin Mid
Actin 3'UTR
C
Actin 3'UTR
Actin 5'UTR
D
Actin
HA
NA
PB1
NP
5'UTR : Mid

2.7 Discussion

Canonical eukaryotic translation initiation is an intricate process and involves more than ten initiation factors. One of the key steps during initiation is the recruitment of the 43S preinitiation complex to the 5' end of an mRNA by eIF4F **(Figure 2.14)**. Mammalian eIF4F is composed of eIF4E, eIF4G, and eIF4A subunits. The eIF4E subunit binds to the m^7G cap structure present at the 5' end of cellular mRNAs; therefore, it is responsible for the placement of eIF4F at the 5' end. The eIF4G subunit is a large scaffolding protein that interacts with eIF4E, eIF4A, mRNA, 43S preinitiation complex (via eIF3), and PABP1 bound to the 3' end of the mRNA. Finally, the eIF4A subunit is an RNA helicase that melts RNA structures in the 5'UTR, which facilitates the recruitment of the 43S preinitiation complex. Interestingly, the concentration of eIF4E in the cell is low and it is the limiting factor for translation initiation [6]. Additionally, the activity of eIF4E is regulated by a phosphorylation/dephosphorylation cycle and by 4EBP [6]. Thus, eIF4E serves as a regulatory hub for translation initiation.

Many viruses subvert canonical translation initiation in order to direct ribosome assembly onto viral mRNA sequences. For example, EMCV activates 4EBP and poliovirus encodes a protease that cleaves eIF4G [41]. Both strategies neutralize eIF4E-dependent translation initiation of capped host mRNAs. These viruses contain an IRES in the 5'UTR regions of their mRNA that directly recruit eIF4G in the case of EMCV or the cleaved eIF4G fragment in the case of poliovirus to proceed with translation initiation [42]. Many such IRES's have been discovered in viral mRNAs whose ability to recruit initiation factors and the ribosome without the need for eIF4E give them a clear

advantage over host mRNA translation [43]. To date no IRES like activity for the IAV 5'UTR have been reported. However, numerous studies have shown that the IAV mRNAs are efficiently translated, whereas the translation of the host mRNAs is dramatically attenuated in infected cells [35,44–49]. This is explained by the inhibition of host RNA polymerase II, and the degradation of host mRNAs after viral infection [7,50–53]. Viral mRNAs escape the fate of the host mRNAs because they are transcribed by the viral polymerase, have a 5'-cap obtained from host mRNAs, and a 3' poly (A) tail added by a specialized process [54–63].

Even though the above-described processes reduce the amount of host mRNAs, there are still significant amounts of host mRNAs in the cytoplasm of infected cells, especially during the early phase of infection that will compete with viral mRNAs for translation [50]. More importantly, IAV infection activates the cellular stress response pathways, which will inhibit global translation [34,41,64–68]. One of the mechanisms for inhibiting global translation during the stress response is by the dephosphorylation of eIF4E and the activation of 4EBPs [34,41,64–68]. The dephosphorylation of eIF4E or the binding of 4EBPs to eIF4E reduces the activity of eIF4E and inhibit canonical cap-dependent mRNA translation [34,41,64–68]. However, many stress response mRNAs escape the inhibition of cap-dependent translation by recruiting PABP1 to their 5'-UTR to initiate translation in an eIF4E-independent mechanism [37].

We propose that IAV mRNAs also use an eIF4E-independent mechanism for translation initiation to compete with cellular mRNAs under virus-induced stress conditions. Indeed, previous studies have shown that downregulating eIF4E during the course of IAV infection does not hinder the overall translation of the viral proteins [17,34–

[36]. These observations can be more fully explained by our findings since PABP1 recognition of the 5'UTR is capable of recruiting eIF4G and thus exclude the need for cap-recognition by eIF4E **(Figure 2.14)**. Additionally, viral mRNA translation may be enhanced because eIF4E, which is the limiting factor for canonical translation initiation, is not needed for translation initiated by PABP1 binding to the 5'UTR.

During infection, the IAV proteins are differentially expressed based on need and stage of the viral life cycle. These different rates of protein synthesis cannot be explained solely by mRNA levels or sequence lengths. Our studies suggest that the levels of expression are coded for in the 5'UTR of each viral mRNA. These 5'UTR sequences are highly conserved across IAV strains, adenine rich, and have biologically relevant affinities for the translation initiation factor PABP1. The binding affinity of PABP1 for the different viral 5'UTRs and the recruitment of eIF4G may modulate translation initiation and regulate the expression of the various viral proteins during infection **(Figure 2.14)**. Even the alternative gene products coding for proteins such as M2, NS2, PA-X or PB1-FX, that are produced by either an alternative reading frame or due to splicing of the RNA segments, contain the 5' UTR of their respective segment and thus the translation of these mRNAs may also be modulated by PABP1 [53,69–72].

The high sequence conservation of the 5'UTR comes as no major surprise considering other studies have also noted the conservation of both the 5'- and 3'- ends of IAV segments allow for the panhandle structure to form for the negative stranded RNA [73]. While this sequence is known to be important for viral replication, our studies suggest that the complementary sequence present in the IAV mRNAs may additionally be important for translation. The panhandle structure could be formed technically by a

variety of sequences that are complementary at the 5’ and 3’ ends of the IAV RNA without the conservation of sequence identity. Therefore, our studies suggest that the conservation of A-rich sequence identity in the 5’-UTR maybe to ensure favorable binding to PABP1. In summary, our unexpected discovery that PABP1 binds with high affinity to the conserved sequence present in the viral 5’UTR and recruits eIF4G to initiate translation is consistent with previous reports that IAV mRNA translation is resistant to eIF4E inhibition [17,34–36]. The alternative mechanism could be used to enhance viral mRNA translation in competition with host mRNAs especially when the activity of eIF4E is reduced [74]. More studies are needed to understand this alternative mechanism of translation initiation on viral mRNAs, which could be targeted to treat IAV infection.

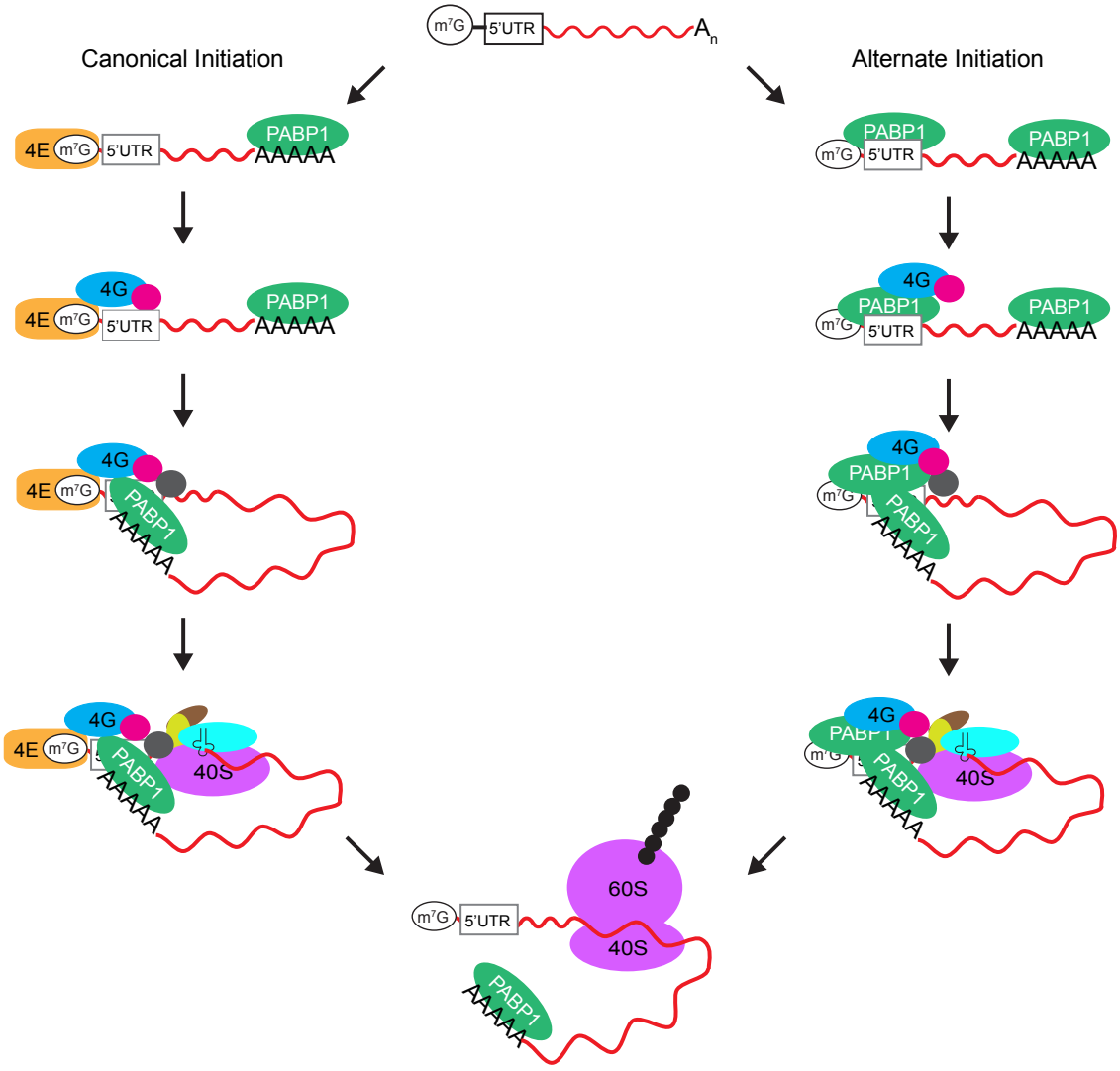

Figure 2.14: Models for translation initiation on IAV mRNAs. The IAV mRNAs have a m^{7}G cap structure at the 5' end, a highly conserved 5'UTR and a poly(A) tail at the 3' end. During canonical translation initiation shown on the left, PABP1 binds to the 3' poly(A) tail and eIF4F consisting of eIF4E, eIF4G and eIF4A subunits binds to the m^{7}G cap at the 5' end (for clarity the binding of eIF4E subunit to the m^{7}G cap is shown as a separate step). This is followed by the recruitment of the 43S preinitiation complex to the mRNA by eIF4F. In the alternate mechanism of initiation shown on the right, PABP1 binds both to the 3' poly(A) tail and to the viral 5'UTR. PABP1 bound to the viral 5'UTR then recruits eIF4G and the 43S preinitiation complex to initiate translation in an eIF4E-independent manner.

Materials and Methods

2.8 LOGO Analysis.

We performed a sequence search on www.fludb.org for all eight IAV segments individually. Search results were filtered based on human infecting IAV strains with duplicate sequences removed by the websites search parameter options. Minimum sequence lengths were also included to enrich results containing the respective 5'UTRs of each segment. Lengths are as follows; PB2 = 2341 nucleotides, PB1 = 2339 nucleotides, PA = 2233 nucleotides, HA = 1760 nucleotides, NP = 1565 nucleotides, NA = 1466 nucleotides, M1 = 1011 nucleotides, and NS = 889 nucleotides. Resulting sequences were trimmed after the first ATG of the sequence and the results were separated by length. Sequences were then analyzed using weblogo.berkeley.edu/logo.cgi.

2.9 Purification of Human PABP1.

Human PABP1 (GenBank accession code BC015958) in the pANT7_cGST vector was purchased from DNASU. The PABP1 gene was subcloned into pMCSG26, which contains a C-terminal six-His tag [75,76]. pMCSG26-PABP1 constructs were transformed into *E. coli* Rosetta 2 (DE3) pLysS cells (Millipore). The cells were grown at 37 °C in LB/ampicillin/chloramphenicol to an OD_{600} of 0.6−0.8, cooled to 18 °C, and then induced with 0.25 mM isopropyl β-D-1-thiogalactopyranoside for 12−18 h. Cells

were pelleted, flash-frozen, and stored at −80 °C. Cells were resuspended in PABP1 lysis buffer [25 mM Tris (pH 7.5), 250 mM NaCl, 10% glycerol, 8mM DTT, 0.5 mM EDTA, 1 mM PMSF, 0.1% Triton X-100, and 5 mM imidazole] and disrupted by sonication. The cell lysate was centrifuged at 20000 x g for 45 min at 4 °C. The supernatant was incubated with 4 mL of Ni-NTA beads for 15 min at 4 °C on a rotator. The slurry was poured over a column and washed with 50 mL of PABP1 wash buffer (lysis buffer with 20 mM imidazole and 1mg/mL Heparin sodium salt from porcine intestinal mucosa (Sigma)). Protein was eluted with PABP1 elution buffer [25 mM Tris (pH 7.5), 250 mM NaCl, 10% glycerol, 8 mM DTT, 0.5 mM EDTA, and 250 mM imidazole]. Fractions were collected and concentrated using a 50K MWCO concentrator until the volume was 1 mL. The protein sample was filtered and further purified using a Superdex 16/60 200 pg column at a flow rate of 1 mL/min using PABP1 storage buffer [25 mM Tris (pH 7.5), 250 mM NaCl, 5% glycerol, and 0.25 mM TCEP]. Sample peaks were collected and analyzed by 10% SDS−PAGE. Fractions free of nucleic acids, based on A_{280}/A_{260} measurements, were pooled and concentrated using a 50K MWCO concentrator, aliquoted, and flash-frozen. Concentrations of purified proteins were determined by the Bradford assay (Bio-Rad).

2.10 Purification of Human eIF4G.

The human eIF4G1 isoform 5 (NP_937884.1) gene (coding from amino acid 88-653) was codon optimized for *E. coli* expression and purchased as a FragmentGENE (GENEWIZ). The gene coding for eIF4G1 88-653 was subcloned using NdeI and SapI

sites into the pTXB1 vector (NEB) which contains a C-terminal Mxe GyrA Intein and a chitin binding domain. An additional threonine was inserted after D653 to enhance cleavage during purification.

The plasmid was transformed into *E. coli* BL21 (DE3) Star cells (Novagen). Cells were grown overnight at 37°C in a 5 ml LB starter culture supplemented with 100 µg/mL ampicillin. A 1 L LB media containing 100 µg/mL ampicillin was inoculated with 3-5 ml of the overnight starter culture and grown at 37°C to OD_{600} ~0.5. The culture was cooled to 30°C then induced with 0.4 mM IPTG and grown at that temperature for 2.5 – 3 hrs. Cells were pelleted at 5000 RPM for 15 min at 4°C and then stored at -80°C.

Cells were resuspended in pTXB1 lysis buffer (20 mM Hepes, 100 mM KCl, 10% Glycerol, 1 mM PMSF, pH 8.5) then lysed by French Press. Lysate was clarified at 50,000g for 30 min at 4°C then loaded into a pre-equilibrated column containing chitin resin (NEB) with a flow rate of ~0.5 ml/min at 4°C. The resin was washed with 10 column volumes of pTXB1 lysis buffer, 10 column volumes of pTXB1 wash buffer (20 mM Hepes, 1M KCl, 10% Glycerol, 1 mg/ml Heparin sodium salt, pH 8.5), and finally an additional 10 column volumes of pTXB1 lysis buffer. The resin was quickly washed with 3 column volumes of cleavage buffer (20 mM Hepes, 100 mM KCl, 10% Glycerol, 50 mM DTT, pH 8.5) before closing the column and incubating in cleavage buffer for 16-20 hrs at room temperature. Fractions were collected, analyzed by SDS-PAGE, then pooled and concentrated to ~5 ml in an Amicon Ultra Centrifugal Filter (Millipore). The protein was further purified on a Superdex 200 16/600 gel filtration column (GE Healthcare) in Storage Buffer (20 mM Hepes, 200 mM KCl, 10% Glycerol, 1 mM DTT,

0.1 mM EDTA pH 7.5). Fractions were analyzed by SDS-PAGE and only the purest fractions were pooled, concentrated, aliquoted, flash-frozen, and stored at -80°C.

2.11 RNAs for Fluorescence Anisotropy.

The poly(A)$_{18}$, ssIAV (5′-AGCAAAAGCAGG-3′), M1 (5′-GGUAGAUA-3′) and ssCR1 (5′-GCUAUCCAGAUUCUGAUU-3′) RNA with a fluorescein dye attached to the 3′-end was purchased from GE Dharmacon. The dsRK1 with a fluorescein dye attached to the 5′-end was synthesized as two complementary RNAs: 5′-FL-CCAUCCUCUACAGGCG-3′ and 5′-FL-CGCCUGUAGAGGAUGG-3′. All RNAs were deprotected and purified by denaturing urea−PAGE. All RNAs were resuspended in water, and their concentrations were determined by measuring the absorbance at 260 nm. All RNAs were stored at −80 °C in small aliquots. To make double-stranded RNA, equimolar amounts of sense and antisense RNAs were heated to 95 °C in 50 mM Tris (pH 8), 50 mM KCl, and 1 mM DTT for 2 min and then allowed to cool slowly to room temperature. The dsRNA was then aliquoted and stored at −80 °C.

2.12 RNA Transcription, Purification, and Capping.

RNAs not directly purchased were synthesized by in vitro transcription using either DNA oligonucleotides purchased from IDT or PCR products. Briefly, complementary sequences to the desired RNA sequence were designed with an additional 5’-CCTATAGTGAGTCGTATTA-3’ sequence at the 3’ end that is

complementary to the 18T7T sequence (5’-TAATACGACTCACTATAG-3’). All DNA oligonucleotides were purified by denaturing urea-PAGE and resuspended in RNase-free water. The quality and yield were assessed with a NanoDrop 2000c (ThermoFischer). The 18T7T was annealed to the oligonucleotide templates and used for in vitro transcription using T7 RNA polymerase to synthesize RNAs. All RNAs were purified by denaturing urea-PAGE. Each RNA was then purified via chloroform extraction followed by ethanol precipitation and resuspended in RNase-free water. The quality and yield were assessed by measuring A260 with a NanoDrop 2000c (ThermoFischer).

For long RNAs used for *in vitro* translation assays, the templates were synthesized by PCR. Briefly, the gene encoding the Renilla luciferase (RLuc) in the pRL-null vector (Promega) was modified with different sequences at the 5’ end and a poly(A)$_{25}$ was inserted at the 3' end of the gene by PCR. Similarly, the bicistronic construct encoding the Firefly luciferase and CrPV driven Renilla luciferase proteins in the pFR-CrPV vector was modified with different sequences at the 5’ end and a poly(A)$_{25}$ was inserted at the 3' end of the gene. The bicistronic constructs were amplified by PCR to add the T7 promoter sequence. The PCR products were used as templates for in vitro transcription by T7 RNA polymerase to synthesize the RNAs. RNAs were purified using the Monarch RNA Cleanup Kit (New England BioLabs) and resuspended in RNase-free water. RNA length and quality were checked using denaturing urea-PAGE and concentration was measured with a NanoDrop 2000c (ThermoFischer).

The mRNAs were 5' capped with 7-methylguanosine (m^7G) using a homemade Vaccinia virus capping enzyme [77]. The mRNAs were first heated for 5 minutes at 65 ºC and then put on ice for 5 minutes. Capping was carried out for 2 hours at 37ºC in 50 µL reactions with 1X capping buffer [50 mM Tris pH 8, 5 mM KCl, 1 mM MgCl2, and 1 mM DTT], 0.5 mM GTP, 0.1 mM SAM, and 4 µL homemade Vaccinia capping enzyme; the amount of mRNA substrate to be modified was limited to maintain a large stoichiometric excess of both GTP and SAM to ensure all mRNA molecules were capped. The 5' m^7G-capped mRNAs were then cleaned up using the Monarch RNA cleanup kit (New England Biolabs) and yield was assessed with a NanoDrop 2000c (ThermoFischer).

2.13 Fluorescence Anisotropy.

Fluorescence anisotropy studies were performed using a fixed concentration of fluorescein-labeled RNA and an increasing concentration of protein in anisotropy buffer [50 mM Tris (pH 8), 50 mM KCl, 50 ng/µL *E. coli* total tRNA, 1 mM DTT, and 0.01% Tween 20] [78]. For the anisotropy experiments, the concentration of RNA was fixed at 1 nM, and the concentration of PABP1 was titrated from 0 to 5 µM. Samples were incubated for 1 h at room temperature and the anisotropy studies were performed using a Tecan Spark plate reader in a 96-well plate. The sample (final volume of 100 µL) was excited at 470 nm, and the polarized emission at 520 nm was measured with 10 nm band slits for both excitation and emission. The G-factor was determined using a control sample with fluorescein-labeled RNA. The anisotropy values were subtracted from their

initial value, plotted, and fit to the following quadratic equation to determine K_D as described previously [78,79]:

$$\frac{[P+FL]}{[FL]} = \frac{\left[[P]+[FL]+K_D-\sqrt{([P]+[FL]+K_D)^2-4[P][FL]}\right]}{(2[P])}$$

where [P+FL]/[FL] is the anisotropy value, [FL] is the fluorescently labeled species and [P] is the protein concentration. GraphPad Prism (GraphPad Software Inc.) was used to perform the curve fits. All experiments were performed a minimum of three times with different protein batches to ensure reproducibility.

2.14 Electrophoretic Mobility Shift Assay (EMSA).

An EMSA was performed by incubating fluorescein-labeled RNA [final concentrations of 100 nM] with protein in anisotropy buffer to a final volume of 11 µL at room temperature for 1 h. After incubation, 1.3 µL of ice-cold 50% glycerol & Xylene cyanol was added to the mix. The complexes were separated from unbound species by electrophoresis on a 0.7% nondenaturing gel using a SEAKEM GTG agarose solution (Lonza) made with 1× TBE buffer. Samples were separated at 4 °C in 1× TBE buffer for 1.5 h at a 66 V constant voltage. The gels were visualized by scanning with a FLA9500 Typhoon instrument using the Cy2 excitation laser at a 600 PMT voltage and 50 µm resolution. In cases where concentrations are not explicit, 500 nM PABP to 100 nM poly(A) RNA ratio was used. Gels were analyzed with ImageJ software [80].

2.15 *In vitro* translation assay.

HeLa extract and translation assays were performed as described previously [81]. Briefly, HeLa cells were cultured in several 10 cm or 15 cm tissue culture plates until > 95% confluency. Cells were trypsinized, collected, spun down, washed with PBS and spun down again. The cell pellet mass was measured in a falcon tube (~ 200 – 300 mg) and resuspended in an equal volume of lysis buffer (10 mM HEPES pH 7.6, 10 mM Potassium Acetate, 0.5 mM Magnesium Acetate, 5 mM Dithiothreitol, 15 mM 2-aminopurine and 1 tablet of cOmplete Mini, EDTA free proteinase inhibitor tablet from Roche). Cells were then lysed with 25 strokes of a 2 mL dounce homogenizer and lysate was clarified via centrifugation. Supernatant was isolated and subjected to a 7-minute incubation at 25 ºC with 15 U/mL of micrococcal nuclease (New England Biolabs) and 0.75 mM calcium chloride. Reaction was stopped with the addition of 3 mM of EGTA pH 7.0 and sample was aliquoted and stored in liquid nitrogen.

The *in vitro* translation reactions were carried out as recommended with some slight modifications [81]. Briefly, HeLa extract made up 40% of each reaction in addition to, with remaining volume made up of translation buffer [16 mM HEPES pH 7.6, 20 mM creatine phosphate, 0.1 µg/µL creatine kinase, 0.1 mM spermidine, 100 µM amino acid mix, 8 mM ATP and 500 µM GTP], 150 mM potassium acetate, 2.5 mM magnesium acetate and 15 nM of RNA. Samples were incubated at 30 ºC for 1.5 hours and luminescence was measured with a Tecan Spark plate reader after adding 3 µM coelenterazine (Promega) for the monocistronic Renilla luciferase mRNAs. Samples of Firefly and Renilla luciferase bicistronic mRNAs were measured using the Dual Reporter Luciferase Assay System kit (Promega). All experiments were performed a minimum of three times with different lysate batches to ensure reproducibility.

2.16 Tissue culture, Virus propagation and IAV infection.

HeLa and A549 cells were cultured in Dulbecco's Modified Eagle Medium (DMEM) with 10% Fetal Bovine Serum in an incubator set a 37 ºC with 5% CO_2. A/Puerto Rico/8/34 (H1N1 ATCC-1469) virus was propagated in MDCK cells and transferred to DMEM supplemented with 25 mM HEPES buffer, 0.2% BSA Fraction V, 2 µg/mL TPCK-trypsin, and 1% penicillin/streptomycin (DMEM-IAV Media). Viral titers were determined via the hemagglutination test in Turkey red blood cells. MDCK cells were infected and used to determine the 50% tissue culture infective dose (TCID50) using the Spearman-Karber method.

Cells used for infection were carried out by passaging 10^6 A549 cells into a 10-cm dish for two days prior to infection with IAV. Infections was done at an MOI of 1 in DMEM-IAV Media and incubated for 1 hour prior to multiple washes with 1x PBS. A mock infected control plate was prepared in parallel. Cells were incubated in DMEM + 10% FBS for 24 hours before harvest. Briefly, media was aspirated and cells were washed twice with cold 1x PBS. A crosslinking solution made up of 0.1% formaldehyde in 1x PBS solution was added to each plate and incubated at room temperature for ten minutes with gentle mixing. Afterwards glycine was added (final concentration of 125 mM) to each plate and incubated for five minutes at room temperature. Solution was removed from each plate and cells were washed twice with cold 1x PBS. Cells were harvested by scraping the plates in 1 mL of 1x PBS using a cell scraper and transferred to an Eppendorf tube. Cells were pelleted, supernatant was aspirated and pellet was

stored at -80 ºC until ready for immunoprecipitation. Experiment was performed a minimum of three time.

2.17 PABP1 Immunoprecipitation.

Pulldown of PABP1 was performed by resuspending the A549 pellets in ice cold RIPA buffer [25 mM Tris pH 7.5, 150 mM NaCl, 1% NP-40, 0.1% SDS, 0.1% SDC and 1 mM EDTA]. Resuspended cells were sonicated on ice for 5 rounds 15 seconds on, 60 seconds off using a Branson Sonifier 450 equipped with a microtip and set at 50% Duty Cycle and an Output Control of 4. Samples were spun down, supernatant was transferred to washed Dynabeads Protein G Magnetic Beads (Invitrogen) with Rabbit IgG (Diagenode Cat. # c15410206) and placed on a rotator for 30 minutes at 4 ºC. Aliquots were collected prior to the next stage to serve as an RNA Input control. Samples were separated from beads and added to anti-PABPC1 rabbit polyclonal antibody (Abcam Cat. # ab21060)) and placed on a rotator for 2 hours at 4 ºC followed by washed Dynabeads Protein G Magnetic Beads for another hour. Supernatant was then discarded and beads were gently washed three times with RIPA buffer. Protein and RNA were eluted off with elution buffer [50 mM Tris-HCl pH 7.5, 5 mM EDTA, 1% SDS and 10 mM DTT] and samples were subjected to a proteinase K (New England Biolabs) treatment at 65ºC for 45 minutes. RNA was separated from beads and then subjected to the Monarch RNA cleanup kit (New England Biolabs) where yield and purity were checked via NanoDrop 2000c (ThermoFischer). Pulldown experiments were

performed a minimum of three times with three different infection experiments to ensure reproducibility.

2.18 Quantitative RT-PCR.

For qPCR, 10 ng of total RNA taken before and after the IP was reverse transcribed with gene specific primers for different sections of the target mRNAs. Briefly, three different reactions per target mRNA were performed using the following primers: HA-5'UTR-Rev: 5'-CGTTGTGGCTGTCTTCGAGC-3', HA-Mid-Rev: 5'-CTGGAAAGGGAGACTGCTGTTTATAGC -3', HA-3'UTR-Rev: 5'-TCAGATGCATATTCTGCACTGCAAAGAT -3', Actin-5'UTR-Rev: 5'-GCCCACATAGGAATCCTTCTGACC-3', Actin-Mid-Rev: 5'-GGTACATGGTGGTGCCGCC-3', Actin-3'UTR-Rev: 5'-TCATTTTTAAGGTGTGCACTTTTATTCAACTGG-3', Tubulin-5'UTR-Rev: 5'-TGCATGTGTTAAAAGGCGCAGG-3', Tubulin-Mid-Rev: 5'-AAGCAGTGATGGAGGACACAATCTG-3', Tubulin-3'UTR-Rev: 5'-GACATTTAAAATGGAAACTTCAATTTTATTAACAATTTACGGC-3', NP-5'UTR-Rev: 5'-AATCACTGAGTTTGAGTTCGGTGCA-3', NP-Mid-Rev: 5'-CCGACCCTCTCAATATGAGTGCA-3', NP-3'UTR-Rev: 5'-TTAATTGTCGTACTCCTCTGCATTGTCTC-3', NA-5'UTR-Rev: 5'-TGATGTTTTGGTTGCATATTCCAGTATGGT-3', NA-Mid-Rev: 5'-TGATTTAGTAACCTTCCCCTTTTCGATCTTG -3', NA-3'UTR-Rev: 5'-CTACTTGTCAATGGTGAATGGCAACTC-3', PB1-5'UTR-Rev: 5'-

CTGAGTACTGATGTGTCCTGTTGACA-3', PB1-Mid-Rev: 5'-TGAATCCCTTCATGATTGGGTGCA-3', PB1-3'UTR-Rev: 5'-CTATTTTTGCCGTCTGAGCTCTTCAATG-3'. The reverse transcriptase used was Superscript III (Invitrogen) and reaction followed manufacturer's protocol.

The qPCR was performed on a Bio-Rad CFX Connect Real-Time System using specific primers for different sections of the target mRNAs. Briefly, qPCR was performed with 2 µL of total cDNA from the above step using the Luna Universal qPCR Master Mix (NEB) and specific primers according to the manufacturer's protocol. The reverse primers used are the same as the aforementioned primers for reverse transcription. The forward primers are as follows: HA-5'UTR-Fwd: 5'-AGCAAAAGCAGGGGAAAATAAAAACAACC-3', HA-Mid-Fwd: 5'-GGAGGATGAACTATTACTGGACCTTGC-3', HA-3'UTR-Fwd: 5'-ATCAATGGGGATCTATCAGATTCTGGC-3', Actin-5'UTR-Fwd: 5'-ACAGAGCCTCGCCTTTGC-3', Actin-Mid-Fwd: 5'-AGCTGCCTGACGGCCAG-3', Actin-3'UTR-Fwd: 5'-TTTTAATCTTCGCCTTAATACTTTTTTATTTTGTTTTATTTTGAATGA-3', Tubulin-5'UTR-Fwd: 5'- CTAAAATGACAGCCTGGTTCAATGGG-3', Tubulin-Mid-Fwd: 5'-CCAGGTTTCCACAGCTGTAGTTGA-3', Tubulin-3'UTR-Fwd: 5'-GACATGGCTGCCCTTGAGAAG-3', NP-5'UTR-Fwd: 5'-AGCAAAAGCAGGGTAGATAATCACTCAC-3', NP-Mid-Fwd: 5'-GGTGAGAATGGACGAAAAACAAGAATTGC-3', NP-3'UTR-Fwd: 5'-ATCTGACATGAGGACCGAAATCATAAGG-3', NA-5'UTR-Fwd: 5'-GCAGGAGTTTAAAATGAATCCAAATCAGAAAATAATAACC-3', NA-Mid-Fwd: 5'-GCAGTGGCTGTATTAAAATACAACGGC-3', NA-3'UTR-Fwd: 5'-

GGAAGTTTCGTTCAACATCCTGAGC-3', PB1-5'UTR-Fwd: 5'-CAGGCAAACCATTTGAATGGATGTCAATC-3', PB1-Mid-Fwd: 5'-CTGCATCATTGAGCCCTGGAATG-3', PB1-3'UTR-Fwd: 5'-TGCTGCAATTTATTTGAAAAATTCTTCCCCAG-3'. Reactions were run in duplicates and the $2^{-\Delta\Delta Ct}$ was calculated by subtracting the C_t values of the samples post pulldown from pre-pulldown and relating different sections of a gene to each other before relating genes to each other. Note that primer efficiency for each pair of primers was validated according to recommended practices [82]. RT-qPCR was done on RNA from three biological replicates. GraphPad Prism was used to perform one-way ANOVA and t-test analysis to obtain P-values. $P < 0.05$ is denoted with one asterisks, $P < 0.01$ is denoted with two asterisks, and $P < 0.0001$ is denoted with four asterisks.

Chapter 2, in full, has been submitted for publication of the material. Cyrus M de Rozières, Alberto Pequeno, Shandy Shahabi, Taryn M Lucas, Kamil Godula, Gourisankar Ghosh and Simpson Joseph. The dissertation author was the primary investigator and author of this material.

References

(1) Ghebrehewet, S.; MacPherson, P.; Ho, A. Influenza. *BMJ* **2016**, i6258. https://doi.org/10.1136/bmj.i6258.

(2) Iuliano, A. D.; Roguski, K. M.; Chang, H. H.; Muscatello, D. J.; Palekar, R.; Tempia, S.; Cohen, C.; Gran, J. M.; Schanzer, D.; Cowling, B. J.; Wu, P.; Kyncl, J.; Ang, L. W.; Park, M.; Redlberger-Fritz, M.; Yu, H.; Espenhain, L.; Krishnan, A.; Emukule, G.; van Asten, L.; Pereira da Silva, S.; Aungkulanon, S.; Buchholz, U.; Widdowson, M.-A.; Bresee, J. S.; Azziz-Baumgartner, E.; Cheng, P.-Y.; Dawood, F.; Foppa, I.; Olsen, S.; Haber, M.; Jeffers, C.; MacIntyre, C. R.; Newall, A. T.; Wood, J. G.; Kundi, M.; Popow-Kraupp, T.; Ahmed, M.; Rahman, M.; Marinho, F.; Sotomayor Proschle, C. V.; Vergara Mallegas, N.; Luzhao, F.; Sa, L.; Barbosa-Ramírez, J.; Sanchez, D. M.; Gomez, L. A.; Vargas, X. B.; Acosta Herrera, aBetsy; Llanés, M. J.; Fischer, T. K.; Krause, T. G.; Mølbak, K.; Nielsen, J.; Trebbien, R.; Bruno, A.; Ojeda, J.; Ramos, H.; an der Heiden, M.; del Carmen Castillo Signor, L.; Serrano, C. E.; Bhardwaj, R.; Chadha, M.; Narayan, V.; Kosen, S.; Bromberg, M.; Glatman-Freedman, A.; Kaufman, Z.; Arima, Y.; Oishi, K.; Chaves, S.; Nyawanda, B.; Al-Jarallah, R. A.; Kuri-Morales, P. A.; Matus, C. R.; Corona, M. E. J.; Burmaa, A.; Darmaa, O.; Obtel, M.; Cherkaoui, I.; van den Wijngaard, C. C.; van der Hoek, W.; Baker, M.; Bandaranayake, D.; Bissielo, A.; Huang, S.; Lopez, L.; Newbern, C.; Flem, E.; Grøneng, G. M.; Hauge, S.; de Cosío, F. G.; de Moltó, Y.; Castillo, L. M.; Cabello, M. A.; von Horoch, M.; Medina Osis, J.; Machado, A.; Nunes, B.; Rodrigues, A. P.; Rodrigues, E.; Calomfirescu, C.; Lupulescu, E.; Popescu, R.; Popovici, O.; Bogdanovic, D.; Kostic, M.; Lazarevic, K.; Milosevic, Z.; Tiodorovic, B.; Chen, M.; Cutter, J.; Lee, V.; Lin, R.; Ma, S.; Cohen, A. L.; Treurnicht, F.; Kim, W. J.; Delgado-Sanz, C.; de mateo Ontañón, S.; Larrauri, A.; León, I. L.; Vallejo, F.; Born, R.; Junker, C.; Koch, D.; Chuang, J.-H.; Huang, W.-T.; Kuo, H.-W.; Tsai, Y.-C.; Bundhamcharoen, K.; Chittaganpitch, M.; Green, H. K.; Pebody, R.; Goñi, N.; Chiparelli, H.; Brammer, L.; Mustaquim, D. Estimates of Global Seasonal Influenza-Associated Respiratory Mortality: A Modelling Study. *The Lancet* **2018**, *391* (10127), 1285–1300. https://doi.org/10.1016/S0140-6736(17)33293-2.

(3) Cozza, V.; Campbell, H.; Chang, H. H.; Iuliano, A. D.; Paget, J.; Patel, N. N.; Reiner, R. C.; Troeger, C.; Viboud, C.; Bresee, J. S.; Fitzner, J. Global Seasonal Influenza Mortality Estimates: A Comparison of 3 Different Approaches. *Am. J. Epidemiol.* **2021**, *190* (5), 718–727. https://doi.org/10.1093/aje/kwaa196.

(4) Molinari, N.-A. M.; Ortega-Sanchez, I. R.; Messonnier, M. L.; Thompson, W. W.; Wortley, P. M.; Weintraub, E.; Bridges, C. B. The Annual Impact of Seasonal Influenza in the US: Measuring Disease Burden and Costs. *Vaccine* **2007**, *25* (27), 5086–5096. https://doi.org/10.1016/j.vaccine.2007.03.046.

(5) Jackson, R. J.; Hellen, C. U. T.; Pestova, T. V. The Mechanism of Eukaryotic Translation Initiation and Principles of Its Regulation. *Nat. Rev. Mol. Cell Biol.* **2010**, *11* (2), 113–127. https://doi.org/10.1038/nrm2838.

(6) Pelletier, J.; Sonenberg, N. The Organizing Principles of Eukaryotic Ribosome Recruitment. *Annu. Rev. Biochem.* **2019**, *88* (1), 307–335. https://doi.org/10.1146/annurev-biochem-013118-111042.

(7) Plotch, S. J.; Bouloy, M.; Ulmanen, I.; Krug, R. M. A Unique Cap(M7GpppXm)-Dependent Influenza Virion Endonuclease Cleaves Capped RNAs to Generate the Primers That Initiate Viral RNA Transcription. *Cell* **1981**, *23* (3), 847–858. https://doi.org/10.1016/0092-8674(81)90449-9.

(8) Gu, W.; Gallagher, G. R.; Dai, W.; Liu, P.; Li, R.; Trombly, M. I.; Gammon, D. B.; Mello, C. C.; Wang, J. P.; Finberg, R. W. Influenza A Virus Preferentially Snatches Noncoding RNA Caps. *RNA* **2015**, *21* (12), 2067–2075. https://doi.org/10.1261/rna.054221.115.

(9) Koppstein, D.; Ashour, J.; Bartel, D. P. Sequencing the Cap-Snatching Repertoire of H1N1 Influenza Provides Insight into the Mechanism of Viral Transcription Initiation. *Nucleic Acids Res.* **2015**, *43* (10), 5052–5064. https://doi.org/10.1093/nar/gkv333.

(10) Sikora, D.; Rocheleau, L.; Brown, E. G.; Pelchat, M. Deep Sequencing Reveals the Eight Facets of the Influenza A/HongKong/1/1968 (H3N2) Virus Cap-Snatching Process. *Sci. Rep.* **2015**, *4* (1), 6181. https://doi.org/10.1038/srep06181.

(11) Sikora, D.; Rocheleau, L.; Brown, E. G.; Pelchat, M. Influenza A Virus Cap-Snatches Host RNAs Based on Their Abundance Early after Infection. *Virology* **2017**, *509*, 167–177. https://doi.org/10.1016/j.virol.2017.06.020.

(12) te Velthuis, A. J. W.; Fodor, E. Influenza Virus RNA Polymerase: Insights into the Mechanisms of Viral RNA Synthesis. *Nat. Rev. Microbiol.* **2016**, *14* (8), 479–493. https://doi.org/10.1038/nrmicro.2016.87.

(13) Bercovich-Kinori, A.; Tai, J.; Gelbart, I. A.; Shitrit, A.; Ben-Moshe, S.; Drori, Y.; Itzkovitz, S.; Mandelboim, M.; Stern-Ginossar, N. A Systematic View on Influenza Induced Host Shutoff. *eLife* **2016**, *5*, e18311. https://doi.org/10.7554/eLife.18311.

(14) Bogdanow, B.; Wang, X.; Eichelbaum, K.; Sadewasser, A.; Husic, I.; Paki, K.; Budt, M.; Hergeselle, M.; Vetter, B.; Hou, J.; Chen, W.; Wiebusch, L.; Meyer, I. M.; Wolff, T.; Selbach, M. The Dynamic Proteome of Influenza A Virus Infection Identifies M Segment Splicing as a Host Range Determinant. *Nat. Commun.* **2019**, *10* (1), 5518. https://doi.org/10.1038/s41467-019-13520-8.

(15) Kummer, S.; Flöttmann, M.; Schwanhäusser, B.; Sieben, C.; Veit, M.; Selbach, M.; Klipp, E.; Herrmann, A. Alteration of Protein Levels during Influenza Virus H1N1 Infection in Host Cells: A Proteomic Survey of Host and Virus Reveals Differential Dynamics. *PLoS ONE* **2014**, *9* (4), e94257. https://doi.org/10.1371/journal.pone.0094257.

(16) Hatada, E.; Hasegawa, M.; Mukaigawa, J.; Shimizu, K.; Fukuda, R. Control of Influenza Virus Gene Expression: Quantitative Analysis of Each Viral RNA Species in Infected Cells. *J. Biochem. (Tokyo)* **1989**, *105* (4), 537–546. https://doi.org/10.1093/oxfordjournals.jbchem.a122702.

(17) Burgui, I.; Yángüez, E.; Sonenberg, N.; Nieto, A. Influenza Virus MRNA Translation Revisited: Is the EIF4E Cap-Binding Factor Required for Viral MRNA Translation? *J. Virol.* **2007**, *81* (22), 12427–12438. https://doi.org/10.1128/JVI.01105-07.

(18) Shapiro, G. I.; Gurney, T.; Krug, R. M. Influenza Virus Gene Expression: Control Mechanisms at Early and Late Times of Infection and Nuclear-Cytoplasmic Transport of Virus-Specific RNAs. *J. Virol.* **1987**, *61* (3), 764–773. https://doi.org/10.1128/JVI.61.3.764-773.1987.

(19) Crooks, G. E. WebLogo: A Sequence Logo Generator. *Genome Res.* **2004**, *14* (6), 1188–1190. https://doi.org/10.1101/gr.849004.

(20) Schneider, T. D.; Stephens, R. M. Sequence Logos: A New Way to Display Consensus Sequences. *Nucleic Acids Res.* **1990**, *18* (20), 6097–6100. https://doi.org/10.1093/nar/18.20.6097.

(21) Furuse, Y.; Oshitani, H. Evolution of the Influenza A Virus Untranslated Regions. *Infect. Genet. Evol.* **2011**, *11* (5), 1150–1154. https://doi.org/10.1016/j.meegid.2011.04.006.

(22) Parvin, J. D.; Moscona, A.; Pan, W. T.; Leider, J. M.; Palese, P. Measurement of the Mutation Rates of Animal Viruses: Influenza A Virus and Poliovirus Type 1. *J. Virol.* **1986**, *59* (2), 377–383. https://doi.org/10.1128/JVI.59.2.377-383.1986.

(23) Nobusawa, E.; Sato, K. Comparison of the Mutation Rates of Human Influenza A and B Viruses. *J. Virol.* **2006**, *80* (7), 3675–3678. https://doi.org/10.1128/JVI.80.7.3675-3678.2006.

(24) Rambaut, A.; Pybus, O. G.; Nelson, M. I.; Viboud, C.; Taubenberger, J. K.; Holmes, E. C. The Genomic and Epidemiological Dynamics of Human Influenza A Virus. *Nature* **2008**, *453* (7195), 615–619. https://doi.org/10.1038/nature06945.

(25) Chen, R.; Holmes, E. C. Avian Influenza Virus Exhibits Rapid Evolutionary Dynamics. *Mol. Biol. Evol.* **2006**, *23* (12), 2336–2341. https://doi.org/10.1093/molbev/msl102.

(26) Sachs, A. B.; Davis, R. W.; Kornberg, R. D. A Single Domain of Yeast Poly(A)-Binding Protein Is Necessary and Sufficient for RNA Binding and Cell Viability. *Mol. Cell. Biol.* **1987**, *7* (9), 3268–3276. https://doi.org/10.1128/mcb.7.9.3268.

(27) Kühn, U.; Pieler, T. Xenopus Poly(A) Binding Protein: Functional Domains in RNA Binding and Protein-Protein Interaction. *J. Mol. Biol.* **1996**, *256* (1), 20–30. https://doi.org/10.1006/jmbi.1996.0065.

(28) Burd, C. G.; Matunis, E. L.; Dreyfuss, G. The Multiple RNA-Binding Domains of the MRNA Poly(A)-Binding Protein Have Different RNA-Binding Activities. *Mol. Cell. Biol.* **1991**, *11* (7), 3419–3424. https://doi.org/10.1128/MCB.11.7.3419.

(29) de Rozières, C. M.; Joseph, S. Influenza A Virus NS1 Protein Binds as a Dimer to RNA-Free PABP1 but Not to the PABP1·Poly(A) RNA Complex. *Biochemistry* **2020**, *59* (46), 4439–4448. https://doi.org/10.1021/acs.biochem.0c00666.

(30) Görlach, M.; Burd, C. G.; Dreyfuss, G. The MRNA Poly(A)-Binding Protein: Localization, Abundance, and RNA-Binding Specificity. *Exp. Cell Res.* **1994**, *211* (2), 400–407. https://doi.org/10.1006/excr.1994.1104.

(31) Simon, L. M.; Morandi, E.; Luganini, A.; Gribaudo, G.; Martinez-Sobrido, L.; Turner, D. H.; Oliviero, S.; Incarnato, D. In Vivo Analysis of Influenza A MRNA Secondary Structures Identifies Critical Regulatory Motifs. *Nucleic Acids Res.* **2019**, *47* (13), 7003–7017. https://doi.org/10.1093/nar/gkz318.

(32) Kozak, M. Structural Features in Eukaryotic MRNAs That Modulate the Initiation of Translation. *J. Biol. Chem.* **1991**, *266* (30), 19867–19870.

(33) Witherell, G. In Vitro Translation Using HeLa Extract. *Curr. Protoc. Cell Biol.* **2000**, *6* (1). https://doi.org/10.1002/0471143030.cb1108s06.

(34) Feigenblum, D.; Schneider, R. J. Modification of Eukaryotic Initiation Factor 4F during Infection by Influenza Virus. *J. Virol.* **1993**, *67* (6), 3027–3035.

(35) Yángüez, E.; Nieto, A. So Similar, yet so Different: Selective Translation of Capped and Polyadenylated Viral MRNAs in the Influenza Virus Infected Cell. *Virus Res.* **2011**, *156* (1–2), 1–12. https://doi.org/10.1016/j.virusres.2010.12.016.

(36) Yángüez, E.; Rodriguez, P.; Goodfellow, I.; Nieto, A. Influenza Virus Polymerase Confers Independence of the Cellular Cap-Binding Factor EIF4E for Viral MRNA Translation. *Virology* **2012**, *422* (2), 297–307. https://doi.org/10.1016/j.virol.2011.10.028.

(37) Gilbert, W. V.; Zhou, K.; Butler, T. K.; Doudna, J. A. Cap-Independent Translation Is Required for Starvation-Induced Differentiation in Yeast. *Science* **2007**, *317* (5842), 1224–1227. https://doi.org/10.1126/science.1144467.

(38) Safaee, N.; Kozlov, G.; Noronha, A. M.; Xie, J.; Wilds, C. J.; Gehring, K. Interdomain Allostery Promotes Assembly of the Poly(A) MRNA Complex with PABP and EIF4G. *Mol. Cell* **2012**, *48* (3), 375–386. https://doi.org/10.1016/j.molcel.2012.09.001.

(39) Deo, R. C.; Bonanno, J. B.; Sonenberg, N.; Burley, S. K. Recognition of Polyadenylate RNA by the Poly(A)-Binding Protein. *Cell* **1999**, *98* (6), 835–845. https://doi.org/10.1016/S0092-8674(00)81517-2.

(40) Vicens, Q.; Kieft, J. S.; Rissland, O. S. Revisiting the Closed-Loop Model and the Nature of MRNA 5′–3′ Communication. *Mol. Cell* **2018**, *72* (5), 805–812. https://doi.org/10.1016/j.molcel.2018.10.047.

(41) Walsh, D.; Mathews, M. B.; Mohr, I. Tinkering with Translation: Protein Synthesis in Virus-Infected Cells. *Cold Spring Harb Perspect Biol* **2013**, *5*, a012351. https://doi.org/10.1101/cshperspect.a012351.

(42) Bushell, M.; Sarnow, P. Hijacking the Translation Apparatus by RNA Viruses. *J. Cell Biol.* **2002**, *158* (3), 395–399. https://doi.org/10.1083/jcb.200205044.

(43) Martinez-Salas, E.; Francisco-Velilla, R.; Fernandez-Chamorro, J.; Embarek, A. M. Insights into Structural and Mechanistic Features of Viral IRES Elements. *Front. Microbiol.* **2018**, *8*, 2629. https://doi.org/10.3389/fmicb.2017.02629.

(44) Katze, M. G.; DeCorato, D.; Krug, R. M. Cellular MRNA Translation Is Blocked at Both Initiation and Elongation after Infection by Influenza Virus or Adenovirus. *J Virol* **1986**, *60*, 1027–1039.

(45) Katze, M. G.; Krug, R. M. Translational Control in Influenza Virus-Infected Cells. *Enzyme* **1990**, *44*, 265–277.

(46) Garfinkel, M. S.; Katze, M. G. Translational Control by Influenza Virus. Selective Translation Is Mediated by Sequences within the Viral MRNA 5'-Untranslated Region. *J Biol Chem* **1993**, *268*, 22223–22226.

(47) Enami, K.; Sato, T. A.; Nakada, S.; Enami, M. Influenza Virus NS1 Protein Stimulates Translation of the M1 Protein. *J Virol* **1994**, *68*, 1432–1437.

(48) de la Luna, S.; Fortes, P.; Beloso, A.; Ortin, J. Influenza Virus NS1 Protein Enhances the Rate of Translation Initiation of Viral MRNAs. *J Virol* **1995**, *69*, 2427–2433.

(49) Kash, J. C.; Goodman, A. G.; Korth, M. J.; Katze, M. G. Hijacking of the Host-Cell Response and Translational Control during Influenza Virus Infection. *Virus Res* **2006**, *119*, 111–120. https://doi.org/10.1016/j.virusres.2005.10.013.

(50) Katze, M. G.; Krug, R. M. Metabolism and Expression of RNA Polymerase II Transcripts in Influenza Virus-Infected Cells. *Mol Cell Biol* **1984**, *4*, 2198–2206.

(51) Beloso, A.; Martinez, C.; Valcarcel, J.; Santaren, J. F.; Ortin, J. Degradation of Cellular MRNA during Influenza Virus Infection: Its Possible Role in Protein Synthesis Shutoff. *J Gen Virol* **1992**, *73 (Pt 3)*, 575–581.

(52) Chen, Z.; Krug, R. M. Selective Nuclear Export of Viral MRNAs in Influenza-Virus-Infected Cells. *Trends Microbiol* **2000**, *8*, 376–383.

(53) Jagger, B. W.; Wise, H. M.; Kash, J. C.; Walters, K. A.; Wills, N. M.; Xiao, Y. L.; Dunfee, R. L.; Schwartzman, L. M.; Ozinsky, A.; Bell, G. L.; Dalton, R. M.; Lo, A.; Efstathiou, S.; Atkins, J. F.; Firth, A. E.; Taubenberger, J. K.; Digard, P. An Overlapping Protein-Coding Region in Influenza A Virus Segment 3 Modulates the Host Response. *Science* **2012**, *337*, 199–204. https://doi.org/10.1126/science.1222213.

(54) Ortin, J.; Martin-Benito, J. The RNA Synthesis Machinery of Negative-Stranded RNA Viruses. *Virology* **2015**, *479-480C*, 532–544. https://doi.org/10.1016/j.virol.2015.03.018.

(55) Ulmanen, I.; Broni, B. A.; Krug, R. M. Role of Two of the Influenza Virus Core P Proteins in Recognizing Cap 1 Structures (M7GpppNm) on RNAs and in Initiating Viral RNA Transcription. *Proc Natl Acad Sci U A* **1981**, *78*, 7355–7359.

(56) Guilligay, D.; Tarendeau, F.; Resa-Infante, P.; Coloma, R.; Crepin, T.; Sehr, P.; Lewis, J.; Ruigrok, R. W.; Ortin, J.; Hart, D. J.; Cusack, S. The Structural Basis for Cap Binding by Influenza Virus Polymerase Subunit PB2. *Nat Struct Mol Biol* **2008**, *15*, 500–506. https://doi.org/10.1038/nsmb.1421.

(57) Yuan, P.; Bartlam, M.; Lou, Z.; Chen, S.; Zhou, J.; He, X.; Lv, Z.; Ge, R.; Li, X.; Deng, T.; Fodor, E.; Rao, Z.; Liu, Y. Crystal Structure of an Avian Influenza Polymerase PA(N) Reveals an Endonuclease Active Site. *Nature* **2009**, *458* (7240), 909–913. https://doi.org/10.1038/nature07720.

(58) Blass, D.; Patzelt, E.; Kuechler, E. Identification of the Cap Binding Protein of Influenza Virus. *Nucleic Acids Res.* **1982**, *10* (15), 4803–4812. https://doi.org/10.1093/nar/10.15.4803.

(59) Dias, A.; Bouvier, D.; Crépin, T.; McCarthy, A. A.; Hart, D. J.; Baudin, F.; Cusack, S.; Ruigrok, R. W. H. The Cap-Snatching Endonuclease of Influenza Virus

Polymerase Resides in the PA Subunit. *Nature* **2009**, *458* (7240), 914–918. https://doi.org/10.1038/nature07745.

(60) Pflug, A.; Lukarska, M.; Resa-Infante, P.; Reich, S.; Cusack, S. Structural Insights into RNA Synthesis by the Influenza Virus Transcription-Replication Machine. *Virus Res.* **2017**, *234*, 103–117. https://doi.org/10.1016/j.virusres.2017.01.013.

(61) Te Velthuis, A. J. W.; Fodor, E. Influenza Virus RNA Polymerase: Insights into the Mechanisms of Viral RNA Synthesis. *Nat. Rev. Microbiol.* **2016**, *14* (8), 479–493. https://doi.org/10.1038/nrmicro.2016.87.

(62) Poon, L. L.; Pritlove, D. C.; Fodor, E.; Brownlee, G. G. Direct Evidence That the Poly(A) Tail of Influenza A Virus MRNA Is Synthesized by Reiterative Copying of a U Track in the Virion RNA Template. *J Virol* **1999**, *73*, 3473–3476.

(63) Pritlove, D. C.; Poon, L. L.; Fodor, E.; Sharps, J.; Brownlee, G. G. Polyadenylation of Influenza Virus MRNA Transcribed in Vitro from Model Virion RNA Templates: Requirement for 5' Conserved Sequences. *J. Virol.* **1998**, *72* (2), 1280–1286.

(64) Kleijn, M.; Vrins, C. L.; Voorma, H. O.; Thomas, A. A. Phosphorylation State of the Cap-Binding Protein EIF4E during Viral Infection. *Virology* **1996**, *217* (2), 486–494. https://doi.org/10.1006/viro.1996.0143.

(65) Joshi-Barve, S.; Rychlik, W.; Rhoads, R. E. Alteration of the Major Phosphorylation Site of Eukaryotic Protein Synthesis Initiation Factor 4E Prevents Its Association with the 48 S Initiation Complex. *J. Biol. Chem.* **1990**, *265* (5), 2979–2983.

(66) Huang, J. T.; Schneider, R. J. Adenovirus Inhibition of Cellular Protein Synthesis Involves Inactivation of Cap-Binding Protein. *Cell* **1991**, *65* (2), 271–280.

(67) Morley, S. J.; Rau, M.; Kay, J. E.; Pain, V. M. Increased Phosphorylation of Eukaryotic Initiation Factor 4 Alpha during Early Activation of T Lymphocytes Correlates with Increased Initiation Factor 4F Complex Formation. *Eur. J. Biochem.* **1993**, *218* (1), 39–48. https://doi.org/10.1111/j.1432-1033.1993.tb18349.x.

(68) Kuss-Duerkop, S. K.; Wang, J.; Mena, I.; White, K.; Metreveli, G.; Sakthivel, R.; Mata, M. A.; Muñoz-Moreno, R.; Chen, X.; Krammer, F.; Diamond, M. S.; Chen, Z. J.; García-Sastre, A.; Fontoura, B. M. A. Influenza Virus Differentially Activates MTORC1 and MTORC2 Signaling to Maximize Late Stage Replication. *PLOS Pathog.* **2017**, *13* (9), e1006635. https://doi.org/10.1371/journal.ppat.1006635.

(69) Lamb, R. A.; Choppin, P. W. Segment 8 of the Influenza Virus Genome Is Unique in Coding for Two Polypeptides. *Proc. Natl. Acad. Sci.* **1979**, *76* (10), 4908–4912. https://doi.org/10.1073/pnas.76.10.4908.

(70) Lamb, R. A.; Choppin, P. W.; Chanock, R. M.; Lai, C. J. Mapping of the Two Overlapping Genes for Polypeptides NS1 and NS2 on RNA Segment 8 of Influenza Virus Genome. *Proc. Natl. Acad. Sci.* **1980**, *77* (4), 1857–1861. https://doi.org/10.1073/pnas.77.4.1857.

(71) Tsai, K.-N.; Chen, G.-W. Influenza Genome Diversity and Evolution. *Microbes Infect.* **2011**, *13* (5), 479–488. https://doi.org/10.1016/j.micinf.2011.01.013.

(72) Vasin, A. V.; Temkina, O. A.; Egorov, V. V.; Klotchenko, S. A.; Plotnikova, M. A.; Kiselev, O. I. Molecular Mechanisms Enhancing the Proteome of Influenza A Viruses: An Overview of Recently Discovered Proteins. *Virus Res.* **2014**, *185*, 53–63. https://doi.org/10.1016/j.virusres.2014.03.015.

(73) Desselberger, U.; Racaniello, V. R.; Zazra, J. J.; Palese, P. The 3' and 5'-Terminal Sequences of Influenza A, B and C Virus RNA Segments Are Highly Conserved and Show Partial Inverted Complementarity. *Gene* **1980**, *8* (3), 315–328. https://doi.org/10.1016/0378-1119(80)90007-4.

(74) Gingras, A. C.; Svitkin, Y.; Belsham, G. J.; Pause, A.; Sonenberg, N. Activation of the Translational Suppressor 4E-BP1 Following Infection with Encephalomyocarditis Virus and Poliovirus. *Proc. Natl. Acad. Sci.* **1996**, *93* (11), 5578–5583. https://doi.org/10.1073/pnas.93.11.5578.

(75) Eschenfeldt, W. H.; Maltseva, N.; Stols, L.; Donnelly, M. I.; Gu, M.; Nocek, B.; Tan, K.; Kim, Y.; Joachimiak, A. Cleavable C-Terminal His-Tag Vectors for Structure Determination. *J. Struct. Funct. Genomics* **2010**, *11* (1), 31–39. https://doi.org/10.1007/s10969-010-9082-y.

(76) Eschenfeldt, W. H.; Lucy, S.; Millard, C. S.; Joachimiak, A.; Mark, I. D. A Family of LIC Vectors for High-Throughput Cloning and Purification of Proteins. In *High Throughput Protein Expression and Purification*; Doyle, S. A., Ed.; Walker, J. M., Series Ed.; Methods in Molecular Biology; Humana Press: Totowa, NJ, 2009; Vol. 498, pp 105–115. https://doi.org/10.1007/978-1-59745-196-3_7.

(77) Fuchs, A.-L.; Neu, A.; Sprangers, R. A General Method for Rapid and Cost-Efficient Large-Scale Production of 5′ Capped RNA. *RNA* **2016**, *22* (9), 1454–1466. https://doi.org/10.1261/rna.056614.116.

(78) Cho, E. J.; Xia, S.; Ma, L.-C.; Robertus, J.; Krug, R. M.; Anslyn, E. V.; Montelione, G. T.; Ellington, A. D. Identification of Influenza Virus Inhibitors Targeting NS1A Utilizing Fluorescence Polarization–Based High-Throughput Assay. *J. Biomol. Screen.* **2012**, *17* (4), 448–459. https://doi.org/10.1177/1087057111431488.

(79) Pollard, T. D. A Guide to Simple and Informative Binding Assays. *Mol. Biol. Cell* **2010**, *21* (23), 4061–4067. https://doi.org/10.1091/mbc.E10-08-0683.

(80) Schneider, C. A.; Rasband, W. S.; Eliceiri, K. W. NIH Image to ImageJ: 25 Years of Image Analysis. *Nat. Methods* **2012**, *9* (7), 671–675. https://doi.org/10.1038/nmeth.2089.

(81) Rakotondrafara, A. M.; Hentze, M. W. An Efficient Factor-Depleted Mammalian in Vitro Translation System. *Nat. Protoc.* **2011**, *6* (5), 563–571. https://doi.org/10.1038/nprot.2011.314.

(82) Nolan, T.; Hands, R. E.; Bustin, S. A. Quantification of MRNA Using Real-Time RT-PCR. *Nat. Protoc.* **2006**, *1* (3), 1559–1582. https://doi.org/10.1038/nprot.2006.236.

Chapter 3:

Influenza A virus NS1 protein binds as a dimer to the RNA-free PABP1 but not to the PABP1•Poly(A) RNA Complex

Abstract

Influenza A virus (IAV) is a highly contagious human pathogen responsible for nearly half a million deaths each year. Non-structural protein 1 (NS1) is a crucial protein expressed by IAV to evade the host immune system. Additionally, NS1 has been proposed to stimulate translation because of its ability to bind poly(A) binding protein 1 (PABP1) and eukaryotic initiation factor 4G (eIF4G). We analyzed the interaction of NS1 with PABP1 using quantitative techniques. Our studies show that NS1 binds as a homodimer to PABP1, and this interaction is conserved across different IAV strains. Unexpectedly, NS1 does not bind to PABP1 that is bound to poly(A) RNA. Instead, NS1 only binds to PABP1 free of RNA, suggesting that translation stimulation does not occur by NS1 interacting with the PABP1 molecule attached to the mRNA 3'-poly(A) tail. More studies are needed to determine the role of NS1-PABP1 interaction, which is conserved across different IAV strains, in the life cycle of IAV.

Introduction

Seasonal Influenza A Virus (IAV) infection causes tens of thousands of deaths each year and billions of dollars lost in productivity with potential for greater severity during epidemics and pandemics.[1] IAV is a negative sense, single-stranded RNA virus that infects the lung's epithelial cells causing acute respiratory distress upon infection.[2] The IAV genome is made up of 8 different segments that code for roughly a dozen proteins required for successful infection and replication.[3–6] One of these viral proteins, Non-structural protein 1 (NS1), is responsible for a multitude of functions to help IAV proliferation, including the downregulation of the innate immune response, regulation of specific signaling pathways, and selective translation.[7] NS1 is a 26 kDa protein made up of an RNA-Binding domain (RBD), a linker region, an effector domain (ED), and a C-terminal tail.[8] NS1 is one of the most highly expressed proteins during IAV infection and yet does not get packaged into new viral particles, emphasizing its importance as a cell regulator during IAV infection. Studies of this protein and its roles have unveiled over a dozen different interactions with both host and viral proteins essential for successful viral replication.[7]

One of these interactions known to exist but not yet well understood is with the eukaryotic cytoplasmic Poly (A) Binding protein 1 (PABP1).[9] PABP1 is a 72 kDa protein made up of four RNA recognition motifs, a homodimerization domain, and the PABC domain at the C terminal end.[10] PABP1 is one of the most abundant proteins in the cell (~4 μM) and is primarily responsible for stimulating translation initiation by binding to the poly(A) tail at the 3' end of the mRNA.[11] PABP1 bound to the 3' poly(A) tail both protects

the mRNA from exonucleases as well as stimulates translation initiation by interacting with eukaryotic initiation factors at the 5' end of the mRNA.[12] While it is unsurprising for viruses to target translation factors to replicate successfully, little is yet known about how IAV makes use of PABP1 during infection.

To date, what is known about the NS1•PABP1 interaction is that NS1 binds to PABP1 with a high affinity (K_D = 20 nM) and primarily involves the RBD of NS1 and the homodimerization domain of PABP1.[9,13] Furthermore, NS1 cannot bind to both RNA and PABP1 simultaneously, suggesting a function that is independent of NS1's other roles as an RNA binder.[13] An interesting facet of this interaction is that the PABP1 homodimerization domain is long (~170 residues) and predicted to be intrinsically disordered. This domain is primarily responsible for PABP1's ability to multimerize on a poly(A) tail.[14] Neither the purpose of this interaction nor the nature of the binding is well understood. We believe that further characterization of the interaction between NS1 and PABP1 is critical to understanding IAV infection. Additionally, identifying the binding mode can help design inhibitors that can specifically target this interaction to inhibit IAV infections. Here, we employed fluorescence polarization and gel-shift assays to study the binding of NS1 to PABP1. Our studies show that NS1 binds as a homodimer to PABP1, and the interaction is primarily electrostatic. Interestingly, NS1 binds to RNA-free PABP1 but does not bind to the poly(A)•PABP1 complex. These results suggest that NS1 does not enhance translation by promoting the interaction of the 3'-poly(A)•PABP1 complex with the translation initiation complex assembled at the 5'-end of the mRNA.[9,15–18]

Materials and Methods

3.1 Purification of Recombinant NS1

H1N1 WSN wtNS1, H5N1 Nigeria wtNS1, H3N2 Udorn wtNS1, H3N2 Udorn WT NS1-RBD and NS1-RBD mutants were LIC cloned into the pETHSUL vector.[19] NS1-RBD mutants were created by site-directed mutagenesis by either insertion of a C-terminal cysteine to make NS1-RBD FL or changing R35 and R46 to alanine to make MUT NS1-RBD. pETHSUL-NS1 constructs were transformed into *E. coli* BL21(DE3) cells. 2 L of cells were grown at 37 °C in LB/ampicillin to an OD_{600} of 0.6−0.8, and then induced with 1 M isopropyl β-D-1-thiogalactopyranoside for 2.5 h. Cells were pelleted, flash-frozen, and stored at −80 °C.

For H1N1 wtNS1 and H3N2 wtNS1 cells were resuspended in lysis buffer [25 mM Tris (pH 7.5), 500 mM NaCl, 5% glycerol, 0.5 mM EDTA, 1 mM PMSF, 0.1% Triton X-100, 8 mM dithiothreitol and 5 mM imidazole] and disrupted by sonication. The cell lysate was centrifuged at 20000g for 45 min at 4 °C. The supernatant was incubated with 4 mL of Ni-NTA beads for 15 min at 4 °C on a rotator. The slurry was poured over a column and washed with 50 mL of wash buffer [25 mM Tris (pH 7.5), 500 mM NaCl, 5% glycerol, 0.5 mM EDTA, 1 M KCl, 8mM dithiothreitol (DTT) and 50 mM imidazole]. Protein was eluted with elution buffer [25 mM Tris (pH 7.5), 500 mM NaCl, 5% glycerol, 8 mM DTT, 0.5 mM EDTA, and 250 mM imidazole]. Elutions were collected and concentrated using a 10K molecular weight cutoff (MWCO) concentrator until the volume was 5 mL. Protein was dialyzed at 4 °C overnight with constant stirring in

storage buffer [25 mM Tris (pH 8.0), 100 mM NaCl, 10% glycerol, and 1mM TCEP-HCl] with Ulp1 protease (1:100) to remove SUMO tag. After dialysis the protein was incubated with 2 mL of Ni-NTA beads for 15 min at 4 °C on a rotator. The slurry was poured over a column and washed with storage buffer. Fractions were collected and analyzed by 12% sodium dodecyl sulfate−polyacrylamide gel electrophoresis (SDS−PAGE). Fractions were pooled and concentrated using a 3K MWCO concentrator, aliquoted, and flash-frozen. Concentrations of purified proteins were determined by the Bradford assay (Bio-Rad). Note that yields for these proteins post cleavage are low.

For H5N1 wtNS1 and H3N2 WT NS1-RBD and RBD mutants, cells were resuspended in lysis buffer [25 mM Tris (pH 7.5), 500 mM NaCl, 5% glycerol, 1 mM PMSF, 0.1% Triton X-100, 1 mM DTT and 20 mM imidazole] and disrupted by sonication. The cell lysate was centrifuged at 20000g for 45 min at 4 °C. Cell lysate was injected into FPLC and run over two HisTrap FF Crude 1 mL columns (Sigma-Aldrich) with FPLC running buffer [25 mM Tris (pH 7.5), 5% glycerol, and 0.5 mM TCEP-HCl]. Columns were washed with FPLC running buffer + 1 M NaCl and proteins were eluted with a step gradient (3%, 50%, 100%) of FPLC running buffer + 1 M Imidazole. Elutions were collected and run over a HiTrap Q 5 mL column (Sigma-Aldrich) with FPLC running buffer. A linear gradient from 0% to 100% FPLC running buffer + 1 M NaCl was used to elute proteins off of the column. Elutions were collected and analyzed by 16% Tricine−PAGE and A_{280}/A_{260} measurements. Elutions free of nucleic acids were collected and concentrated using a 10K MWCO concentrator until the volume was 5 mL. Protein was incubated at 4 °C overnight on a rotator with Ulp1

protease (1:100) to remove SUMO tag. Protein post cleavage was injected into FPLC and run over two HisTrap FF Crude 1 mL columns (Sigma-Aldrich) with FPLC running buffer. The flow through fractions were pooled, concentrated and buffer exchanged with NS1-RBD Buffer [25 mM Tris (pH 7.5), 150 mM NaCl, 5% glycerol, and 0.5 mM TCEP-HCl] using a 3K MWCO concentrator, aliquoted, and flash-frozen. Concentrations of purified proteins were determined by the Bradford assay (Bio-Rad).

3.2 Tryptophan Polarization Assay

Polarization studies were performed by using 2 μM of WT NS1-RBD or MUT NS1-RBD in NS1-RBD Buffer. Each sample (200 μL final volume) was transferred to a quartz cuvette and placed in a fluorometer (Jasco FP-8500) with a xenon lamp. The samples were excited at 295 nm, and the fluorescence emission intensity was measured at 350 nm. The excitation and emission bandwidth were set to 5 nm. A measurement of just NS1-RBD Buffer served as background. Three independent experiments were performed with three batches of protein.

3.3 RNAs for Fluorescence Anisotropy

The poly$(A)_{18}$ and ssCR1 (5′-GCUAUCCAGAUUCUGAUU-3′) RNA with a fluorescein dye attached to the 3′-end was purchased from GE Dharmacon. The dsRK1 with a fluorescein dye attached to the 5′-end was synthesized as two complementary RNAs: 5′-FL-CCAUCCUCUACAGGCG-3′ and 5′-FL-CGCCUGUAGAGGAUGG-3′. The

S17 with a fluorescein dye attached to the 3′-end was synthesized as 5'-GGGTGACAGTCCTGTTT-FL-3'. All RNAs were deprotected and purified by denaturing urea−PAGE. All RNAs were resuspended in water, and their concentrations were determined by measuring the absorbance at 260 nm. All RNAs were stored at −80 °C in small aliquots. To make double-stranded RNA, equimolar amounts of sense and antisense RNAs were heated to 95 °C in 50 mM Tris (pH 8), 50 mM KCl, and 1 mM DTT for 2 min and then allowed to cool slowly to room temperature. The dsRNA was then aliquoted and stored frozen at −80 °C.

3.4 Electrophoretic Mobility Shift Assay (EMSA)

An EMSA was performed by incubating proteins with Cy5 or fluorescein-labeled molecules [final concentrations of 100 nM] in anisotropy buffer to a final volume of 11 μL at room temperature for 1 h. After incubation, 1.3 μL of ice-cold 50% glycerol was added to the mix. The complexes were separated from unbound species by electrophoresis on a 0.7% nondenaturing gel using a SEAKEM GTG agarose solution (Lonza) made with 1× TBE buffer. Samples were separated at 4 °C in 1× TBE buffer for 1.5 h at a 66 V constant voltage. The gels were visualized by scanning with a FLA9500 Typhoon instrument using the Cy2 or Cy5 excitation laser at a 600 PMT voltage and 50 μm resolution. In cases where concentrations are not explicit, 500 nM PABP to 100 nM poly(A) RNA ratio was used with 5 μM NS1 when excess NS1 was used. Gels were analyzed and quantified with ImageJ software.[20]

3.5 Fluorescence Anisotropy

Fluorescence anisotropy studies were performed using a fixed concentration of fluorescein-labeled RNA and an increasing concentration of protein in anisotropy buffer [50 mM Tris (pH 8), 50 mM KCl, 50 ng/μL *E. coli* total tRNA, 1 mM DTT, and 0.01% Tween 20].[21] Note that the 50 mM KCl in the anisotropy buffer was exchanged for varying concentrations of NaCl where applicable. For the NS1 anisotropy experiments, the concentration of RNA or fluorescein labelled NS1-RBD protein was fixed at 10 nM, and the concentration of either NS1 or PABP1 was titrated from 0 to 5 μM. Note for the PABP1 binding to fluorescein labelled poly(A)$_{18}$ experiments, poly(A)$_{18}$ concentration was fixed at 1 nM. Samples were incubated for 1 h at room temperature and the anisotropy studies were performed using a Tecan Spark plate reader in a 96-well plate. The sample (final volume of 100 μL) was excited at 470 nm, and the polarized emission at 520 nm was measured with 10 nm band slits for both excitation and emission. The G-factor was determined using a control sample with fluorescein-labeled RNA. The anisotropy values were subtracted from their initial value, plotted, and fit to the following quadratic equation to determine K_D as described previously: [21,22]

$$\frac{[P+FL]}{[FL]} = \frac{\left[[P]+[FL]+K_D-\sqrt{([P]+[FL]+K_D)^2-4[P][FL]}\right]}{(\,2[P]\,)}$$

where [P+FL]/[FL] is the anisotropy value, [FL] is the fluorescently labeled species and [P] is the protein concentration. GraphPad Prism (GraphPad Software Inc.) was used to perform the curve fits. All experiments were performed a minimum of three times with different protein batches to ensure reproducibility.

3.6 Purification of Human PABP1

Human PABP1 (GenBank accession code BC015958) in the pANT7_cGST vector was purchased from DNASU. The PABP1 gene was subcloned into pMCSG26, which contains a C-terminal six-His tag.[23,24] pMCSG26-PABP1 constructs were transformed into *E. coli* Rosetta 2 (DE3) pLysS cells (Millipore). The cells were grown at 37 °C in LB/ampicillin/chloramphenicol to an OD_{600} of 0.6−0.8, cooled to 18 °C, and then induced with 0.25 mM isopropyl β-D-1-thiogalactopyranoside for 12−18 h. Cells were pelleted, flash-frozen, and stored at −80 °C. Cells were resuspended in PABP1 lysis buffer [25 mM Tris (pH 7.5), 250 mM NaCl, 10% glycerol, 8mM DTT, 0.5 mM EDTA, 1 mM PMSF, 0.1% Triton X-100, and 5 mM imidazole] and disrupted by sonication. The cell lysate was centrifuged at 20000g for 45 min at 4 °C. The supernatant was incubated with 4 mL of Ni-NTA beads for 15 min at 4 °C on a rotator. The slurry was poured over a column and washed with 50 mL of PABP1 wash buffer (lysis buffer with 20 mM imidazole and 1mg/mL Heparin sodium salt from porcine intestinal mucosa (Sigma)). Protein was eluted with PABP1 elution buffer [25 mM Tris (pH 7.5), 250 mM NaCl, 10% glycerol, 8 mM DTT, 0.5 mM EDTA, and 250 mM imidazole]. Fractions were collected and concentrated using a 50K MWCO concentrator until the volume was 1 mL. The protein sample was filtered and further purified using a Superdex 16/60 200 pg column at a flow rate of 1 mL/min using PABP1 storage buffer [25 mM Tris (pH 7.5), 250 mM NaCl, 5% glycerol, and 0.25 mM TCEP]. Sample peaks were collected and analyzed by 10% SDS−PAGE. Fractions free of nucleic acids, based on A_{280}/A_{260} measurements, were pooled and concentrated using a 50K MWCO

concentrator, aliquoted, and flash-frozen. Concentrations of purified proteins were determined by the Bradford assay (Bio-Rad).

3.7 Purification of GST Protein

Plasmid pGEX-3X was used to overexpress and purify the GST protein from *E. coli* BL21 cells as described previously.[13] The protein was purified using glutathione-Sepharose 4B beads (GE Healthcare) concentrated and flash-frozen in GST buffer [25 mM Tris (pH 7.5), 25 mM NaCl, 10% glycerol, and 0.25 mM TCEP or 0.5 mM DTT] were identified by analyzing aliquots by 12% SDS−PAGE.

3.8 Fluorescence labelling

NS1-RBD FL was labeled with *N*-(5-Fluoresceinyl) maleimide (Sigma-Aldrich) or cyanine 5 (Cy5) maleimide (GE Bioscience), according to the manufacturer's instructions and as described previously.[25] Labelled protein was separated from free dye by FPLC on a HiPrep 26/10 Desalting column (Sigma-Aldrich) with NS1-RBD Buffer. Fractions were collected and analyzed by 16% Tricine−PAGE scanned on a FLA9500 Typhoon instrument using the Cy2 or Cy5 excitation laser at a 600 PMT voltage and 50 μm resolution and stained with Coomassie. Fractions free of dye were pooled and concentrated using a 3K MWCO concentrator, aliquoted, and flash-frozen. Concentrations and labelling efficiency of proteins were determined by the Bradford assay (Bio-Rad) and nanodrop.

Results and Discussion

3.9 Design of an NS1 RBD mutant that does not form a homodimer

Studies of NS1 have elucidated its ability to dimerize and oligomerize as part of its many functions.[7,26] Examples include RBD – RBD dimerization to bind directly to RNA as well as ED – ED interactions for the binding to CPSF30 **(Figure 3.1A)**.[27–29] We purified the full-length NS1 and the RNA binding domain of NS1 (WT NS1-RBD) because previous studies using pull-down assays showed that the RBD is sufficient for binding to PABP1.[9] Additionally, the NS1 RBD only forms homodimers, which makes it easier study. To characterize the minimum oligomerization state NS1 must adopt to interact with PABP1, we designed a mutant NS1-RBD that cannot form a homodimer. Previous studies have shown that alanine substitution at Arg 35 and Arg 46 of NS1 disrupts the RBD – RBD interaction.[28] These mutations were incorporated into an NS1-RBD construct (MUT NS1-RBD), and the protein was purified along with the WT NS1-RBD **(Figure 3.1B)**. To determine the oligomeric states of the wild type and mutant NS1 RBDs, we analyzed the intrinsic tryptophan-fluorescence polarization of both proteins when they are excited with light at 295 nm wavelength.[30–32] Based on reports regarding fluorescence polarization of proteins, we expect to see a dimer of NS1 RBD (~ 16.8 kDa) to polarize light more than the monomer (~ 8.4 kDa). As predicted, WT NS1-RBD polarizes light more than MUT NS1-RBD, with the difference being in agreement with reports on UV-fluorescence polarization of proteins **(Figure 3.1C)**.[33]

Another method for testing the oligomeric states of the NS1-RBD constructs is the ability to bind double-stranded RNA (dsRNA). Based on previous reports that NS1-RBD must be a dimer to bind to dsRNA, we tested the binding of WT NS1-RBD and MUT NS1-RBD to a double-stranded RNA (dsRK1) using an electrophoretic mobility shift assay (EMSA).[27] We used one of the single-stranded RK1 (ssRK1) sequence as a negative control for the assay. The WT NS1-RBD bound to dsRK1 and slowed its migration on the gel. In contrast, the MUT NS1-RBD did not affect the migration of dsRK1, indicating that the MUT NS1-RBD cannot dimerize to bind to dsRNA **(Figure 3.1D)**. Additionally, both RBDs do not bind to ssRK1, which is consistent with the specificity of NS1 for dsRNA and not for ssRNA **(Figure 3.1D)**.

To validate these results, we used a fluorescence anisotropy-based quantitative assay to analyze the binding of NS1-RBDs to dsRK1. Binding experiments were performed by incubating increasing concentrations of NS1-RBD with a fixed concentration of fluorescein-labeled dsRK1 (10 nM), and the change in anisotropy was measured. WT NS1-RBD bound to dsRK1 with a K_D of 76 nM ± 9 nM, which is stronger than what has been previously reported for the full-length NS1 **(Figure 3.1E)**.[13,21] MUT NS1-RBD incubated with dsRK1 showed no change in anisotropy, indicating that it cannot form a dimer to bind to the dsRNA. Thus, the lower intrinsic tryptophan-fluorescence polarization value of the MUT NS1-RBD and its inability to bind to dsRNA, taken together, supports the conclusion that the MUT NS1-RBD behaves as a monomer in solution.

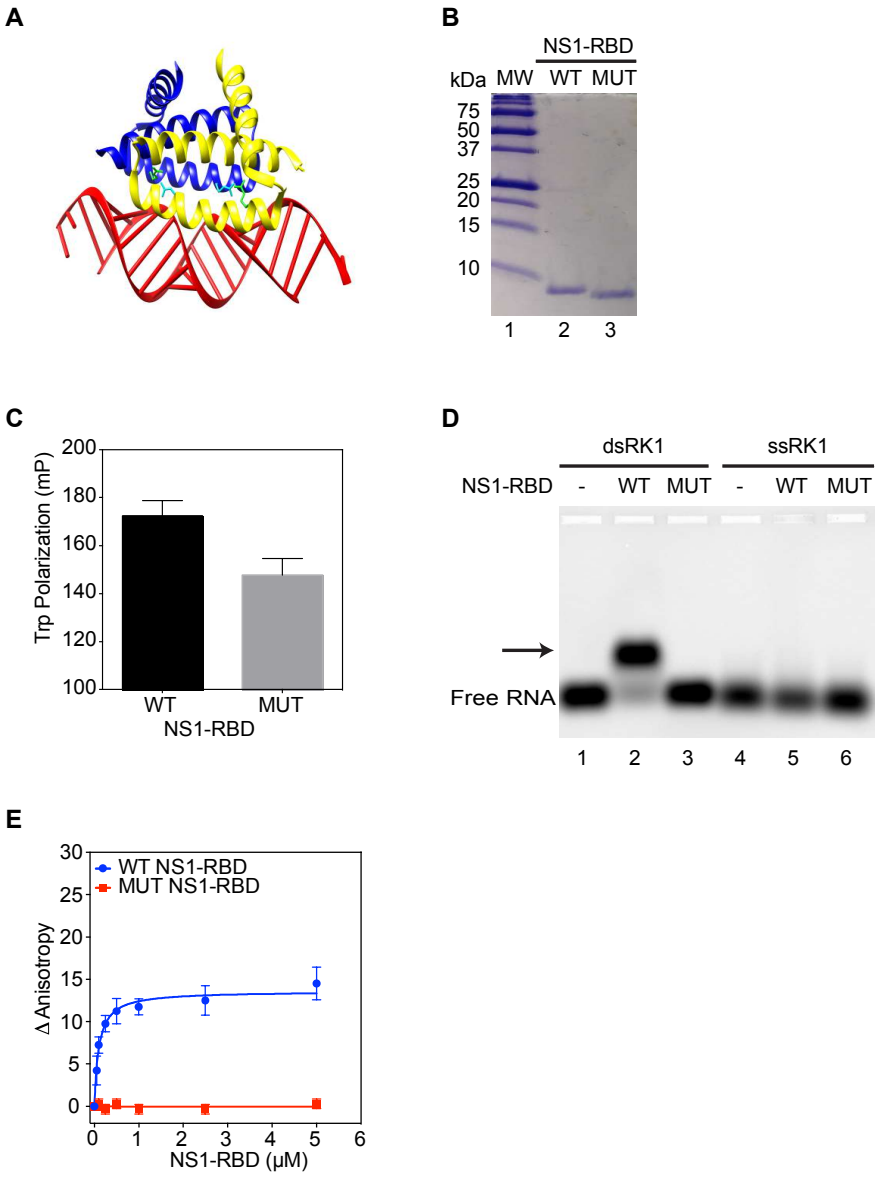

Figure 3.1: NS1 binds to PABP1 as a dimer. (A) Structure of NS1 RBD dimer (blue and yellow) bound to dsRNA (red) (PDB:2ZKO).[29] (B) Tricine-PAGE gel of purified WT NS1 RBD and MUT NS1 RBD proteins. (C) Tryptophan polarization of WT NS1-RBD and MUT NS1-RBD. (D) EMSA assay comparing binding of WT NS1 RBD and MUT NS1-RBD to single-stranded RK1 (ssRK1) and double stranded RK1 (dsRK1) RNA. Minus sign indicates no protein was added to the lane. Arrow points to the shifted protein-RNA complex. (E) Anisotropy assay of WT NS1-RBD and MUT NS1-RBD binding to dsRK1 RNA. The final concentration of the RNAs was 10 nM, and the final concentration of NS1 was increased from 0 to 5 μM. The change in anisotropy is shown on the y-axis. The error bars represent the standard deviation from three independent experiments.

3.10 Interaction of NS1 with the PABP1•poly(A) RNA complex

We used EMSA to monitor the binding of PABP1 to poly(A) RNA. Briefly, PABP1 was incubated with a 3' fluorescein-labeled poly adenosine sequence consisting of 18 nucleotides ($poly(A)_{18}$).[13] In the presence of increasing concentrations of PABP1, we first observe a shift of $poly(A)_{18}$ to an intermediate position on the gel and at a much higher concentration a shift to a higher position compared to the free $poly(A)_{18}$ **(Figure 3.2A)**. We interpret the complex that migrates to the intermediate position to be a monomer of PABP1 bound to a $poly(A)_{18}$ and the complex that migrates to the higher position to be a PABP1 dimer bound to a $poly(A)_{18}$ RNA molecule. The $poly(A)_{18}$ is short such that only one PABP1 molecule can directly bind to it, and the second PABP1 molecule binds by weaker protein-protein interaction.[14,34,35] This interpretation is consistent with the fact that PABP1 monomer binds with a high affinity to poly(A) RNA, whereas PABP1 dimers are formed only at much higher concentrations.[36,37]

After establishing the EMSA to monitor the binding of PABP1 to $poly(A)_{18}$, we analyzed the effect of NS1 on the PABP1•$poly(A)_{18}$ complex. In the absence of NS1, we observed the two shifted bands corresponding to the PABP1 monomer bound to $poly(A)_{18}$ and the PABP1 dimer bound to $poly(A)_{18}$. Interestingly, in the presence of the full-length NS1, we predominantly observed the band corresponding to the PABP1 monomer bound to $poly(A)_{18}$ **(Figure 3.2B)**. Similarly, in the presence of the WT NS1-RBD, PABP1 bound as a monomer to $poly(A)_{18}$. These results also agree with previous reports that the RBD is sufficient for binding to PABP1.[9] As a control, the addition of BSA did not affect the formation of the PABP1 dimer on $poly(A)_{18}$. Additionally, PABP1

does not bind to a control RNA (CR1). These results suggest that NS1, which is present in excess concentration over PABP1, is binding to PABP1 and inhibiting the formation of the PABP1 dimer on poly(A)$_{18}$.

Finally, we analyzed whether the MUT NS1-RBD that is incapable of forming a homodimer affects the binding of PABP1 to poly(A)$_{18}$. Interestingly, in the presence of MUT NS1-RBD, both the PABP1 monomer and the dimer were formed on poly(A)$_{18}$ indicating that the mutant NS1 cannot bind to the PABP1•poly(A) complex, possibly because it cannot homodimerize to form the binding interface needed for interacting with PABP1 **(Figure 3.2C)**. Thus, NS1 binds as a homodimer to PABP1.

3.11 NS1•PABP1 interaction is conserved across different IAV strains

To date, NS1•PABP1 interaction has been demonstrated only with H3N2 IAV strains, namely A/Victoria/3/75 and A/Udorn/307/1973.[9,13] Our studies show that in the presence of full-length recombinant A/Udorn/307/1973 NS1, the PABP1 dimer species is disrupted, leaving only the PABP1 monomer bound to poly(A)$_{18}$. To determine whether this interaction occurs with other IAV strains, we purified NS1 proteins from two other strains, namely A/WSN/1933 (H1N1) and A/chicken/Nigeria/2007 (H5N1) **(Figure 3.2D)**. The NS1 proteins corresponding to the different IAV strains were incubated with the PABP1•poly(A)$_{18}$ complex, and the change in RNA migration was monitored by EMSA. The results show that the different variants of NS1 also disrupt the PABP1 homodimer suggesting that the NS1•PABP1 interaction is conserved across IAV strains.

The NS1•PABP1 interaction is conserved across the different IAV strains, most likely due to the RBD's high sequence homology **(Figure 3.3A)**.

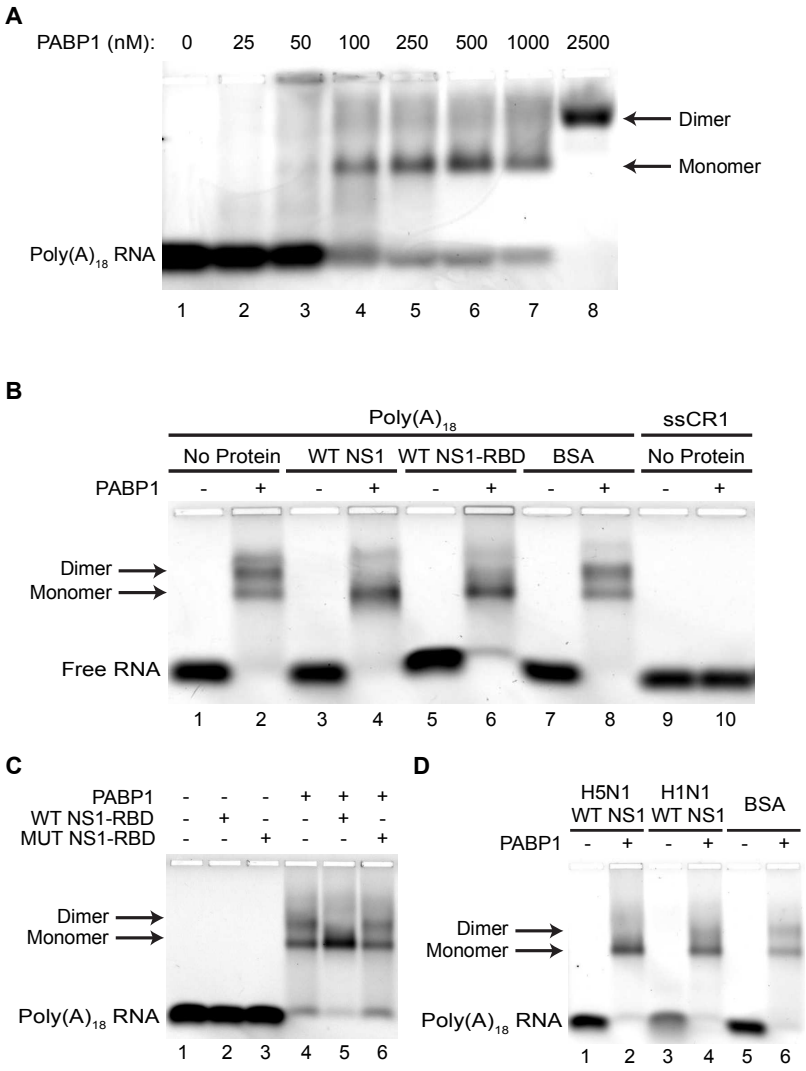

Figure 3.2: Binding of PABP1 to Poly(A)$_{18}$ RNA in the presence or absence of NS1. (A) PABP1 titration with Poly(A)$_{18}$ RNA. (B) Binding of PABP1 to Poly(A)$_{18}$ RNA in the presence or absence of excess full length H3N2 Udorn NS1 (WT NS1) or the RNA binding domain of H3N2 Udorn NS1 (WT NS1-RBD). BSA serves as a control for the presence of NS1 protein. ssCR1 serves as a control for non-specific binding by PABP1 and NS1. (C) Binding of WT NS1-RBD or MUT NS1-RBD to the PABP1•Poly(A)$_{18}$ complex. (D) Binding of full length H5N1 Nigeria WT NS1 and H1N1 WSN WT NS1 to the PABP1•Poly(A)$_{18}$ complex. Arrows indicate the monomer and dimer of PABP1 on the RNA. Minus and plus signs indicate the absence and presence of NS1, respectively. Arrow points to the shifted protein-RNA complex. The final concentration of the RNA was 100 nM, the final concentration of PABP1 was 500 nM (when not indicated) and the final concentration of NS1 or BSA was 5 μM. Note the gel rig used in (A) differs from (B) – (D) to enable the existence of both PABP1 states simultaneously.

3.12 Binding of NS1 RBD to PABP1 monitored using a quantitative polarization assay

Although the EMSA results unequivocally show that NS1-RBD binds to PABP1, we wanted a simple, quantitative assay to measure the binding affinity of NS1-RBD for PABP1. Therefore, we decided to develop a fluorescence polarization assay to monitor the binding of NS1-RBD to PABP1. Due to the small size of WT NS1-RBD (~ 8.4 kDa), we anticipated that a fluorescence polarization assay would be sensitive to the increase in size when NS1-RBD binds to PABP1. WT NS1-RBD has an endogenous cysteine; however, our studies showed that it could not be labeled because it is buried in the protein structure's interior and is inaccessible to the reactive dye **(Figure 3.3B)**. Therefore, we added a C-terminal cysteine to WT NS1-RBD (NS1-RBD FL) to label the protein with fluorescein-5-maleimide. Control experiments showed that NS1-RBD with the C-terminal cysteine binds to dsRK1 with the same affinity as WT NS1-RBD, indicating that it is functional **(Figure 3.3C)**. Additionally, EMSA showed that the NS1-RBD FL decreased the band corresponding to the PABP1 dimer bound to poly(A)$_{18}$, indicating that it is behaving similar to the WT NS1-RBD **(Figure 3.3D)**.

We next performed the polarization assay to monitor the binding of NS1-RBD FL to PABP1. As predicted, NS1-RBD FL exhibits an increase in anisotropy as the PABP1 concentration increases, showing that the two proteins form a complex **(Figure 3.4A)**. As a control, we titrated GST protein and did not observe the large increase in anisotropy observed with PABP1. The change in anisotropy with increasing concentrations of PABP1 was plotted, and the data were analyzed by nonlinear regression to obtain a K_D of 349 nM ± 69 nM **(Figure 3.4A)**. The affinity of NS1-RBD for

PABP1 is much weaker than the previously reported K_D = ~20 nM between the full-length NS1 and PABP1, which suggests that the ED also contributes to the binding without being necessary.[13] Furthermore, this weaker binding is consistent with the Nieto group's qualitative results, where the signal of NS1-RBD used in their pull-down was visibly weaker compared to the full-length NS1.[9] The new polarization assay can be used to determine the binding affinity of NS1-RBD for PABP1 and could also be used for identifying small molecules that inhibit this interaction.

NS1 binds to the PABP1 homodimerization domain, which contains interspersed proline residues, polar residues, and positively charged residues that are hallmarks of one type of intrinsically disordered proteins.[38] We hypothesized that if the interactions were electrostatic, binding of NS1 and PABP1 should weaken as the salt concentration increases. We used the polarization assay to determine the affinity of NS1-RBD FL for PABP1 with increasing concentrations of NaCl to see how sensitive the binding was to competing ions. We found that the affinity of NS1•PABP1 weakened with increasing salt concentrations. For example, the affinity between NS1-RBD FL and PABP1 changed from ~350 nM at 50 mM NaCl to greater than 1 μM at 150 mM NaCl **(Figure 3.4B)**. This suggests that NS1 is using the positively charged residues in the homodimerization domain to bind to PABP1.

3.13 NS1 does not bind to the PABP1•poly(A) RNA complex

The EMSA assays' results made us curious as to where NS1 was migrating on the gel when bound to PABP1. Our studies showed that the addition of NS1 to the

PABP1•poly(A)$_{18}$ complex resulted in the disappearance of the band corresponding to the PABP1 dimer bound to poly(A)$_{18}$. Whereas, the PABP1 monomer bound to poly(A)$_{18}$ remained intact. However, we did not detect the potential formation of an NS1•PABP1•poly(A)$_{18}$ complex by EMSA. First, this could be because NS1 binds to the PABP1•poly(A)$_{18}$ complex, and the corresponding change in the isoelectric point of the complex offsets the change in mass giving the appearance of a PABP1 monomer with poly(A)$_{18}$ on the gel. The second possibility is that NS1 cannot bind to the PABP1•poly(A)$_{18}$ complex and is binding only to PABP1 that is free of RNA. However, the formation of the NS1•PABP1 complex cannot be detected because there is no fluorescent dye directly attached to either of the proteins. To resolve these two possibilities, we labeled the NS1-RBD FL construct with the Cy5 dye so that its emission wavelength (670 nm) is distinct from the emission wavelength of the fluorescein dye (521 nm) attached to poly(A)$_{18}$ **(Figure 3.3E)**. This will allow us to monitor the migration pattern of both NS1-RBD and the PABP1•poly(A) complex simultaneously in the EMSA gels.

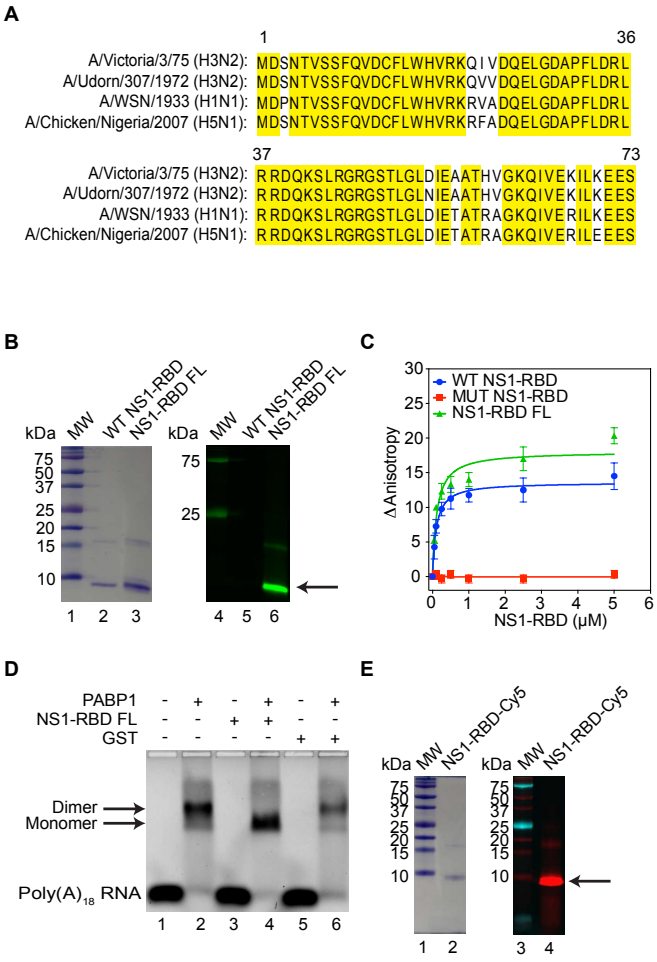

Figure 3.3: NS1 quality control. (A) Primary sequence alignment of the RNA Binding domain of the four NS1 strains used to demonstrate binding to PABP1. Yellow background highlights residues that are identical across all four strains. (B) Tricine-PAGE of WT NS1-RBD and NS1-RBD FL after fluorescein labeling. Gel on left is after Coomassie staining. Gel on right is scanned with the Typhoon FLA9500 using the Cy2 channel. (C) Polarization assay comparing the RNA binding properties of WT NS1-RBD, MUT NS1-RBD, and NS1-RBD FL with dsRK1. The final concentration of the RNA was 10 nM, and the final concentration of NS1 was increased from 0 to 5 μM. The change in anisotropy is shown on the y-axis. The error bars represent the standard deviation from three independent experiments. The K_D for WT NS1-RBD, and NS1-RBD FL binding to dsRK1 are 96 nM ± 19 nM and 115 nM ± 27 nM, respectively. (D) EMSA showing the binding of NS1-RBD FL to PABP1•poly(A)$_{18}$ complex. The concentrations of poly(A)$_{18}$, PABP1, and NS1-RBD FL are 100 nM, 500 nM and 5000 nM, respectively. GST at 5000 nM was used as a control for NS1-RBD FL. (-) and (+) indicate the absence and presence of the protein, respectively. The arrows indicate the PABP1 monomer and dimer bands. (E) Tricine-PAGE of NS1-RBD FL after Cy5 labeling. Gel on left is after Coomassie staining. Gel on right is scanned with the Typhoon FLA9500 using the Cy5 channel.

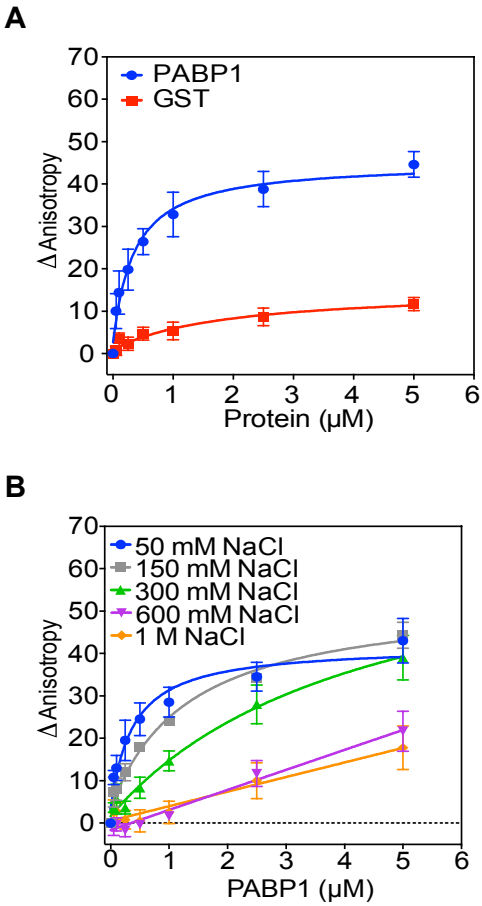

Figure 3.4: Binding of PABP1 to NS1 RBD monitored with a polarization assay. (A) Plot showing the change in anisotropy when NS1-RBD FL binds to PABP1 or GST as a control. (B) Binding of NS1-RBD FL to PABP1 in the presence of increasing concentrations of NaCl. The final concentration of NaCl ranged from 50 mM to 1M. The final concentration of the NS1-RBD FL was 10 nM, and the final concentration of PABP1 was increased from 0 to 5 μM. The change in anisotropy is shown on the y-axis. The error bars represent the standard deviation from three independent experiments.

We analyzed the binding of the Cy5-labeled NS1-RBD (NS1-RBD-Cy5) to PABP1 and the PABP1•poly(A)$_{18}$ complex by EMSA. Our studies show that the NS1-RBD-Cy5 does not co-localize with the PABP1•poly(A)18 complex but migrates as a smear above and below the PABP1•poly(A)$_{18}$ complex **(Figure 3.5A and B, compare lanes 3, 4, and 6)**. To verify this observation, we analyzed the binding of NS1-RBD-Cy5 to PABP1 with longer poly(A)$_{60}$ RNA. PABP1 binds to poly(A)$_{60}$ as a dimer that is unaffected in the presence of excess WT NS1 **(Figure 3.7A and 3.7B)**.[35,39] Again, the NS1-RBD-Cy5 does not co-localize with the PABP1•poly(A)$_{60}$ complex but binds to the free PABP1 present in the reaction **(Figure 3.5A and 3.5B, lanes 9 and 10)**. Furthermore, we noticed that the NS1-RBD-Cy5 enters the gel only when PABP1 is present **(Figure 3.5A, lanes 5 and 6)**. To follow up on this observation, we performed a PABP1 titration experiment with a fixed concentration of NS1-RBD-Cy5, which showed that NS1-RBD-Cy5 migrates into the gel only in the presence of PABP1 **(Figure 3.5C)**.

To confirm our results that NS1-RBD binds to the RNA-free PABP1 but not to the PABP1•poly(A) complex, we performed the polarization assay with fixed concentrations of NS1-RBD FL and PABP1 and titrating the concentration of poly(A)$_{18}$. As the concentration of poly(A)$_{18}$ is increased in the reaction, the anisotropy value decreased, indicating that more and more NS1-RBD FL is dissociating from PABP1 because PABP1 is preferentially binding to poly(A)$_{18}$ to form the PABP1•poly(A)$_{18}$ complex. More importantly, the result shows that an NS1•PABP1•poly(A)$_{18}$ complex does not form. A similar experiment with increasing concentrations of the control S17 RNA showed a smaller decrease in anisotropy, consistent with the much lower binding affinity PABP1

has for S17 **(Figure 3.7C)**. Thus, these results show that NS1 does not bind to the PABP1•poly(A) RNA complex.

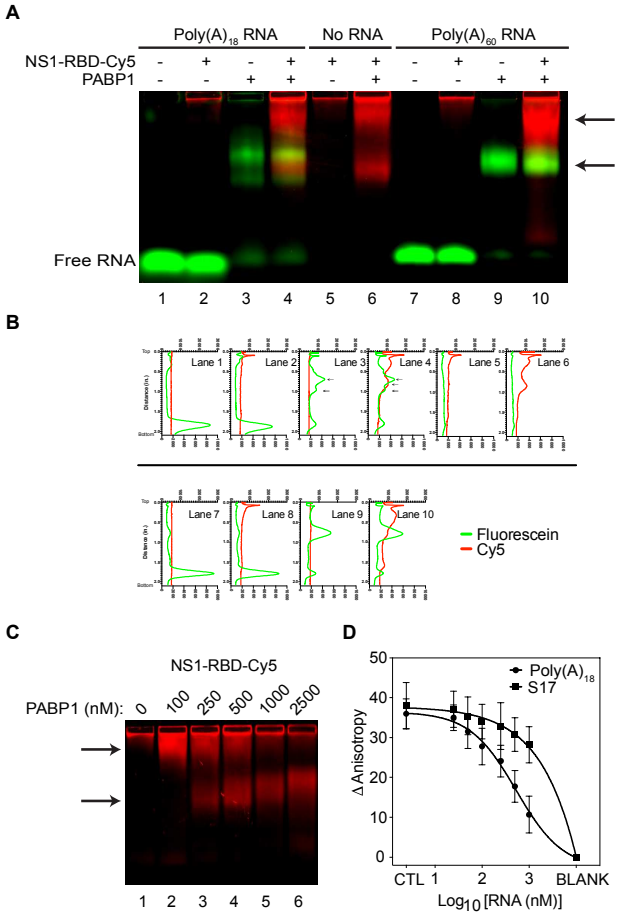

Figure 3.5: NS1 does not bind to PABP1•Poly(A)$_{18}$ complex. (A) EMSA assay of NS1-RBD labelled with Cy5 (in red) incubated with PABP1 and either Poly(A)$_{18}$ or Poly(A)$_{60}$ RNA labelled with fluorescein (in green). Minus and plus signs indicate the absence and presence of NS1, respectively. Arrows point to the shifted complexes. (B) ImageJ plot of the fluorescence intensity profile for each lane of the EMSA gel in (A). Top axis of each plot represents the intensity (in arbitrary units) of fluorescein (in green) ranging from 0 to 30,000. Bottom axis of each plot represents the intensity (in arbitrary units) of Cy5 (in red) ranging from 0 to 10,000. Left axis of each plot represents relative distance from the well (in inches) ranging from 0 to 2.1. Axes in all plots are scaled the same. (C) EMSA of NS1-RBD binding to varying PABP1 concentrations. NS1-RBD FL is labelled with Cy5. Arrows point to the shifted complexes. (D) Polarization assay with PABP1 pre-bound to NS1-RBD FL (labelled with fluorescein) in the presence of increasing amount of Poly(A)$_{18}$ RNA or S17 RNA. CTL refers to the PABP1•NS1-RBD FL complex in the absence of RNA. BLANK refers to NS1-RBD FL without PABP1 or RNA. The final concentration of the NS1-RBD FL was 10 nM, the final concentration of PABP1 was 500 nM and the final concentration of Poly(A)$_{18}$ RNA and S17 RNA were increased from 0 to 1 μM.

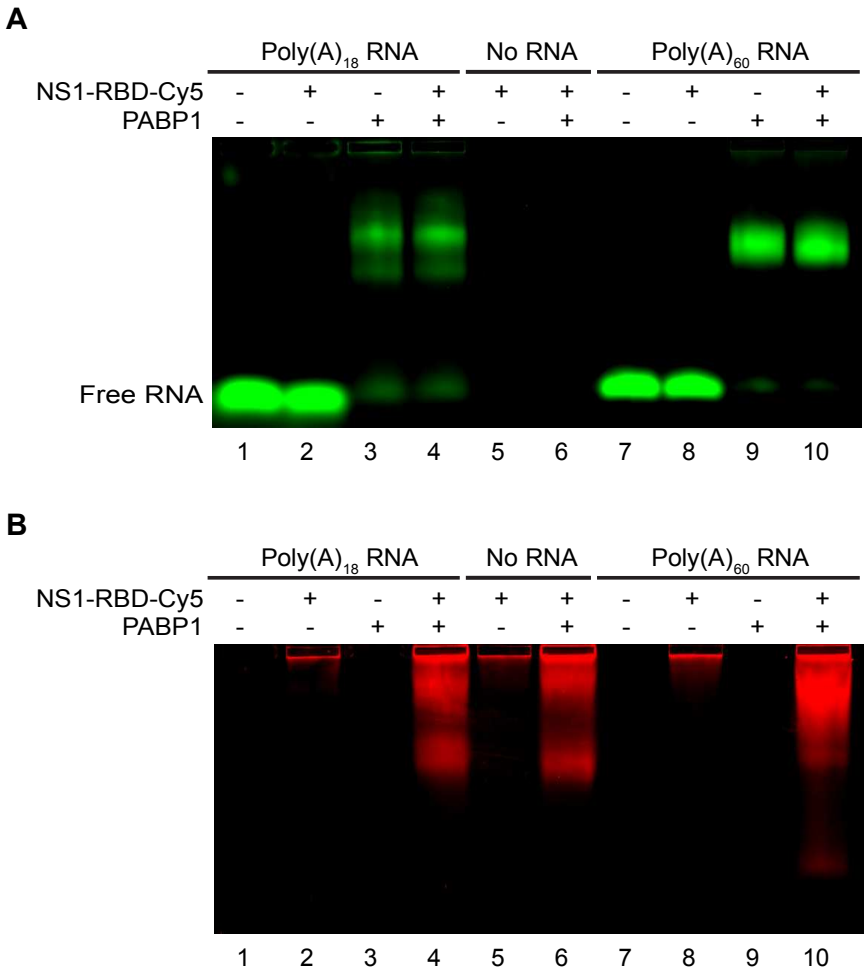

Figure 3.6. The Figure 3.5A EMSA gel showing the two color channels separately. NS1-RBD labelled with Cy5 (in red) was incubated with PABP1 and either Poly(A)$_{18}$ or Poly(A)$_{60}$ RNA labelled with fluorescein (in green). Minus and plus signs indicate the absence and presence of NS1, respectively. (A) Gel scanned to show the fluorescein dye. (B) Gel scanned to show the Cy5 dye.

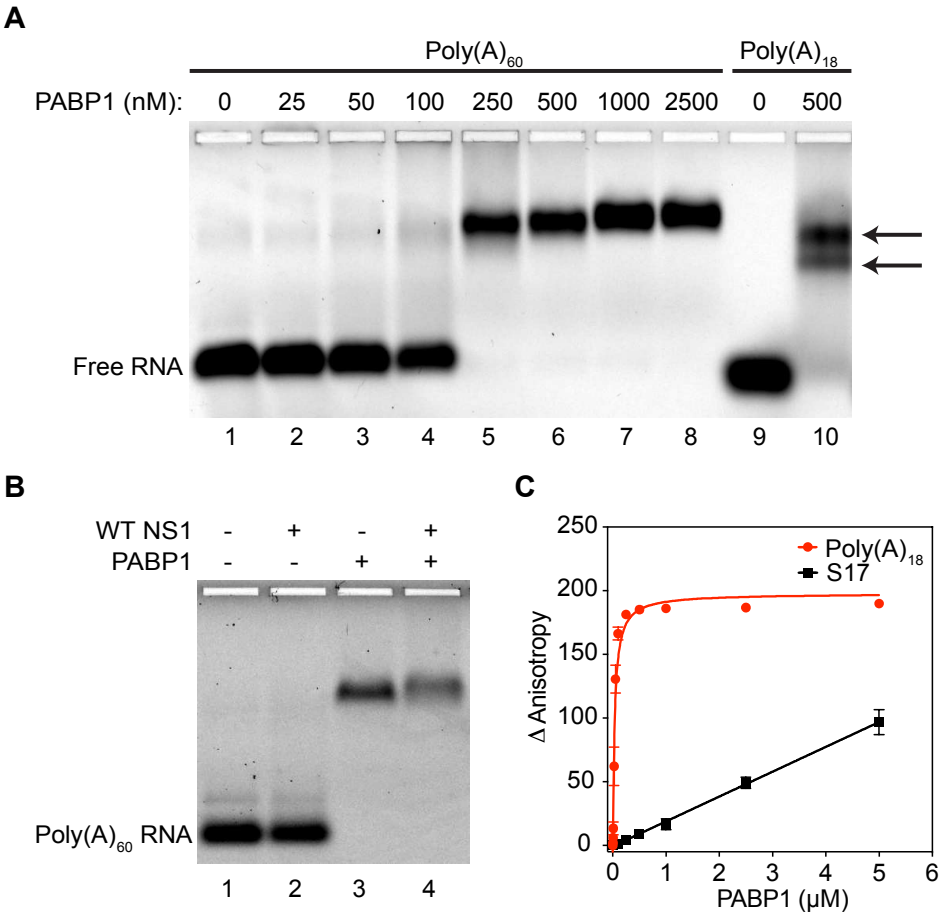

Figure 3.7: Binding of PABP1 to RNA. (A) EMSA showing the binding of PABP1 to the fluorescein-labeled poly(A)$_{60}$ RNA. The concentration of the RNA is 100 nM and the concentration of PABP1 was titrated, as indicated. Poly(A)$_{18}$ at 100 nM concentration was used as a control. The arrows indicate the PABP1 monomer and dimer bands. (B) Binding of PABP1 to Poly(A)$_{60}$ RNA in the presence or absence of excess full length H3N2 Udorn NS1 (WT NS1). (C) Polarization assay showing the binding of PABP1 to poly(A)$_{18}$ and S17 RNA. The final concentrations of the fluorescein-labeled poly(A)$_{18}$ and S17 RNA were 1 nM and 10 nM respectively, and the final concentration of NS1 was increased from 0 to 5 μM. The change in anisotropy is shown on the y-axis. The error bars represent the standard deviation from three independent experiments.

3.14 Discussion

The NS1 protein is a multifunctional protein that binds to dsRNA and to several host proteins to enable IAV to replicate efficiently in host cells.[7,40,41] NS1 can form dimers and oligomers by itself, and a long tube-like multimer that wraps around dsRNA.[42] Previous studies also showed that NS1 binds as a dimer to TRIM25, CPSF30, DHX30 and dsRNA.[28,43–45] Thus, depending on the interacting partner, NS1 displays various oligomeric states that are critical for its function.[41] Here we show that NS1 monomer cannot bind to PABP1, but NS1 that can form dimers bind to PABP1. This is not unexpected because NS1 is expressed to high levels in the infected cells and may exist predominantly as dimers or other higher-order structures.[46,47]

PABP1 is one of the most highly expressed proteins in the cell and plays an essential role during translation initiation.[11,48] PABP1 binds to the 3' poly(A) tail of mRNA and protects the mRNA from degradation by exonucleases.[49,50] Additionally, PABP1 interacts with the eIF4F complex, which is bound to the 5' 7-methyl guanosine cap structure, to bring the 5'- and 3'-ends close together to form the mRNA closed-loop structure.[51] The mRNA closed-loop structure is thought to stimulate translation by recycling the terminating ribosome back to the 5'-end of the mRNA to initiate translation.[52] PABP1 binds to poly(A) with a high affinity (K_D ~ 5 nM) and can bind to a poly(A) sequence as short as 12 nucleotides with no change in binding affinity.[34,35] Although PABP1 can bind to short poly(A) tails with high affinity using its RRM domains, PABP1 covers about 30 nucleotides because of steric occlusion by the rest of the protein.[14,34,35,39] Recent studies indicate that most mRNAs have a poly(A) tail that is 30

nt in length,[53] suggesting that only one PABP1 is directly bound to the mRNA, and possibly a second PABP1 may bind via protein-protein interaction. Our results show that NS1 cannot bind to PABP1 bound to the mRNA poly(A) tail. This suggests that the poly(A) RNA bound to the RRM domains sterically blocks the binding of NS1 to the homodimerization domain of PABP1. Alternatively, NS1 can only bind to the RNA-free PABP1 because it has a different conformation than the PABP1 bound to the poly(A) RNA. Importantly, the function of the NS1•PABP1 complex appears to be distinct from the classical role of PABP1 in translation initiation, when it is bound to the 3'-poly(A) tail of mRNA.

Previously, we showed that NS1 could not bind simultaneously to both dsRNA and PABP1.[13] The RBD of NS1 is responsible for binding to dsRNA and PABP1, and it can accommodate only one of these partners. Here, we show that NS1 binds to PABP1 free of poly(A). Thus, both proteins can interact with each other only when they are not bound to RNA. We expect PABP1 will bind to all the available mRNA poly(A) tails because the affinity of PABP1 for poly(A) is significantly higher than for NS1. However, PABP1 is present in excess over the total cellular mRNA concentration, and it is estimated that only 30% of the PABP1 molecules are bound to the poly (A) tail.[11] Thus, NS1 can interact with the large pool of PABP1 molecules that are not bound to the poly(A) RNA.

The functional significance of the interaction of NS1 with PABP1 for the life cycle of IAV is unknown. Because NS1 also interacts with eIF4G, it has been suggested that NS1 may stimulate the translation of viral mRNAs by promoting the binding of the 3' poly(A)•PABP1 complex to the eIF4F complex present at the 5'-end of the mRNA.[9,15–18]

However, our results are not consistent with this model because we show that NS1 cannot bind to PABP1 that is bound to poly(A) RNA. Interestingly, PABP1 interacts with the ribosome directly, and this interaction was shown to enhance translation in a dose-dependent manner.[54] It has been proposed that PABP1 may stimulate translation initiation by promoting the recruitment of the 40S and 60S subunits to the eIF4F initiation complex that is assembled at the 5'-end of the mRNA.[54–58] Additionally, NS1 is a general enhancer of translation, and a recent report showed that NS1 stimulates the binding of the ribosome to the mRNA.[59–61] Taken together, we propose that NS1's ability to bind to both eIF4G and the RNA-free PABP1 may be a mechanism to recruit PABP1 to the 5'-end of the mRNA. The NS1•eIF4F•PABP1 complex at the 5'-end of the mRNA may then stimulate translation by enhancing the recruitment of the ribosomal subunits to the initiation complex.

Chapter 3, in full, is a reprint of the material as it appears in Influenza A Virus NS1 Protein Binds as a Dimer to RNA-Free PABP1 but Not to the PABP1·Poly(A) RNA Complex, Biochemistry, 2020. de Rozieres, Cyrus M.; Joseph, Simpson, 2020. The dissertation author was the primary investigator and author of this paper.

References

(1) Molinari, N.-A. M.; Ortega-Sanchez, I. R.; Messonnier, M. L.; Thompson, W. W.; Wortley, P. M.; Weintraub, E.; Bridges, C. B. The Annual Impact of Seasonal Influenza in the US: Measuring Disease Burden and Costs. *Vaccine* 2007, *25* (27), 5086–5096. https://doi.org/10.1016/j.vaccine.2007.03.046.

(2) Rogers, G. N.; Paulson, J. C. Receptor Determinants of Human and Animal Influenza Virus Isolates: Differences in Receptor Specificity of the H3 Hemagglutinin Based on Species of Origin. *Virology* 1983, *127* (2), 361–373. https://doi.org/10.1016/0042-6822(83)90150-2.

(3) Wise, H. M.; Foeglein, A.; Sun, J.; Dalton, R. M.; Patel, S.; Howard, W.; Anderson, E. C.; Barclay, W. S.; Digard, P. A Complicated Message: Identification of a Novel PB1-Related Protein Translated from Influenza A Virus Segment 2 MRNA. *J. Virol.* 2009, *83* (16), 8021–8031. https://doi.org/10.1128/JVI.00826-09.

(4) Jagger, B. W.; Wise, H. M.; Kash, J. C.; Walters, K.-A.; Wills, N. M.; Xiao, Y.-L.; Dunfee, R. L.; Schwartzman, L. M.; Ozinsky, A.; Bell, G. L.; Dalton, R. M.; Lo, A.; Efstathiou, S.; Atkins, J. F.; Firth, A. E.; Taubenberger, J. K.; Digard, P. An Overlapping Protein-Coding Region in Influenza A Virus Segment 3 Modulates the Host Response. *Science* 2012, *337* (6091), 199–204. https://doi.org/10.1126/science.1222213.

(5) Lamb, R. A.; Choppin, P. W. Segment 8 of the Influenza Virus Genome Is Unique in Coding for Two Polypeptides. *Proc. Natl. Acad. Sci.* 1979, *76* (10), 4908–4912. https://doi.org/10.1073/pnas.76.10.4908.

(6) Lamb, R. A.; Choppin, P. W.; Chanock, R. M.; Lai, C. J. Mapping of the Two Overlapping Genes for Polypeptides NS1 and NS2 on RNA Segment 8 of Influenza Virus Genome. *Proc. Natl. Acad. Sci.* 1980, *77* (4), 1857–1861. https://doi.org/10.1073/pnas.77.4.1857.

(7) Hale, B. G.; Randall, R. E.; Ortín, J.; Jackson, D. The Multifunctional NS1 Protein of Influenza A Viruses. *J. Gen. Virol.* 2008, *89* (10), 2359–2376. https://doi.org/10.1099/vir.0.2008/004606-0.

(8) Hale, B. G. Conformational Plasticity of the Influenza A Virus NS1 Protein. *J. Gen. Virol.* 2014, *95* (10), 2099–2105. https://doi.org/10.1099/vir.0.066282-0.

(9) Burgui, I.; Aragón, T.; Ortín, J.; Nieto, A. PABP1 and EIF4GI Associate with Influenza Virus NS1 Protein in Viral MRNA Translation Initiation Complexes. *J. Gen. Virol.* 2003, *84* (12), 3263–3274. https://doi.org/10.1099/vir.0.19487-0.

(10) Eliseeva, I. A.; Lyabin, D. N.; Ovchinnikov, L. P. Poly(A)-Binding Proteins: Structure, Domain Organization, and Activity Regulation. *Biochem. Mosc.* 2013, *78* (13), 1377–1391. https://doi.org/10.1134/S0006297913130014.

(11) Görlach, M.; Burd, C. G.; Dreyfuss, G. The MRNA Poly(A)-Binding Protein: Localization, Abundance, and RNA-Binding Specificity. *Exp. Cell Res.* 1994, *211* (2), 400–407. https://doi.org/10.1006/excr.1994.1104.

(12) Sachs, A.; Wahle, E. Poly(A) Tail Metabolism and Function in Eucaryotes. *J. Biol. Chem.* 1993, *268* (31), 22955–22958.

(13) Arias-Mireles, B. H.; de Rozieres, C. M.; Ly, K.; Joseph, S. RNA Modulates the Interaction between Influenza A Virus NS1 and Human PABP1. *Biochemistry* 2018, *57* (26), 3590–3598. https://doi.org/10.1021/acs.biochem.8b00218.

(14) Sawazaki, R.; Imai, S.; Yokogawa, M.; Hosoda, N.; Hoshino, S.; Mio, M.; Mio, K.; Shimada, I.; Osawa, M. Characterization of the Multimeric Structure of Poly(A)-Binding Protein on a Poly(A) Tail. *Sci. Rep.* 2018, *8* (1), 1455. https://doi.org/10.1038/s41598-018-19659-6.

(15) Aragón, T.; de la Luna, S.; Novoa, I.; Carrasco, L.; Ortín, J.; Nieto, A. Eukaryotic Translation Initiation Factor 4GI Is a Cellular Target for NS1 Protein, a Translational Activator of Influenza Virus. *Mol. Cell. Biol.* 2000, *20* (17), 6259–6268. https://doi.org/10.1128/MCB.20.17.6259-6268.2000.

(16) Burgui, I.; Yángüez, E.; Sonenberg, N.; Nieto, A. Influenza Virus MRNA Translation Revisited: Is the EIF4E Cap-Binding Factor Required for Viral MRNA Translation? *J. Virol.* 2007, *81* (22), 12427–12438. https://doi.org/10.1128/JVI.01105-07.

(17) Rodriguez, P.; Pérez-Morgado, M. I.; Gonzalez, V. M.; Martín, M. E.; Nieto, A. Inhibition of Influenza Virus Replication by DNA Aptamers Targeting a Cellular Component of Translation Initiation. *Mol. Ther. - Nucleic Acids* 2016, *5*, e308. https://doi.org/10.1038/mtna.2016.20.

(18) Yángüez, E.; Nieto, A. So Similar, yet so Different: Selective Translation of Capped and Polyadenylated Viral MRNAs in the Influenza Virus Infected Cell. *Virus Res.* 2011, *156* (1–2), 1–12. https://doi.org/10.1016/j.virusres.2010.12.016.

(19) Weeks, S. D.; Drinker, M.; Loll, P. J. Ligation Independent Cloning Vectors for Expression of SUMO Fusions. *Protein Expr. Purif.* 2007, *53* (1), 40–50. https://doi.org/10.1016/j.pep.2006.12.006.

(20) Schneider, C. A.; Rasband, W. S.; Eliceiri, K. W. NIH Image to ImageJ: 25 Years of Image Analysis. *Nat. Methods* 2012, *9* (7), 671–675. https://doi.org/10.1038/nmeth.2089.

(21) Cho, E. J.; Xia, S.; Ma, L.-C.; Robertus, J.; Krug, R. M.; Anslyn, E. V.; Montelione, G. T.; Ellington, A. D. Identification of Influenza Virus Inhibitors Targeting NS1A Utilizing Fluorescence Polarization–Based High-Throughput Assay. *J. Biomol. Screen.* 2012, *17* (4), 448–459. https://doi.org/10.1177/1087057111431488.

(22) Pollard, T. D. A Guide to Simple and Informative Binding Assays. *Mol. Biol. Cell* 2010, *21* (23), 4061–4067. https://doi.org/10.1091/mbc.E10-08-0683.

(23) Eschenfeldt, W. H.; Maltseva, N.; Stols, L.; Donnelly, M. I.; Gu, M.; Nocek, B.; Tan, K.; Kim, Y.; Joachimiak, A. Cleavable C-Terminal His-Tag Vectors for Structure Determination. *J. Struct. Funct. Genomics* 2010, *11* (1), 31–39. https://doi.org/10.1007/s10969-010-9082-y.

(24) Eschenfeldt, W. H.; Lucy, S.; Millard, C. S.; Joachimiak, A.; Mark, I. D. A Family of LIC Vectors for High-Throughput Cloning and Purification of Proteins. In *High Throughput Protein Expression and Purification*; Doyle, S. A., Ed.; Walker, J. M., Series Ed.; Methods in Molecular Biology; Humana Press: Totowa, NJ, 2009; Vol. 498, pp 105–115. https://doi.org/10.1007/978-1-59745-196-3_7.

(25) Chen, E.; Sharma, M. R.; Shi, X.; Agrawal, R. K.; Joseph, S. Fragile X Mental Retardation Protein Regulates Translation by Binding Directly to the Ribosome. *Mol. Cell* 2014, *54* (3), 407–417. https://doi.org/10.1016/j.molcel.2014.03.023.

(26) Nemeroff, M. E.; Qian, X. Y.; Krug, R. M. The Influenza Virus NS1 Protein Forms Multimers in Vitro and in Vivo. *Virology* 1995, *212* (2), 422–428. https://doi.org/10.1006/viro.1995.1499.

(27) Wang, W.; Riedel, K.; Lynch, P.; Chien, C.-Y.; Montelione, G. T.; Krug, R. M. RNA Binding by the Novel Helical Domain of the Influenza Virus NS1 Protein Requires Its Dimer Structure and a Small Number of Specific Basic Amino Acids. *RNA* 1999, *5* (2), 195–205. https://doi.org/10.1017/S1355838299981621.

(28) Das, K.; Ma, L.-C.; Xiao, R.; Radvansky, B.; Aramini, J.; Zhao, L.; Marklund, J.; Kuo, R.-L.; Twu, K. Y.; Arnold, E.; Krug, R. M.; Montelione, G. T. Structural Basis for Suppression of a Host Antiviral Response by Influenza A Virus. *Proc. Natl. Acad. Sci.* 2008, *105* (35), 13093–13098. https://doi.org/10.1073/pnas.0805213105.

(29) Cheng, A.; Wong, S. M.; Yuan, Y. A. Structural Basis for DsRNA Recognition by NS1 Protein of Influenza A Virus. *Cell Res.* 2009, *19* (2), 187–195. https://doi.org/10.1038/cr.2008.288.

(30) Held, P. Quantitation of Peptides and Amino Acids with a Synergy^{TM}HT using UV Fluorescence

https://www.biotek.com/resources/docs/Synergy_HT_Quantitation_of_Peptides_and_Amino_Acids.pdf.

(31) Wilcox, W.; Eisenberg, D. Thermodynamics of Melittin Tetramerization Determined by Circular Dichroism and Implications for Protein Folding. *Protein Sci.* 1992, *1* (5), 641–653. https://doi.org/10.1002/pro.5560010510.

(32) Kumar, S.; Swaminathan, R. Employing the Fluorescence Anisotropy and Quenching Kinetics of Tryptophan to Hunt for Residual Structures in Denatured Proteins. *J. Chem. Sci.* 2007, *119* (2), 141–145. https://doi.org/10.1007/s12039-007-0021-9.

(33) Held, P.; Davis, K. UV Fluorescence Polarization as a Means to Investigate Protein Conformational and Mass Change https://www.biotek.com/resources/application-notes/uv-fluorescence-polarization-as-a-means-to-investigate-protein-conformational-and-mass-change-using-intrinsic-tryptophan-fluorescence-in-conjunction-with-uv-capable-polarizers/.

(34) Sachs, A. B.; Davis, R. W.; Kornberg, R. D. A Single Domain of Yeast Poly(A)-Binding Protein Is Necessary and Sufficient for RNA Binding and Cell Viability. *Mol. Cell. Biol.* 1987, *7* (9), 3268–3276. https://doi.org/10.1128/mcb.7.9.3268.

(35) Kühn, U.; Pieler, T. Xenopus Poly(A) Binding Protein: Functional Domains in RNA Binding and Protein-Protein Interaction. *J. Mol. Biol.* 1996, *256* (1), 20–30. https://doi.org/10.1006/jmbi.1996.0065.

(36) Lin, J.; Fabian, M.; Sonenberg, N.; Meller, A. Nanopore Detachment Kinetics of Poly(A) Binding Proteins from RNA Molecules Reveals the Critical Role of C-Terminus Interactions. *Biophys. J.* 2012, *102* (6), 1427–1434. https://doi.org/10.1016/j.bpj.2012.02.025.

(37) Melo, E. O.; Dhalia, R.; Martins de Sa, C.; Standart, N.; de Melo Neto, O. P. Identification of a C-Terminal Poly(A)-Binding Protein (PABP)-PABP Interaction Domain: Role in Cooperative Binding to Poly (A) and Efficient Cap Distal Translational Repression. *J. Biol. Chem.* 2003, *278* (47), 46357–46368. https://doi.org/10.1074/jbc.M307624200.

(38) Forman-Kay, J. D.; Mittag, T. From Sequence and Forces to Structure, Function, and Evolution of Intrinsically Disordered Proteins. *Structure* 2013, *21* (9), 1492–1499. https://doi.org/10.1016/j.str.2013.08.001.

(39) Baer, B. W.; Kornberg, R. D. The Protein Responsible for the Repeating Structure of Cytoplasmic Poly(A)-Ribonucleoprotein. *J. Cell Biol.* 1983, *96* (3), 717–721. https://doi.org/10.1083/jcb.96.3.717.

(40) Rückle, A.; Haasbach, E.; Julkunen, I.; Planz, O.; Ehrhardt, C.; Ludwig, S. The NS1 Protein of Influenza A Virus Blocks RIG-I-Mediated Activation of the Noncanonical NF-KB Pathway and P52/RelB-Dependent Gene Expression in Lung Epithelial Cells. *J. Virol.* 2012, *86* (18), 10211–10217. https://doi.org/10.1128/JVI.00323-12.

(41) Ayllon, J.; Russell, R. J.; García-Sastre, A.; Hale, B. G. Contribution of NS1 Effector Domain Dimerization to Influenza A Virus Replication and Virulence. *J. Virol.* 2012, *86* (23), 13095–13098. https://doi.org/10.1128/JVI.02237-12.

(42) Bornholdt, Z. A.; Prasad, B. V. V. X-Ray Structure of NS1 from a Highly Pathogenic H5N1 Influenza Virus. *Nature* 2008, *456* (7224), 985–988. https://doi.org/10.1038/nature07444.

(43) Koliopoulos, M. G.; Lethier, M.; van der Veen, A. G.; Haubrich, K.; Hennig, J.; Kowalinski, E.; Stevens, R. V.; Martin, S. R.; Reis e Sousa, C.; Cusack, S.; Rittinger, K. Molecular Mechanism of Influenza A NS1-Mediated TRIM25 Recognition and Inhibition. *Nat. Commun.* 2018, *9* (1), 1820. https://doi.org/10.1038/s41467-018-04214-8.

(44) Chen, G.; Ma, L.-C.; Wang, S.; Woltz, R. L.; Grasso, E. M.; Montelione, G. T.; Krug, R. M. A Double-Stranded RNA Platform Is Required for the Interaction between a Host Restriction Factor and the NS1 Protein of Influenza A Virus. *Nucleic Acids Res.* 2020, *48* (1), 304–315. https://doi.org/10.1093/nar/gkz1094.

(45) Chien, C.; Xu, Y.; Xiao, R.; Aramini, J. M.; Sahasrabudhe, P. V.; Krug, R. M.; Montelione, G. T. Biophysical Characterization of the Complex between Double-Stranded RNA and the N-Terminal Domain of the NS1 Protein from Influenza A Virus: Evidence for a Novel RNA-Binding Mode †. *Biochemistry* 2004, *43* (7), 1950–1962. https://doi.org/10.1021/bi030176o.

(46) Kummer, S.; Flöttmann, M.; Schwanhäusser, B.; Sieben, C.; Veit, M.; Selbach, M.; Klipp, E.; Herrmann, A. Alteration of Protein Levels during Influenza Virus H1N1 Infection in Host Cells: A Proteomic Survey of Host and Virus Reveals Differential Dynamics. *PLoS ONE* 2014, *9* (4), e94257. https://doi.org/10.1371/journal.pone.0094257.

(47) Shapiro, G. I.; Gurney, T.; Krug, R. M. Influenza Virus Gene Expression: Control Mechanisms at Early and Late Times of Infection and Nuclear-Cytoplasmic Transport of Virus-Specific RNAs. *J. Virol.* 1987, *61* (3), 764–773. https://doi.org/10.1128/JVI.61.3.764-773.1987.

(48) Jackson, R. J.; Hellen, C. U. T.; Pestova, T. V. The Mechanism of Eukaryotic Translation Initiation and Principles of Its Regulation. *Nat. Rev. Mol. Cell Biol.* 2010, *11* (2), 113–127. https://doi.org/10.1038/nrm2838.

(49) Bernstein, P.; Peltz, S. W.; Ross, J. The Poly(A)-Poly(A)-Binding Protein Complex Is a Major Determinant of MRNA Stability in Vitro. *Mol. Cell. Biol.* 1989, *9* (2), 659–670. https://doi.org/10.1128/mcb.9.2.659.

(50) Ford, L. P.; Bagga, P. S.; Wilusz, J. The Poly(A) Tail Inhibits the Assembly of a 3'-to-5' Exonuclease in an in Vitro RNA Stability System. *Mol. Cell. Biol.* 1997, *17* (1), 398–406. https://doi.org/10.1128/mcb.17.1.398.

(51) Vicens, Q.; Kieft, J. S.; Rissland, O. S. Revisiting the Closed-Loop Model and the Nature of MRNA 5′–3′ Communication. *Mol. Cell* 2018, *72* (5), 805–812. https://doi.org/10.1016/j.molcel.2018.10.047.

(52) Archer, S. K.; Shirokikh, N. E.; Hallwirth, C. V.; Beilharz, T. H.; Preiss, T. Probing the Closed-Loop Model of MRNA Translation in Living Cells. *RNA Biol.* 2015, *12* (3), 248–254. https://doi.org/10.1080/15476286.2015.1017242.

(53) Lima, S. A.; Chipman, L. B.; Nicholson, A. L.; Chen, Y.-H.; Yee, B. A.; Yeo, G. W.; Coller, J.; Pasquinelli, A. E. Short Poly(A) Tails Are a Conserved Feature of Highly Expressed Genes. *Nat. Struct. Mol. Biol.* 2017, *24* (12), 1057–1063. https://doi.org/10.1038/nsmb.3499.

(54) Machida, K.; Shigeta, T.; Yamamoto, Y.; Ito, T.; Svitkin, Y.; Sonenberg, N.; Imataka, H. Dynamic Interaction of Poly(A)-Binding Protein with the Ribosome. *Sci. Rep.* 2018, *8* (1), 17435. https://doi.org/10.1038/s41598-018-35753-1.

(55) Sachs, A. B.; Davis, R. W. The Poly(A) Binding Protein Is Required for Poly(A) Shortening and 60S Ribosomal Subunit-Dependent Translation Initiation. *Cell* 1989, *58* (5), 857–867. https://doi.org/10.1016/0092-8674(89)90938-0.

(56) Kahvejian, A.; Svitkin, Y. V.; Sukarieh, R.; M'Boutchou, M.-N.; Sonenberg, N. Mammalian Poly(A)-Binding Protein Is a Eukaryotic Translation Initiation Factor, Which Acts via Multiple Mechanisms. *Genes Dev.* 2005, *19* (1), 104–113. https://doi.org/10.1101/gad.1262905.

(57) Searfoss, A.; Dever, T. E.; Wickner, R. Linking the 3' Poly(A) Tail to the Subunit Joining Step of Translation Initiation: Relations of Pab1p, Eukaryotic Translation Initiation Factor 5b (Fun12p), and Ski2p-Slh1p. *Mol. Cell. Biol.* 2001, *21* (15), 4900–4908. https://doi.org/10.1128/MCB.21.15.4900-4908.2001.

(58) Tarun, S. Z.; Sachs, A. B. A Common Function for MRNA 5' and 3' Ends in Translation Initiation in Yeast. *Genes Dev.* 1995, *9* (23), 2997–3007. https://doi.org/10.1101/gad.9.23.2997.

(59) Panthu, B.; Terrier, O.; Carron, C.; Traversier, A.; Corbin, A.; Balvay, L.; Lina, B.; Rosa-Calatrava, M.; Ohlmann, T. The NS1 Protein from Influenza Virus Stimulates Translation Initiation by Enhancing Ribosome Recruitment to MRNAs.

J. Mol. Biol. 2017, *429* (21), 3334–3352. https://doi.org/10.1016/j.jmb.2017.04.007.

(60) Anastasina, M.; Terenin, I.; Butcher, S. J.; Kainov, D. E. A Technique to Increase Protein Yield in a Rabbit Reticulocyte Lysate Translation System. *BioTechniques* 2014, *56* (1). https://doi.org/10.2144/000114125.

(61) Kainov, D. E.; Müller, K. H.; Theisen, L. L.; Anastasina, M.; Kaloinen, M.; Muller, C. P. Differential Effects of NS1 Proteins of Human Pandemic H1N1/2009, Avian Highly Pathogenic H5N1, and Low Pathogenic H5N2 Influenza A Viruses on Cellular Pre-MRNA Polyadenylation and MRNA Translation. *J. Biol. Chem.* 2011, *286* (9), 7239–7247. https://doi.org/10.1074/jbc.M110.203489.

Chapter 4: Conclusions and Future Directions

Characterization of the interactions between the different components involved in translation initiation of IAV mRNAs proposes new and exciting avenues of research. My studies showed that: (1) PABP1 binds to the different IAV 5'UTRs with varying affinities, (2) translation of mRNAs having the IAV 5'UTR is resistant to eIF4E inhibition, and (3) PABP1 is enriched at the IAV 5'UTRs in vivo suggesting that IAV may use the viral 5'UTRs as an IRES to selectively translate viral mRNAs. This potential mechanism warrants further research as it could provide more insight into IAV replication as well as guide new approaches to suppress IAV infection. Second, the binding between NS1 and PABP1 must be investigated further to determine how the two molecules bind in order to better understand what role their interaction plays during infection.

Our studies investigating why IAV targets PABP1 led us to uncover the significant binding affinity PABP1 has for the viral 5'UTRs. Conservation analysis of these regions across thousands of unique IAV sequences suggests that each 5'UTR is sensitive to changes, pointing to the importance of the 5' UTR for the viability and proliferation of IAV [1]. These sequences have high adenosine content which can be targeted by PABP1. The varying binding affinities (K_D) PABP1 has for each 5' UTR sequence are all well below the 4 μM intracellular concentration of PABP1, and thus predict that PABP1 is likely to bind these sequences *in vivo* [2]. Furthermore, the measured affinities of PABP1 for the 5' UTRs of the eight RNA segments were found to correlate with the reported protein levels translated from those mRNAs [3,4].

The *in vitro* translation studies investigating the suppression of cap-dependent translation led us to discover a resistance to inhibition of mRNAs driven by the IAV 5'UTRs compared to model host mRNA [5,6]. We also observed a positive correlation

between the affinity PABP1 has for the viral 5' UTR sequence and protein synthesis of the reporter mRNAs when cap-dependent translation was suppressed. This further points to the possibility that IAV utilizes the 5' UTR as an IRES.

Finally, our PABP1 pulldown studies and RT-qPCR analysis found an enrichment of 5'UTR-containing fragments relative to CDS fragments of the HA, NA, NP and PB1 RNA segments. The relative levels of 5' end fragments measured were significantly more enriched than those of Actin and Tubulin, which we assume only undergoes canonical cap-dependent translation. This study further suggests that PABP1 is indeed located on the 5' ends of viral mRNA segments during infection. These findings put together suggests that PABP1 is selectively initiating certain viral mRNAs over others in order meet the needs for successful IAV replication.

Further investigation is necessary to understand whether, and under what conditions, IAV may utilize PABP1 in a cap-independent manner. This mechanism may be more favored under conditions of host stress where cap-dependent translation is suppressed [7]. It has already been shown that viral protein production is unaffected when infected cells are depleted of eIF4E [8]. Furthermore, PABP1 has been reported by several groups to be located on adenosine-rich stretches at the 5' end of mRNAs in yeast during stress [9] and even under normal conditions of eukaryotic cells as elucidated by CLIP-Seq [10]. Investigations via NGS studying the location of PABP1 during infection would be an invaluable step towards better demonstrating whether PABP1 is actively found on IAV 5'UTRs. NGS-based methods would not only help corroborate the RT-qPCR results but also show the relative abundance and distribution of the 8 viral 5'UTRs pulled down by PABP1. Coupled with studies examining how the abundance of

5’UTR sequences change when subjected to cap-dependent translational suppression by using rapamycin, would go a long way towards supporting the model that IAV utilizes alternative mechanisms to initiate translation of its chosen RNAs.

Furthermore, our studies suggest that RNAs driven solely by the 5’UTR without the cap-snatched sequence translate as well as RNAs with the cap-snatched sequence. This observation raises the question of whether the method of translation and translation initiation are temporally regulated during the course of IAV infection. While some studies suggest that viral cRNAs are not present in high abundance compared to viral mRNAs [11], more recent sequencing-based studies seem to suggest that cRNAs may make up a significant portion of total RNAs during late stages of infection [12]. In the context of our work this might suggest that the cRNAs potentially serve as templates for both transcription and translation. To test this particular IRES-like driven mechanism proposed by our studies, targeted experiments must be done to determine whether or not PABP1 can be found specifically on the 5’ end of cRNAs.

Another question to arise from our studies is based on the high conservation found in the 5’ UTR sequences of each viral segment. Our studies suggest this sequence is important for modulating the rates of translation initiation and thus synthesis of the different viral proteins during infection. A follow up study to test this hypothesis would be to swap the 5' UTRs of one viral RNA segment for another. A system of transfecting 293T cells with eight plasmids each containing one of the vRNAs has been successful in producing infectious viral particles [13]. These plasmids can be modified to change any aspect of the vRNA sequence to study the effects of each change on viral proliferation. Such a system could thus be used to study how production

of one or several of the major viral proteins change if the UTR of one vRNA segment was swapped with another. The influence these changes have on protein production can then be assayed quantitatively with an ELISA or other comparable protein quantification method.

The other avenue of research to come out of our investigations identified certain conditions under which NS1 can successfully bind to PABP1. Previous studies have demonstrated that NS1 cannot bind to both PABP1 and dsRNA simultaneously [14]. Our investigations further demonstrate that despite the multiple oligomeric states adopted by NS1, it is the dimeric state that binds to PABP1 [15,16]. Furthermore, binding of NS1 to PABP1 can only occur in the absence of poly(A) sequences, suggesting NS1's role in binding to PABP1 is independent of the canonical translation initiation process.

Follow up studies on this interaction should look towards the exact mechanism NS1 employs to bind to PABP1. The original reports on the NS1 – PABP1 complex were able to identify the intrinsically-disordered homodimerization domain of PABP1 as the NS1-binding region [17]. Using the binding assay developed to study the affinity between NS1-RBD and PABP1 [16], one could measure how much the affinity between NS1 and PABP1 changes when different regions of the homodimerization domain are mutated (e.g. via alanine scanning) or deleted. While certain deletions may cause large changes in affinity, results may not always be consistent due to global changes in protein folding and stability. Therefore, to complement deletion studies, different regions of the homodimerization domain could be purified and used in fluorescence anisotropy experiments with NS1-RBD.

There is the possibility that NS1 does not completely discriminate across different portions of the PABP1 homodimerization domain. Indeed our investigations suggested that the interaction between NS1 and PABP1 is predominantly stabilized by electrostatic forces [16]. Given that the homodimerization domain of PABP1 contains a somewhat even distribution of positively charged residues, almost every region tested for binding to NS1-RBD could be expected to have some level of affinity if our hypothesis is correct. This would further implicate the negatively charged residues of NS1 as residues necessary for binding to PABP1.

During the course of our NS1-RBD and PABP1 binding studies, we made an additional discovery that might further help characterize the interaction. When using an NS1-RBD construct with a native N-terminus, we observed binding to PABP1 via EMSA. However, when we used an NS1-RBD construct with a hexahistidine tag upstream of the N-terminus, we did not observe binding to PABP1 via EMSA (data not shown). Coupling the clues from the results presented thus far of the NS1-PABP1 interaction with evidence that an N-terminal hexahistidine tag prevents the interaction from occurring may help identify the important residues involved in the interaction between NS1 and PABP1. NS1-RBD has eleven negatively charged residues in its primary sequence at positions 2, 12, 24, 26, 29, 34, 39, 55, 66, 71 and 72; many of which are involved in salt bridges important for the secondary structure. However, based on crystal structures of the NS1-RBD dimer, Asp2, Asp24 and Glu26 are all solvent-exposed and close enough to the N-terminus to be affected by any steric hindrance caused by an N-terminal hexahistidine sequence [18]. Mutational studies of these negatively charged residues on NS1 may be the quickest and most effective

approach to identify the residues that mediate NS1 binding to PABP1. These NS1 residues could then be targeted in a reverse genetics approach to elucidate the significance of the NS1 – PABP1 interaction during infection. This could be performed via the aforementioned eight plasmid system by mutating the necessary residues of the NS1 plasmid, transfecting the 8 plasmids encoding the eight viral proteins into mammalian cells, and monitoring virus production and virulence when NS1 cannot bind to PABP1 [13]. Finally, the NS1-RBD – PABP1 fluorescence anisotropy assay can then be employed to screen therapeutic candidates that target the key interaction residues with the goal of potentially treating cases of influenza in humans [16].

While previous investigations suggested that a minimum of a dimer of NS1 is necessary to bind to PABP1, it is unclear whether or not multiple NS1 proteins are capable of oligomerizing and assembling onto the homodimerization domain of PABP1. In light of the preliminary experiments suggesting NS1 potentially has multiple binding sites to PABP1, this opens up an exciting opportunity to potentially use structure-based approaches to better understand this interaction. While the structure of NS1 has been solved via both X-ray crystallography and solution NMR spectroscopy [19–22], structure-based methods have only been able to elucidate the RRMs and PABC portions of PABP1 in the absence of its homodimerization domain [23–25]. Our investigations into NS1 – PABP1 open up an opportunity to not only visualize the binding mode between these two proteins but also provide a more complete structure of PABP1. Given that the PABP1 homodimerization domain is intrinsically disordered, it is challenging to visualize with current techniques. It is possible that NS1 binding to this region could stabilize it enough to be captured by modern cryo-EM technology [26]. The minimum size of NS1-

PABP1 is expected to be at least 124 kDa, which is larger than the current minimum size limit cryo-EM can resolve of ~ 50 kDa [27]. Future endeavors in pursuit of this structure would contribute greatly to the understanding of influenza biology as well as eukaryotic translation initiation.

Finally, the question still remains why NS1 targets PABP1 and how that contributes to the reported enhancement of viral mRNA translation. We have described the potential importance of PABP1 acting as a translation initiation factor on the 5' end of the viral mRNA in an IRES-like fashion. Future studies with NS1 should look into whether the combination of the two enhances that effect further.

Approaches to understand this relationship can utilize a variation of the pulldown approach used to study PABP1 and the 5'UTRs. Experiments using infected cells selecting for PABP1 followed by NS1 have shown that these two proteins interact with each other *in vivo* [28]. A pulldown method selecting for complexes that contain both proteins could be designed to examine this interaction. Furthermore, if any RNAs are also pulled down, they could be analyzed with NGS to provide clues further characterizing this protein-protein interaction.

The *in vitro* translation assay is another method that could be useful for understanding this interaction. Previous studies in rabbit reticulocyte lysate identified that the presence of NS1can enhance the translation of luciferase mRNA depending on its 5'UTR sequence [29–31]. Additionally, our studies in HeLa lysate suggest that the viral 5'UTRs impart a resistance to cap-dependent translation suppression on their own. While NS1 has been shown to drive the expression of a variety of 5'UTR-driven sequences, there is still little evidence as to whether it has this effect on viral mRNAs in

a human system. Therefore, coupling the HeLa based *in vitro* translation system of IAV 5'UTR driven mRNAs in the presence of NS1 could help link the stage of infection at which NS1 – PABP1 is useful for IAV.

Given that NS1 has been shown to bind to eIF4G and the ribosome, biochemical and *in vivo* approaches should also examine the nature and significance of this interaction [17,31]. Many of the experiments reported and proposed to study NS1 – PABP1 can also be applied to understand the interactions between NS1 and the other initiation factors. Should NS1 be found as part of a complex with the eukaryotic translation initiation factors, single-molecule spectroscopy could be used to study the translation initiation in the context of IAV [32,33].

In conclusion, a great deal of work remains to elucidate the dynamic processes of translation and translation initiation in the context of viral infection. Some of this work may provide solely a mechanistic understanding of the IAV life cycle and translation while other work may lead to new avenues of therapeutic research. What is clear is that IAV and viruses in general continue to evolve new ways of infecting and manipulating their host cellular machinery, but by relentlessly pursuing them we can better understand biological processes and promote human health.

References

(1) Furuse, Y.; Oshitani, H. Evolution of the Influenza A Virus Untranslated Regions. *Infect. Genet. Evol.* **2011**, *11* (5), 1150–1154. https://doi.org/10.1016/j.meegid.2011.04.006.

(2) Görlach, M.; Burd, C. G.; Dreyfuss, G. The MRNA Poly(A)-Binding Protein: Localization, Abundance, and RNA-Binding Specificity. *Exp. Cell Res.* **1994**, *211* (2), 400–407. https://doi.org/10.1006/excr.1994.1104.

(3) Kummer, S.; Flöttmann, M.; Schwanhäusser, B.; Sieben, C.; Veit, M.; Selbach, M.; Klipp, E.; Herrmann, A. Alteration of Protein Levels during Influenza Virus H1N1 Infection in Host Cells: A Proteomic Survey of Host and Virus Reveals Differential Dynamics. *PLoS ONE* **2014**, *9* (4), e94257. https://doi.org/10.1371/journal.pone.0094257.

(4) Bogdanow, B.; Wang, X.; Eichelbaum, K.; Sadewasser, A.; Husic, I.; Paki, K.; Budt, M.; Hergeselle, M.; Vetter, B.; Hou, J.; Chen, W.; Wiebusch, L.; Meyer, I. M.; Wolff, T.; Selbach, M. The Dynamic Proteome of Influenza A Virus Infection Identifies M Segment Splicing as a Host Range Determinant. *Nat. Commun.* **2019**, *10* (1), 5518. https://doi.org/10.1038/s41467-019-13520-8.

(5) Kozak, M. Compilation and Analysis of Sequences Upstream from the Translational Start Site in Eukaryotic MRNAs. *Nucleic Acids Res.* **1984**, *12* (2), 857–872. https://doi.org/10.1093/nar/12.2.857.

(6) Kozak, M. Structural Features in Eukaryotic MRNAs That Modulate the Initiation of Translation. *J. Biol. Chem.* **1991**, *266* (30), 19867–19870.

(7) Liu, B.; Qian, S.-B. Translational Reprogramming in Cellular Stress Response: Translational Reprogramming in Stress. *Wiley Interdiscip. Rev. RNA* **2014**, *5* (3), 301–305. https://doi.org/10.1002/wrna.1212.

(8) Burgui, I.; Yángüez, E.; Sonenberg, N.; Nieto, A. Influenza Virus MRNA Translation Revisited: Is the EIF4E Cap-Binding Factor Required for Viral MRNA Translation? *J. Virol.* **2007**, *81* (22), 12427–12438. https://doi.org/10.1128/JVI.01105-07.

(9) Gilbert, W. V.; Zhou, K.; Butler, T. K.; Doudna, J. A. Cap-Independent Translation Is Required for Starvation-Induced Differentiation in Yeast. *Science* **2007**, *317* (5842), 1224–1227. https://doi.org/10.1126/science.1144467.

(10) Kini, H. K.; Silverman, I. M.; Ji, X.; Gregory, B. D.; Liebhaber, S. A. Cytoplasmic Poly(A) Binding Protein-1 Binds to Genomically Encoded Sequences within Mammalian MRNAs. *RNA* **2016**, *22* (1), 61–74. https://doi.org/10.1261/rna.053447.115.

(11) Shapiro, G. I.; Gurney, T.; Krug, R. M. Influenza Virus Gene Expression: Control Mechanisms at Early and Late Times of Infection and Nuclear-Cytoplasmic Transport of Virus-Specific RNAs. *J. Virol.* **1987**, *61* (3), 764–773. https://doi.org/10.1128/JVI.61.3.764-773.1987.

(12) Phan, T.; Fay, E. J.; Lee, Z.; Aron, S.; Hu, W.-S.; Langlois, R. A. Segment-Specific Kinetics of MRNA, CRNA and VRNA Accumulation during Influenza Infection. *J. Virol.* **2021**, JVI.02102-20, jvi;JVI.02102-20v1. https://doi.org/10.1128/JVI.02102-20.

(13) Neumann, G.; Watanabe, T.; Ito, H.; Watanabe, S.; Goto, H.; Gao, P.; Hughes, M.; Perez, D. R.; Donis, R.; Hoffmann, E.; Hobom, G.; Kawaoka, Y. Generation of Influenza A Viruses Entirely from Cloned CDNAs. *Proc. Natl. Acad. Sci.* **1999**, *96* (16), 9345–9350. https://doi.org/10.1073/pnas.96.16.9345.

(14) Arias-Mireles, B. H.; de Rozieres, C. M.; Ly, K.; Joseph, S. RNA Modulates the Interaction between Influenza A Virus NS1 and Human PABP1. *Biochemistry* **2018**, *57* (26), 3590–3598. https://doi.org/10.1021/acs.biochem.8b00218.

(15) Nemeroff, M. E.; Qian, X. Y.; Krug, R. M. The Influenza Virus NS1 Protein Forms Multimers in Vitro and in Vivo. *Virology* **1995**, *212* (2), 422–428. https://doi.org/10.1006/viro.1995.1499.

(16) de Rozières, C. M.; Joseph, S. Influenza A Virus NS1 Protein Binds as a Dimer to RNA-Free PABP1 but Not to the PABP1·Poly(A) RNA Complex. *Biochemistry* **2020**, *59* (46), 4439–4448. https://doi.org/10.1021/acs.biochem.0c00666.

(17) Burgui, I.; Aragón, T.; Ortín, J.; Nieto, A. PABP1 and EIF4GI Associate with Influenza Virus NS1 Protein in Viral MRNA Translation Initiation Complexes. *J. Gen. Virol.* **2003**, *84* (12), 3263–3274. https://doi.org/10.1099/vir.0.19487-0.

(18) Chien, C. Y.; Tejero, R.; Huang, Y.; Zimmerman, D. E.; Ríos, C. B.; Krug, R. M.; Montelione, G. T. A Novel RNA-Binding Motif in Influenza A Virus Non-Structural Protein 1. *Nat. Struct. Biol.* **1997**, *4* (11), 891–895. https://doi.org/10.1038/nsb1197-891.

(19) Bornholdt, Z. A.; Prasad, B. V. V. X-Ray Structure of NS1 from a Highly Pathogenic H5N1 Influenza Virus. *Nature* **2008**, *456* (7224), 985–988. https://doi.org/10.1038/nature07444.

(20) Bornholdt, Z. A.; Prasad, B. V. V. X-Ray Structure of Influenza Virus NS1 Effector Domain. *Nat. Struct. Mol. Biol.* **2006**, *13* (6), 559–560. https://doi.org/10.1038/nsmb1099.

(21) Chien, C.; Xu, Y.; Xiao, R.; Aramini, J. M.; Sahasrabudhe, P. V.; Krug, R. M.; Montelione, G. T. Biophysical Characterization of the Complex between Double-Stranded RNA and the N-Terminal Domain of the NS1 Protein from Influenza A Virus: Evidence for a Novel RNA-Binding Mode †. *Biochemistry* **2004**, *43* (7), 1950–1962. https://doi.org/10.1021/bi030176o.

(22) Wang, W.; Riedel, K.; Lynch, P.; Chien, C.-Y.; Montelione, G. T.; Krug, R. M. RNA Binding by the Novel Helical Domain of the Influenza Virus NS1 Protein Requires Its Dimer Structure and a Small Number of Specific Basic Amino Acids. *RNA* **1999**, *5* (2), 195–205. https://doi.org/10.1017/S1355838299981621.

(23) Safaee, N.; Kozlov, G.; Noronha, A. M.; Xie, J.; Wilds, C. J.; Gehring, K. Interdomain Allostery Promotes Assembly of the Poly(A) MRNA Complex with PABP and EIF4G. *Mol. Cell* **2012**, *48* (3), 375–386. https://doi.org/10.1016/j.molcel.2012.09.001.

(24) Deo, R. C.; Bonanno, J. B.; Sonenberg, N.; Burley, S. K. Recognition of Polyadenylate RNA by the Poly(A)-Binding Protein. *Cell* **1999**, *98* (6), 835–845. https://doi.org/10.1016/S0092-8674(00)81517-2.

(25) Kozlov, G.; Trempe, J.-F.; Khaleghpour, K.; Kahvejian, A.; Ekiel, I.; Gehring, K. Structure and Function of the C-Terminal PABC Domain of Human Poly(A)-Binding Protein. *Proc. Natl. Acad. Sci.* **2001**, *98* (8), 4409–4413. https://doi.org/10.1073/pnas.071024998.

(26) Glover, K.; Mei, Y.; Sinha, S. C. Identifying Intrinsically Disordered Protein Regions Likely to Undergo Binding-Induced Helical Transitions. *Biochim. Biophys. Acta BBA - Proteins Proteomics* **2016**, *1864* (10), 1455–1463. https://doi.org/10.1016/j.bbapap.2016.05.005.

(27) Henderson, R. The Potential and Limitations of Neutrons, Electrons and X-Rays for Atomic Resolution Microscopy of Unstained Biological Molecules. *Q. Rev. Biophys.* **1995**, *28* (2), 171–193. https://doi.org/10.1017/S003358350000305X.

(28) Bier, K.; York, A.; Fodor, E. Cellular Cap-Binding Proteins Associate with Influenza Virus MRNAs. *J. Gen. Virol.* **2011**, *92* (7), 1627–1634. https://doi.org/10.1099/vir.0.029231-0.

(29) Kainov, D. E.; Müller, K. H.; Theisen, L. L.; Anastasina, M.; Kaloinen, M.; Muller, C. P. Differential Effects of NS1 Proteins of Human Pandemic H1N1/2009, Avian Highly Pathogenic H5N1, and Low Pathogenic H5N2 Influenza A Viruses on Cellular Pre-MRNA Polyadenylation and MRNA Translation. *J. Biol. Chem.* **2011**, *286* (9), 7239–7247. https://doi.org/10.1074/jbc.M110.203489.

(30) Anastasina, M.; Terenin, I.; Butcher, S. J.; Kainov, D. E. A Technique to Increase Protein Yield in a Rabbit Reticulocyte Lysate Translation System. *BioTechniques* **2014**, *56* (1). https://doi.org/10.2144/000114125.

(31) Panthu, B.; Terrier, O.; Carron, C.; Traversier, A.; Corbin, A.; Balvay, L.; Lina, B.; Rosa-Calatrava, M.; Ohlmann, T. The NS1 Protein from Influenza Virus Stimulates Translation Initiation by Enhancing Ribosome Recruitment to MRNAs. *J. Mol. Biol.* **2017**, *429* (21), 3334–3352. https://doi.org/10.1016/j.jmb.2017.04.007.

(32) Chen, J.; Choi, J.; O'Leary, S. E.; Prabhakar, A.; Petrov, A.; Grosely, R.; Puglisi, E. V.; Puglisi, J. D. The Molecular Choreography of Protein Synthesis: Translational Control, Regulation, and Pathways. *Q. Rev. Biophys.* **2016**, *49*, e11. https://doi.org/10.1017/S0033583516000056.

(33) Prabhakar, A.; Choi, J.; Wang, J.; Petrov, A.; Puglisi, J. D. Dynamic Basis of Fidelity and Speed in Translation: Coordinated Multistep Mechanisms of Elongation and Termination: Dynamic Basis of Fidelity and Speed in Translation. *Protein Sci.* **2017**, *26* (7), 1352–1362. https://doi.org/10.1002/pro.3190.